Title
Morphology Control of Noble Metal Nanoparticle Catalysts Using Strategic Organic Capping Agents in Colloidal Phase Synthesis

Author
Roeser, Kayla Mae

Publication Date
2014

Peer reviewed|Thesis/dissertation

UNIVERSITY OF CALIFORNIA

Los Angeles

Morphology Control of Noble Metal Nanoparticle Catalysts Using Strategic Organic Capping Agents in Colloidal Phase Synthesis

A dissertation submitted in partial satisfaction of the requirements for the degree Doctor of Philosophy in Chemistry

by

Kayla Mae Roeser

2014

ABSTRACT OF THE DISSERTATION

Morphology Control of Noble Metal Nanoparticle
Catalysts Using Strategic Organic Capping Agents
in Colloidal Phase Synthesis

by

Kayla Mae Roeser
Doctor of Philosophy in Chemistry
University of California, Los Angeles, 2014
Professor Xiangfeng Duan, Chair

Noble metals are the most sought after elements for catalysis because of their versatility, activity, and recyclability for a variety of applications; however they are limited as a resource and expensive. Noble metal nanoparticles offer a solution for use in catalysis because their high surface area to volume ratio maximizes their available surface sites while minimizing the amount of metal used. Additionally, particularly exposed facets of nanoparticles can increase surface energies for superior catalytic activity and induce novel electronic/physical properties. In the first chapter of my thesis, I synthesized palladium, platinum, and semiconductor titania nanoparticles through a biomimetic approach by using peptides to preferentially bind to and expose particular crystal facets of nanoparticles. Using a combinatorial approach called biopanning to find highly

selective surface energy modifiers for particular facets of materials gave insight to unique binding motifs for materials as well as induced morphology controlled nanoparticles at ambient conditions. There are limitless combinations of solvents, capping agents, and inorganic precursors for inorganic nanoparticle synthesis. Understanding these systems in terms of more global trends would circumvent the current colossal approach of empirically screening systems. To do this, considering the inorganic-organic interfacial relationship is key. In the second chapter, I report unique aryl small molecules which preferentially bind to palladium surfaces through electrostatic potentials and epitaxial binding in nanoparticle synthesis. These results offer an understanding to the dynamic binding relationship between capping agents and nanoparticle surfaces. Lastly, I report on the synthesis of gold-palladium nanoparticles and their activity for the benzyl alcohol oxidation reaction. It was found that the (100) facets of gold-palladium were more catalytically active than the (111) surface. Details of the nanoparticle shape, size, and activity add to the understanding how this material behaves at the atomic level and will help to impact future advances in this field of catalysis. The syntheses described here are important because they are environmentally friendly, they offer information about the binding mechanisms at the organic-inorganic interface of the systems, and give insight to catalytic behavior. All of this work is necessary to further exploit nanoparticle synthesis, assembly and provide the precise engineering of nanostructured materials.

The dissertation of Kayla Mae Roeser is approved.

Jeffrey Zink

Yu Huang

Xiangfeng Duan, Committee Chair

University of California, Los Angeles

2014

TABLE OF CONTENTS

ACKNOWLEDGEMENTS

I would like to thank Dr. Xiangfeng Duan and Dr. Yu Huang for their unconditional support and guidance through my graduate experience. I would like to thank Dr. Sarah Tolbert for motivating me to be a better scientist and inspiring teacher.

I would like to acknowledge the following funding source for making some of the entailed research possible: IGERT Materials Creation Training Program (NSF DGE-0114443 and DGE-0654431, California NanoSystems Institute, and the National Science Foundation).

My graduate experience at UCLA has been both humbling and exhilarating; I couldn't have done it without the limitless support of all my family and friends.

BIOGRAPHY

Kayla Mae Roeser received her B. S. in Chemistry at University of California, San Diego, in spring 2008. During her undergraduate research at UCSD, Kayla worked in Dr. Bill Trogler's Inorganic laboratory synthesizing silicon-based materials for explosives testing. She received her M. S. in Chemistry in the field of Inorganic Chemistry at University of California, Los Angeles in fall 2010. Kayla joined Dr. Xiangfeng Duan and Dr. Yu Huang's labs in spring 2009. In 2010, she received a two-year Materials Creation Training Fellowship (MCTP) supported by the National Science Foundation (NSF) and California NanoSystems Institute for her research. Kayla's graduate research interests focused on controlling noble metal nanoparticle shapes/morphologies using novel organic capping agents including peptides and small molecules. Additionally, she tested her nanoparticles in catalytic experiments. As part of her fellowship, Kayla studied and performed research at Roma Tré University in the summer of 2012 under the guidance of Dr. Igor Luisetto and Dr. Simonetta Tuti. There she synthesized iron, nickel, and cobalt nanoparticles for methane reforming reactions. During her studies at UCLA, she was a teaching assistant in the Chemistry Department for various courses including general chemistry laboratories and lectures as well as the Materials Chemistry Laboratory. In her spare time, Kayla participated in the MCTP Outreach/Nanoscience Program, where she led workshops teaching high school teachers nanoscience experiments. Additionally, she helped to lead Nanoscience Summer Camps for high school students in 2011, 2013, and 2014.

INTRODUCTION

Colloidal nanocrystal growth has proven to be a successful approach for making noble metal and semiconductor nanoparticles for a wide range of useful applications such as in the oxygen reduction reaction in fuel cells,[1-4] the water splitting reaction in photocatalysis,[5-7] numerous types of heterogeneous organic catalysis,[8-10] electronics,[11,12] as well as provides building blocks for the bottom-up assembly of novel electronic and catalytic complex 3D structures.[13-15] Colloidal nanocrystals are defined by nanometer-sized inorganic particles made in solution and capped by a "mono"-layer of surfactants.[16] There are limitless combinations of solvents, capping agents, and inorganic precursors in this type of synthesis for inorganic nanocrystals, and due to the increasing applications of nanoparticles, there is a driving force in the field to begin understand these systems in terms of larger, more catalogued systems instead of empirically screening capping agents individually. To do this, understanding the mechanisms of nanoparticle growth is vital to determine successful systems for different nanoparticle synthesis.

The most common approaches to solution-phase inorganic nanocrystal growth are co-precipitation in aqueous phase, reverse micelle synthesis, the hydrothermal/solvothermal method, impregnation, deposition precipitation, sol-immobilisation, and synthesis by surfactant-controlled growth.[16-20] Synthesis by surfactant-controlled growth offers superior benefits to other growth methods because it can be performed in aqueous solutions at ambient conditions providing a more environmentally friendly approach to synthesis (avoiding the need for high temperatures, organic solvents, and large capping agents) and more importantly may incorporate

capping agents that alter the growth kinetics in solution allowing for size and shape control. My work detailed in the following dissertation exploited this type of nanoparticle synthesis with different types of capping agents to control size and morphology.

Inorganic nanoparticle synthesis in an aqueous phase at room temperature requires organic capping agents, metal (inorganic) precursors, and a reducing agent which all must be soluble in water. Additionally, the inorganic precursor should have good leaving groups so that the desired reactive inorganic species is readily available in the reaction solution. For noble metal precursors, metal-halide salts are often used; metal oxide precursors vary as they are more sensitive to the reducing agent and capping agent. Generic surfactants such as citric acid, polyvinylpyrrolidone (PVP) cetrimonium bromide (CTAB), and trioctylphosphine oxide (TOPO) are used for simple controlling size and dispersity of nanocrystals, but spherical nanoparticles often result due to non-preferential binding and the mechanisms regarding their selective adsorption to metal surfaces remain elusive due to the complexity of the synthetic systems and multiple binding/interaction motifs of these larger surfactants.[21,22] For morphology and shape control of nanoparticles at ambient conditions, peptides,[23] RNA/DNA,[24] and small organic molecules[25] are among the newest rationally-selected capping agents for nanoparticle synthesis at ambient conditions. They offer high specificity in shape control for particles through surface energy modification of crystallographic faces in addition to keeping nanoparticles monodisperse in solution. They are also smaller than most generic surfactants and can provide models for studying specific capping agent-metal surface interactions.

Colloidal synthesis involved two steps: 1) nucleation of seeds and 2) subsequent growth. For ambient condition synthesis, nucleation occurs upon the addition of a reducing agent in a

solution with an inorganic precursor and organic capping agent. Nucleation forms reactive atomic or molecular species, known as monomers, from the inorganic precursor. Subsequently, growth may occur through two different currently accepted mechanisms: monomer attachment and coalescence. The type of growth mechanism that will occur is largely based on the monomer concentration formed, the type of metal being used, and the type and amount of reducing agent present to induce nucleation. Monomer attachment growth typically provides the best route for single crystalline material, whereas coalescence growth often forms nanoparticles with multiple twin structures and/or high-energy facets.[26-30] My work promoted monomer attachment growth and prevented coalescence for the formation of single crystalline nanoparticles.

According to the classic model of kinetic growth by La Mer and Dinegar,[31] monomer attachment growth of nanoparticles with homogeneous size distribution are formed when there is a discrete, fast nucleation step followed by growth. Without a discrete nucleation stage, a wide range of nanoparticle size is obtained. Figure 1 illustrates the La Mer and Dinegar model of size distribution of nanoparticles based on the separation of nucleation and growth steps.

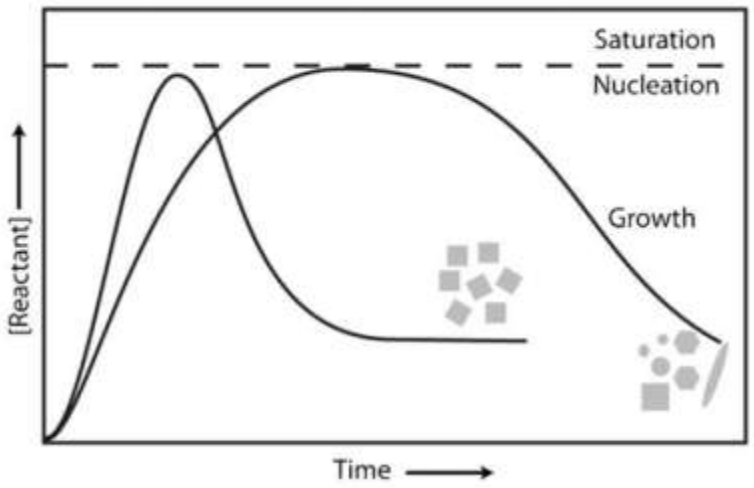

Figure 1 A graph illustrating the La Mer and Dinegar kinetic growth model showing the difference between homogeneous and heterogeneous nanoparticle size based on the time separation of the nucleation and growth steps.[18]

The details of the La Mer/Dinegar growth model was improved by Howard Reiss[32] and was described through size focusing and defocusing processes. These processes rely on several key facts. Very small nanoparticles have active surface atoms due to curvature and strain which can dissolve back into solution; therefore nanoparticles below a certain threshold size have negative growth rates. This phenomenon is well described by the Gibbs-Thompson effect.[33] At a threshold, known as the critical size, nanoparticles neither grow nor shrink.[34] And above this threshold, nanoparticles have a smaller "active" surface to volume ratio and instead of breaking down in solution will grow due to the attachment from monomers in solution. In this regime, smaller nanoparticles will grow faster than larger nanoparticles because they have relatively higher surface energy for monomers to attach. The peak in growth rate of nanoparticles occurs due to a geometric factor, where monomers prefer to attach to smaller nanoparticles with higher surface energies than larger nanoparticles with lower surface energies, preventing further growth of any large nanoparticles.[16,32] Figure 2 illustrates the critical size and growth rate as a function overall size of nanoparticles at high and low monomer concentrations.

When there is a high concentration of monomers present, the critical size of nanoparticles is relatively small. In this situation, the critical size of the particles is outside the range of the average size of the nanoparticles present and creates a driving force of growth of the nanoparticles below the average size to "catch up." Ultimately nanoparticles with narrow size distribution are obtained in this process known as "focusing." This situation is best obtained when there is a "burst" of nucleation creating a high monomer concentration, followed by "focused" growth.

On the other hand, when there is a low monomer concentration present, the critical size of nanoparticles falls within the distribution of nanoparticle sizes present and does not create any driving force of growth of the bunch of nanoparticles. Instead, classic Ostwald ripening occurs, where nanoparticles that are very small get smaller due to active surface atoms that are released into solution and larger nanoparticles grow due to the addition of monomers in solution. This phenomenon leads to a wide range of size distribution of nanoparticles and is known as "defocusing." Low monomer concentration often occurs through a slow nucleation step (assuming there is enough inorganic precursor present to create a saturated solution).

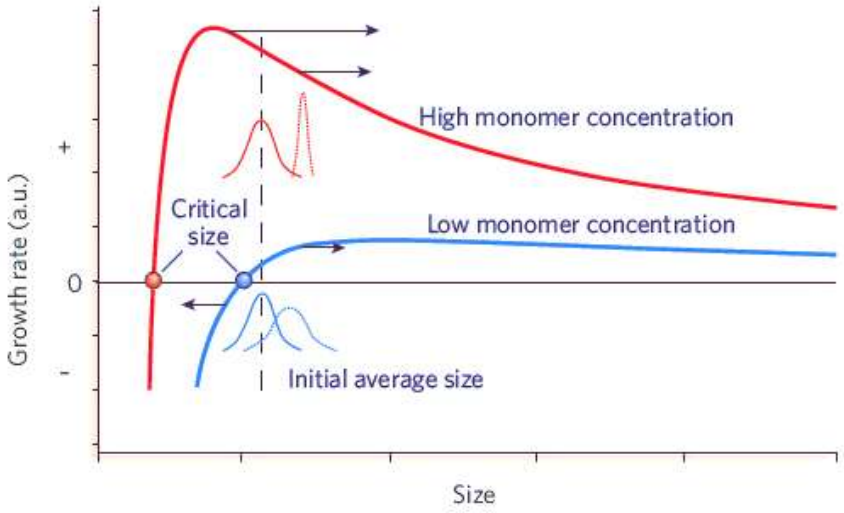

Figure 2 A graph illustrating size focusing (red line) and size defocusing (blue line) depending on the monomer concentration present in solution during the nucleation step of growth.[16]

For ambient condition nanoparticle synthesis, the best way to obtain a high monomer concentration is to induce nucleation on a very short time scale by the addition of a rapidly reacting reducing agent. It is also necessary to add enough inorganic precursor initially so that when nucleation occurs, a nearly saturated solution, or high monomer concentration, can be obtained. Focusing is a kinetically controlled growth process, as smaller nanoparticles with

higher energy surfaces will grow faster than larger nanoparticles with lower energy surfaces. However this classic description of kinetic growth does incorporate mention morphology control but rather is a generic growth mechanism for the monomer attachment model of spherical nanoparticles.

For nanoparticle synthesis in this work, nanoparticles grow from a high monomer concentration in the kinetically-controlled growth (focusing) regime. In this regime, it is understood that surfaces with higher-energy surfaces will grow more quickly than lower-energy surfaces. When capping agents with preferential binding affinities to particular facets are introduced to this mechanism, surfaces with bound capping agent will have lower surface energies, leaving exposed facets with higher surface energies vulnerable for additional growth. Eventually, nanoparticles are produced with shapes defined by the surfaces that the capping agents preferred to bind. The binding of capping agents to favored surfaces is a thermodynamic property driven by lowering both the capping agent and inorganic surface's overall energy in solution. However, kinetic control nanoparticle growth is still the dominant mechanism in this type of colloidal nanoparticle synthesis, where higher energy facets grow faster than lower energy facets.

These fundamental growth mechanisms determined decades ago through indirect observational effects and theoretical calculations are now extensively studied now through computer software models[35] and direct observations of growth trajectories[26,30,36] due to recent advances in technology. For example, Zheng and coworkers[26] observed real-time platinum nanoparticle growth upon the irradiation of a TEM beam by using a liquid cell reactor placed in a TEM sample holder. They found that both monomer attachment growth and coalescence growth

happened in the same reaction but still induced homogeneous size distribution. In Figure 3a and b, the nanoparticle growing by monomer attachment in the first column grows continuously until it reaches a saturation stage and follows a classic focusing, ensemble behavior (Figure 3d, blue line, and e, blue line). On the other hand, the nanoparticles grown by coalescing become bigger immediately after coalescence but then go through a "relaxation" time period where growth stops, slight shrinkage occurs and the crystallinity is re-established, followed by focusing of nanoparticles (Figure 3a and b, second column, Figure 3d, red line, and 3e, red/green/black lines). Altogether, this synthesis follows a traditional homogeneous growth model as shown in Figure 3c (green line) despite the two growth mechanisms. This report provides direct evidence of the monomer attachment and coalescence models as well as offers insight and encourages further studies of the details of these mechanisms.

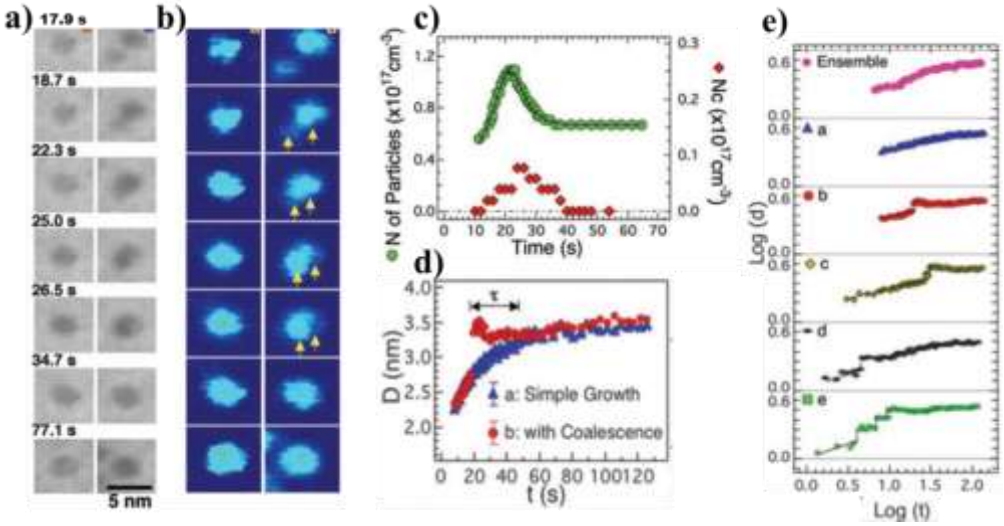

Figure 3 (a and b) In-situ Transmission Electron Microscopy (TEM) images of platinum nanoparticles growing through the monomer attachment mechanism (1st column) and coalescence mechanism (2nd column). (c) A graph illustrating the number of particles (green line) and number of coalescence events (red line) in solution as a function of time. (d) A graph of nanoparticle diameter as a function of time for a nanoparticle grown through monomer attachment (blue line) and coalescence (red line). (e) The logarithmic relationship of particle size as a function of growth time for monomer attachment particles (blue line) and coalesced particles (red, green, and black lines).[26]

Directly studying the nucleation stage of synthesis is still difficult due to its short time period as well as the difficulty of observing small, atomic-sized monomers. However, Harada[37] and colleagues performed a time-resolved in-situ small angle X-ray scattering (SAXS) technique in combination with UV-Vis and TEM and were able to monitor distinct stages of palladium nanoparticle growth in aqueous solutions referred to as the autocatalytic-nucleation, nucleation-growth, Ostwald ripening, and dynamic coalescence growth stages. As shown in Figure 4, the group was able to observe and isolate the autocatalytic-nucleation and nucleation-growth phases, as well as approximate the size of monomers, number of monomers and other important information dependent on concentration. Although visually observing autocatalytic-nucleation through microscopy has still yet to be done, this work provided an advance in studying the early stages of nanoparticle growth.

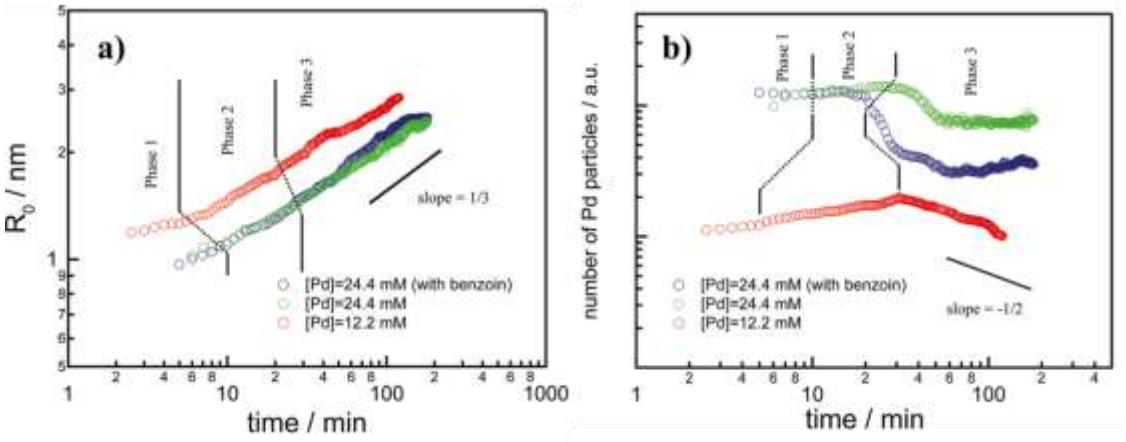

Figure 4 (a) A graph illustrating the average nanoparticle radius as a function of time for the various phases of palladium nanoparticle synthesis. (b) A graph illustrating the average number of particles as a function of time for the various phases in palladium nanoparticle synthesis.[37]

Selective adhesion affects in combination with kinetic control of nanoparticle growth offers the possibility for nanoparticle synthesis with narrow size distribution and a wide range of exposed crystallographic facets. Understanding the mechanisms of growth in solution-phase

nanoparticle synthesis is important for selecting the precise conditions to promote fine control of nanoparticles with a narrow size distribution. Controlling the ways that colloids grow in solution is fundamental for making more advanced leaps in nanoparticle synthesis in the fields of electronics, photovoltaics, catalysis, and more. In the following chapters, great care is taken in choosing capping agents that affect the morphology of nanoparticles while providing the correct environment for monomer attachment growth.

References

1 Debe, M. K. Electrocatalyst approaches and challenges for automotive fuel cells. *Nature* **486**, 43-51, doi:10.1038/nature11115 (2012).

2 Marković, N. M., Schmidt, T. J., Stamenković, V. & Ross, P. N. Oxygen Reduction Reaction on Pt and Pt Bimetallic Surfaces: A Selective Review. *Fuel Cells* **1**, 105-116, doi:10.1002/1615-6854(200107)1:2<105::AID-FUCE105>3.0.CO;2-9 (2001).

3 Gasteiger, H. A., Kocha, S. S., Sompalli, B. & Wagner, F. T. Activity benchmarks and requirements for Pt, Pt-alloy, and non-Pt oxygen reduction catalysts for PEMFCs. *App. CatB. Env.* **56**, 9-35, doi:http://dx.doi.org/10.1016/j.apcatb.2004.06.021 (2005).

4 Koenigsmann, C. *et al.* Enhanced Electrocatalytic Performance of Processed, Ultrathin, Supported Pd–Pt Core–Shell Nanowire Catalysts for the Oxygen Reduction Reaction. *J Am Chem Soc* **133**, 9783-9795, doi:10.1021/ja111130t (2011).

5 Linsebigler, A. L., Lu, G. & Yates, J. T. Photocatalysis on TiO2 Surfaces: Principles, Mechanisms, and Selected Results. *Chemical Reviews* **95**, 735-758, doi:10.1021/cr00035a013 (1995).

6 Ni, M., Leung, M. K. H., Leung, D. Y. C. & Sumathy, K. A review and recent developments in photocatalytic water-splitting using for hydrogen production. *Renewable and Sustainable Energy Reviews* **11**, 401-425, doi:http://dx.doi.org/10.1016/j.rser.2005.01.009 (2007).

7 Ashokkumar, M. An overview on semiconductor particulate systems for photoproduction of hydrogen. *International Journal of Hydrogen Energy* **23**, 427-438, doi:http://dx.doi.org/10.1016/S0360-3199(97)00103-1 (1998).

8 Hashmi, A. S. K. & Hutchings, G. J. Gold Catalysis. *Ang. Chem. Int. Ed.* **45**, 7896-7936, doi:10.1002/anie.200602454 (2006).

9 Miyaura, N. & Suzuki, A. Palladium-Catalyzed Cross-Coupling Reactions of Organoboron Compounds. *Chemical Reviews* **95**, 2457-2483, doi:10.1021/cr00039a007 (1995).

10 Landon, P., Collier, P. J., Papworth, A. J., Kiely, C. J. & Hutchings, G. J. Direct formation of hydrogen peroxide from H2/O2 using a gold catalyst. *Chem. Comm.*, 2058-2059, doi:10.1039/B205248M (2002).

11 Tao, A., Sinsermsuksakul, P. & Yang, P. Polyhedral Silver Nanocrystals with Distinct Scattering Signatures. *Ang. Chem. Int. Ed.* **45**, 4597-4601, doi:10.1002/anie.200601277 (2006).

12 Xia, Y. & Halas, N. J. Shape-Controlled Synthesis and Surface Plasmonic Properties of Metallic Nanostructures. *MRS Bulletin* **30**, 338-348, doi:doi:10.1557/mrs2005.96 (2005).

13 Macfarlane, R. J. *et al.* Nanoparticle Superlattice Engineering with DNA. *Science* **334**, 204-208, doi:10.1126/science.1210493 (2011).

14 Tao, A. *et al.* Langmuir−Blodgett Silver Nanowire Monolayers for Molecular Sensing Using Surface-Enhanced Raman Spectroscopy. *Nano. Lett.* **3**, 1229-1233, doi:10.1021/nl0344209 (2003).

15 Tao, A., Sinsermsuksakul, P. & Yang, P. Tunable plasmonic lattices of silver nanocrystals. *Nat Nano* **2**, 435-440, doi:http://www.nature.com/nnano/journal/v2/n7/suppinfo/nnano.2007.189_S1.html (2007).

16 Yin, Y. A., P. Colloidal Nanocrystal Synthesis and the Organic–Inorganic Interface. *Nature* **437**, 664-670, doi:10.1038/nature04165 (2005).

17 Hayashi, H. & Hakuta, Y. Hydrothermal Synthesis of Metal Oxide Nanoparticles in Supercritical Water. *Materials* **3**, 3794-3817 (2010).

18 Tao, A. R., Habas, S. & Yang, P. Shape Control of Colloidal Metal Nanocrystals. *Small* **4**, 310-325, doi:10.1002/smll.200701295 (2008).

19 Cushing, B. L., Kolesnichenko, V. L. & O'Connor, C. J. Recent Advances in the Liquid-Phase Syntheses of Inorganic Nanoparticles. *Chemical Reviews* **104**, 3893-3946, doi:10.1021/cr030027b (2004).

20 Pileni, M.-P. The role of soft colloidal templates in controlling the size and shape of inorganic nanocrystals. *Nat Mater* **2**, 145-150 (2003).

21 Puntes, V. F. K., K. M. Alivisatos, Paul A. Colloidal Nanocrystal Shape and Size Control: The Case of Cobalt. *Science* **291**, 2115-2117, doi:10.1126/science.1058495 (2001).

22 Sau, T. K. & Murphy, C. J. Room Temperature, High-Yield Synthesis of Multiple Shapes of Gold Nanoparticles in Aqueous Solution. *J Am Chem Soc* **126**, 8648-8649, doi:10.1021/ja047846d (2004).

23 Chiu, C.-Y. Platinum nanocrystals selectively shaped using facet-specific peptide sequences. *Nature Chemistry* **3**, 393-399, doi:10.1038/nchem.1025 (2011).

24 Gugliotti, L. A., Feldheim, D. L. & Eaton, B. E. RNA-Mediated Metal-Metal Bond Formation in the Synthesis of Hexagonal Palladium Nanoparticles. *Science* **304**, 850-852, doi:10.1126/science.1095678 (2004).

25 Chiu, C.-Y. *et al.* Facet-Selective Adsorption on Noble Metal Crystals Guided by Electrostatic Potential Surfaces of Aromatic Molecules. *J Am Chem Soc* **135**, 15489-15500, doi:10.1021/ja406018u (2013).

26 Zheng, H. *et al.* Observation of Single Colloidal Platinum Nanocrystal Growth Trajectories. *Science* **324**, 1309-1312 (2009).

27 Zhu, Y. T. *et al.* Formation of single and multiple deformation twins in nanocrystalline fcc metals. *Acta Materialia* **57**, 3763-3770, doi:http://dx.doi.org/10.1016/j.actamat.2009.04.020 (2009).

28 Li, D. *et al.* Direction-Specific Interactions Control Crystal Growth by Oriented Attachment. *Science* **336**, 1014-1018, doi:10.1126/science.1219643 (2012).

29 Liao, H.-G., Cui, L., Whitelam, S. & Zheng, H. Real-Time Imaging of Pt3Fe Nanorod Growth in Solution. *Science* **336**, 1011-1014, doi:10.1126/science.1219185 (2012).

30 Yuk, J. M. *et al.* High-Resolution EM of Colloidal Nanocrystal Growth Using Graphene Liquid Cells. *Science* **336**, 61-64, doi:10.1126/science.1217654 (2012).

31 LaMer, V. K. & Dinegar, R. H. Theory, Production and Mechanism of Formation of Monodispersed Hydrosols. *J Am Chem Soc* **72**, 4847-4854, doi:10.1021/ja01167a001 (1950).

32 Reiss, H. The Growth of Uniform Colloidal Dispersions. *The Journal of Chemical Physics* **19**, 482-487, doi:doi:http://dx.doi.org/10.1063/1.1748251 (1951).

33 Lifshitz, I. M. & Slyozov, V. V. The kinetics of precipitation from supersaturated solid solutions. *Journal of Physics and Chemistry of Solids* **19**, 35-50, doi:http://dx.doi.org/10.1016/0022-3697(61)90054-3 (1961).

34 Sugimoto, T. Preparation of monodispersed colloidal particles. *Advances in Colloid and Interface Science* **28**, 65-108, doi:http://dx.doi.org/10.1016/0001-8686(87)80009-X (1987).

35 van Embden, J., Sader, J. E., Davidson, M. & Mulvaney, P. Evolution of Colloidal Nanocrystals: Theory and Modeling of their Nucleation and Growth. *J Phys Chem C* **113**, 16342-16355, doi:10.1021/jp9027673 (2009).

36 Meng, F. & Jin, S. The Solution Growth of Copper Nanowires and Nanotubes is Driven by Screw Dislocations. *Nano. Lett.* **12**, 234-239, doi:10.1021/nl203385u (2011).

37 Harada, M., Tamura, N. & Takenaka, M. Nucleation and Growth of Metal Nanoparticles during Photoreduction Using In Situ Time-Resolved SAXS Analysis. *J Phys Chem C* **115**, 14081-14092, doi:10.1021/jp203119a (2011).

CHAPTER 1: PEPTIDE SELECTION FOR FACET SPECIFIC NANOPARTICLE SYNTHESIS

1.1 The Biomimetic Approach: Biopanning

In this report of nanoparticle synthesis, peptides were chosen as unique organic capping agents through a rational biomimetic approach called biopanning. Biopanning is a technique where specific peptides are determined to be strongly binding to a particular substrate of interest from a large library of peptides residing on the outer coat of a bacteriophage. Before biopanning, a library of bacteriophage is genetically engineered to contain identical copies of peptide sequences on a portion of their protein coat. The library is introduced to a substrate of interest and through binding and selection processes, the strongest binding peptides are determined. Binding of peptides occurs through electrostatic, polar, hydrogen, and Van der Waals forces through both peptide conformations and chemical functional groups.[1-3] In my work, this process was used in order to determine strongly binding peptides that could be used as capping agents in subsequent synthesis with the materials of interest including palladium (Pd), platinum (Pt), and titania (TiO_2). Once selected, the peptides were identified and synthesized separately to use as capping agents in nanoparticle synthesis.

The library of bacteriophage used in this work was called a phage display library (pH. D. library, New England BioLabs) and was genetically engineered to express five identical copies of different peptide sequences on the pIII portion of the outer surface protein of a M13 bacteriophage. In nature, the M13 virion is a non-lytic bacteriophage which infects gram-negative bacteria. It is 6.5 nm in diameter and ~1 μm in length. It contains single stranded DNA

made up of 6400 nucleotides. There are five surface coat proteins on the bacteriophage: five copies of the pIII protein hanging off one end of the phage, five copies of the pVI protein just above the pIII protein, 2700 copies of the pVIII protein extending along the length of the shaft of the phage, and 5 copies each of the pVII and pIX proteins on the other end of the phage.

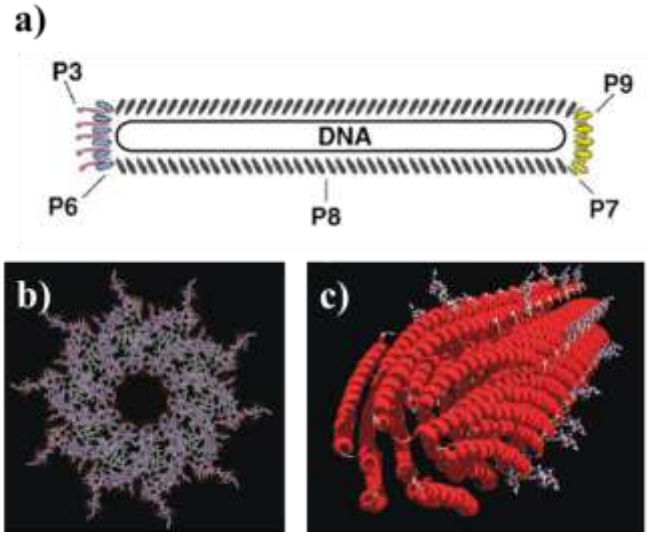

Figure 1.1 (a) Illustration of the M13 bacteriophage with its respective surface proteins labeled.[4] (b) Head-on and c) angled view illustrations of the pVIII protein of the M13 bacteriophage illustrating the symmetry of the protein.[5]

Different types of substrates are created for biopanning. In general, a substrate used in biopanning must not degrade (chemically or physically) in solution, must have a clean bare surface for binding, and must be small enough to fit into a micro-centrifuge tube for the biopanning process but large enough to be physically removed with tweezers or by another convenient method. For example, microparticles of materials could be used if they were large enough to be easily centrifuged out of solution or could be pulled down with a magnet, as in the case with magnetite microparticles. Peptides selected for non-specific platinum surfaces have been performed in our lab with wires ~1 mm in diameter and ~1 cm in length in solution.[6] For selection with specific facets of metals, nano-cubes and/or nano-octahedra were synthesized and

placed on a 1 cm X 1 cm silicon substrate for biopanning, as in the case of palladium in this report. When peptides selected for semi-conductors or other metals that exist naturally as hard, single crystals, a 1 cm X 1 cm X 0.5 mm pieces were placed into solution, as in the case of titania in this report.

The phage display process has become a more established route for selecting highly unique capping agents for metal synthesis.[5-8] The pIII protein is commonly exploited in biopanning because of the ease of genetically engineering it and because of the effective location of the protein for binding to materials, followed by the pVIII protein.[9] Because only one portion of the bacteriophage is genetically engineered to be different from every other phage, the difference in binding of the phage to the surface is attributed to the peptide that is unique to that phage.

In our work, each phage in the library expressed five identical copies of a peptide sequence for a total of ~$2E^9$ different pIII peptide sequences per microliter present in the initial biopanning solution. Phage display libraries of seven, twelve, and other amino acid peptide chains can all be genetically engineered on the pIII portion of the bacteriophage. For palladium and platinum biopanning, a phage display library of seven amino acid peptide chains on the pIII portion of the bacteriophage was chosen, and for titania a phage display library of twelve amino acid peptide chains was chosen. In a typical cycle of biopanning, 10 µL of the phage display library solution was injected into a micro-centrifuge tube at room temperature containing the substrate of interest and 990 µL solution of tris-(hydroxymethyl)-aminomethane (Tris-HCl)/sodium chloride, collectively known as tris-buffered saline solution "TBS," Sigma). The solution was rocked automatically for one hour at room temperature to allow the phages to bind

to the substrate of interest. After one hour, the solution was removed from the tube so that only the substrate and phages bound to the substrate remained. The bound phages were removed from the substrate by eluting them with an acidic solution, glycine-HCl (Sigma), and then added to Tris-HCl to stabilize the phages in a slightly basic buffer solution. The process of introducing phages to the substrate for a given period and collecting those that stayed attached to the substrate while discarding those that did not was considered one round of biopanning.

The bound phages were amplified in order to work with them for succeeding rounds of biopanning. Having only one phage with a strong binding peptide is not practical for being isolated and characterized. Through amplification, the phage could be tested in more rounds of biopanning and would be concentrated enough to collect its DNA for determining its pIII amino acid sequence. A titering process was performed to amplify the bound phages, where the phages infected E. Coli (New England BioLabs) and multiplied over a 5 hour period. The phages were separated from the bacteria and placed back into a buffer TBS solution.

After amplification, the bound phages needed to be tested for their strength to the substrate so that only the strongest binding peptides were selected. To do this, another cycle of biopanning was performed. Before collecting the bound phages from the substrate, the substrate was washed with a 0.1 - 1.0 % Tween-20 (Fluka) solution made of TBS and Tween-20. The remaining phages were then eluted, collected, and amplified. This process was done for several cycles. Each succeeding cycle was washed with a more stringent concentration of Tween-20 so that in the end, only the strongest binding phages were being amplified. As elution and amplification cycles occurred, the concentrations of phages in solution were monitored by plating infected E. Coli on LB XGal/IPTG plates (Sigma).

After several cycles of biopanning, the strongest binding phages out-numbered all other phages in solution. Eventually, the phage solution converged to contain bacteriophages with only several pIII amino acid sequences. For determination of phages with strong binding peptides, E. Coli was infected with the phage solution. Then, individual infected E. Coli colonies (representing a phage which infected that colony) was amplified, collected, processed (QIAprep Spin M13 Kit) and sent to a DNA testing lab at UCLA to determine the nucleotide sequence that corresponded to the amino acid sequence of the pIII protein of interest. Based on this process, strong binding peptide sequences were discovered for palladium (100) and (111) nanoparticles, platinum wire, and rutile (titania) (100) and (110) single crystals. Figure 1.2 illustrates the process of biopanning.

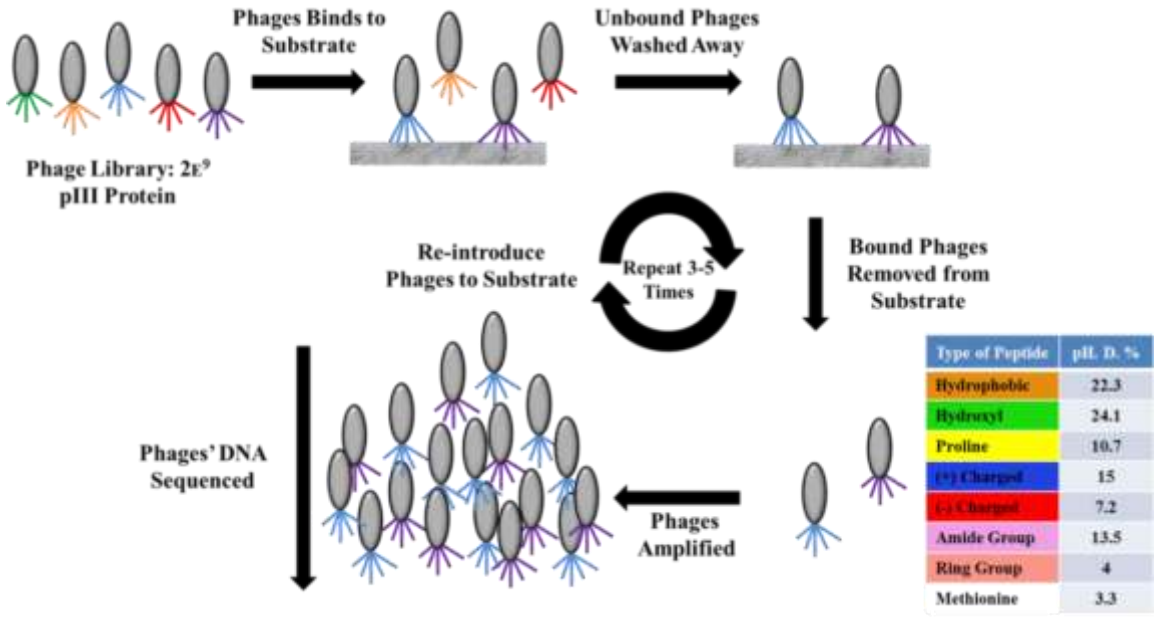

Figure 1.2 A schematic illustrating the process of biopanning including a table of the percentages of each type of amino acid in the phage display library.

Peptides that were selected through biopanning were analyzed for their legitimacy. For example, literature has shown that both hydroxyl groups and amide groups bind well to noble

metal and oxide surfaces.[1,10,11] For biopanning with noble metals/metal oxides, peptides with hydroxyl groups and/or amide groups were expected and selected for use in synthesis before peptides without these groups. Additionally, peptides were selected based on their ease of synthesis. For example, the amino acid methionine is very difficult to synthesize within a peptide as it is toxic while synthesizing and is not stable in air for long periods. Peptides with this amino acid were typically avoided for nanoparticle synthesis.

Once the peptides were selected through biopanning, they were synthesized with a peptide synthesizer (CS336X, C S Bio Co.) and capped with an acetyl group on the N terminus end and an amide group on the C terminus end. Subsequently, the peptides were purified by High Performance Liquid Chromatography, (HPLC, Varian ProStar) and tested for purity with Liquid Chromatography Mass Spectrometer (LCMS, Shimadzu 2010 EV). Peptides used for synthesis had >95 % purity. Finally, the peptides were used as capping agents in solution-phase nanoparticle synthesis.

Instead of empirically choosing capping agents for nanoparticle synthesis through trial and error, biopanning provides a systematic way of determining highly selective capping agents from a large library of potential candidates. The peptides selected are unique to a particular metal surface and offers the inference of important motifs for the successful binding of the organic-inorganic phases.[11] Additionally, selective capping agents in solution may provide more opportunity for dynamic heterostructures. Lastly, nanoparticle synthesis with peptides is performed in aqueous solutions at ambient conditions while still forming single crystal facet-controlled particles, which provides a "green" alternative to more traditional methods of single crystal nanoparticle synthesis.

1.2 Biopanning with Palladium Nano-Cubes and Nano-Octahedra

Biopanning was performed on palladium nano-cubes and nano-octahedra in order to find facet selective peptides for palladium. The nano-cubes were synthesized based on a report in literature,[12] and nano-octahedra were made from the nano-cube seeds. The syntheses are reported in detail in Chapter 3. Figure 1.3 shows TEM images of palladium nano-cubes and nano-octahedra that were made for biopanning.

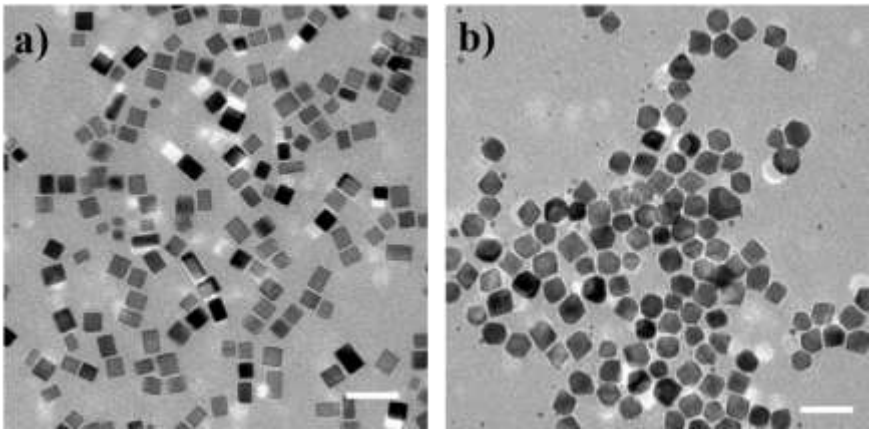

Figure 1.3 (a) Transmission electron microscope (TEM) image of palladium nano-cubes used for biopanning. (b) TEM image of palladium nano-octahedra used for biopanning. Scale bars 50 nm.

Once the nanoparticles were made and washed, they were spin-coated onto a clean silicon substrate with 1 cm X 1 cm X 0.5 mm dimensions and used for biopanning. The silicon substrate prevented aggregation and allowed for easy removal of the nanoparticles during biopanning. Scanning electron microscope images were taken of the substrate before and after biopanning to ensure the nanoparticles were intact and evenly dispersed on the substrate. Figure 1.4 shows Scanning Electron Microscope (SEM) images of palladium nano-octahedra on a silicon substrate after biopanning.

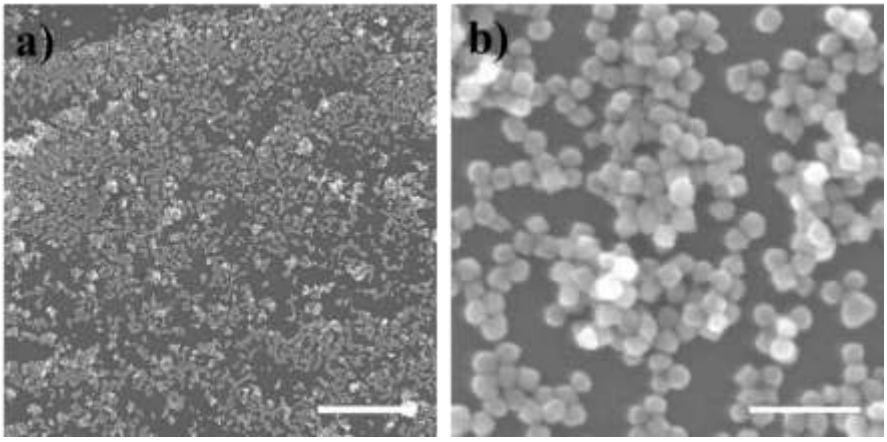

Figure 1.4 (a) Scanning Electron Microscope (SEM) image of palladium nano-octahedra on a silicon substrate after biopanning. Scale bar 1 μm. (b) Magnified SEM image of palladium nano-octahedra on the silicon substrate after biopanning. Scale bar 100 nm.

It was important to make sure the metal surfaces used in biopanning were clean and bare so that peptides could bind directly to the metal. Two cleaning techniques, flame cleaning and ozone treatment, were employed to remove the capping agent, polyvinylpyrrolidone (PVP), from the palladium nanoparticles and then tested to see which technique was more suitable for use in biopanning. In the flame cleaning process, a hydrogen flame was swiped evenly across the surface of the nanoparticle-silicon substrate. Each swipe was considered one cycle of flame treatment. In the ozone cleaning treatment, a more common technique for cleaning noble metal surfaces,[13] 10 cycles of 15 minutes of ozone exposure was used. To test the effectiveness of these techniques, the nanoparticles were placed on a gold substrate, cleaned through either flame cleaning or ozone cleaning, and then tested with X-ray photoelectron spectroscopy (XPS) for palladium's electronic surface properties. Figure 1.5 shows XPS data for palladium black (Sigma), untreated palladium octahedra, octahedra that went through a flame cleaning treatment, and octahedra that went through ozone treatment.

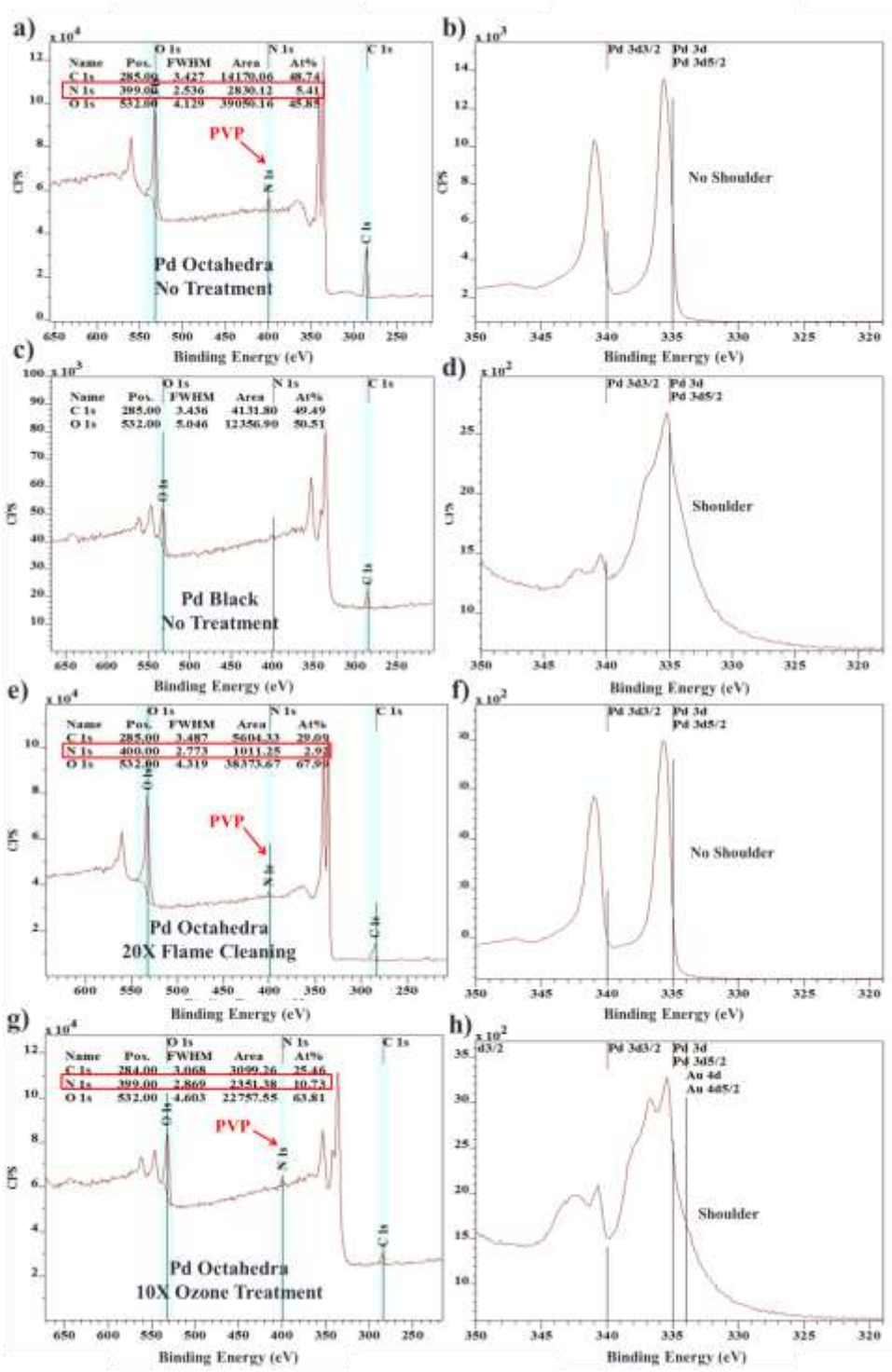

Figure 1.5 (a and b) X-Ray Photoelectron Spectroscopy (XPS) data on untreated palladium octahedra. (c and d) XPS data on untreated palladium black. (e and f) XPS data on palladium octahedra after 20 flame treatment cycles. (g and h) XPS data on palladium octahedra after 10 cycles of ozone treatment.

The untreated sample of palladium octahedra showed peaks associated with carbon and nitrogen binding around 285 eV and 400 eV, respectively (Figure 5a). These peaks were due to the binding of PVP[14,15] and their relative areas were used as a measure of how much PVP was removed from the surface of palladium through each type of cleaning cycle. There was also a peak at 532 eV due to a weak binding mode of palladium with oxygen from the sample being in air. The Pd $3d_{5/2}$ peak at 336 eV is often used as a measure of true oxidation of the Pd surface; the more of a shoulder the peak has around 335 eV, the more Pd-O modes are occurring and the more palladium (II) oxide is present.[16] This peak was observed during the cleaning processes to make sure oxidation of palladium did not occur as a result of the cleaning processes. In the untreated sample of palladium octahedra (Figure 5b), there was no oxidative Pd-O modes, indicating the surface of untreated Pd octahedra was made up of Pd^0 atoms. Palladium black had no nitrogen peak at 400 eV (Figure 5c) and had a shoulder peak at 335 eV (Figure 5d) from oxidation in air over time. This was consistent with its known properties; palladium black is not made with any nitrogen-based capping agents so should not have any nitrogen peaks associated with it. Additionally, it is stored in air over long periods of time and therefore was expected to have a lot of palladium (II) oxide on its surface. These measurements were used for comparing the cleaning techniques by how much each treatment removed the nitrogen peak from the sample and caused oxidation of the palladium surface. The carbon peak at 285 eV in palladium black was due to its synthesis but also showed up when PVP was present; therefore it was not a key peak for comparing cleaning processes.

The flame cleaning process removed about half of the PVP originally on the surface of palladium octahedra (Figure 5e). Additionally, no oxidation of palladium occurred through this process (Figure 5f). More flame cleaning may have removed more PVP and oxidation most

likely would not have occurred, but this was considered clean enough to move forward with biopanning. It is important to note that before either cleaning process, some of the PVP was also removed through stringent ethanol/acetone washing techniques in solution; therefore half of the PVP removed from what was left from solution cleaning indicated a large amount of clean, bare palladium surface for biopanning. The ozone treatment process did not remove as much PVP as the flame cleaning process (Figure 5g), and this process was not pushed forward as oxidation of palladium began to occur (Figure 5h). Less ozone cleaning time/less cycles of ozone cleaning did prevent some palladium oxidation but also decreased the amount of PVP removed. Ultimately, the flame cleaning process provided a cleaner palladium surface for biopanning than ozone treatment while preventing over oxidation. This experiment was useful for determining the correct cleaning process for noble metals in biopanning with palladium and was also important for other systems in our lab when the amount of oxidation needed to be considered when creating a clean substrate for catalysis or otherwise.

Following the first round of biopanning, a "negative" biopanning cycle was applied to the palladium nanoparticle system because the substrate of interest was placed on silicon. Phages that preferentially bound to silicon needed to be excluded from the selection process in order to find phages that only bound strongly to palladium. The eluted phage solution from the first round of biopanning was introduced to a pure silicon substrate. Then, the solution was removed and used for subsequent biopanning. Any peptides that would have preferred silicon binding were discarded with the silicon substrate.

Figure 1.6a shows the peptide found from biopanning with palladium nano-cubes. Out of billions of phages in solution after four rounds of biopanning, 20 were chosen at random from

infected E. Coli colonies to determine the composition of their pIII proteins. The peptide, TGSLSGV was found multiple times. The synthesized and capped chemical formula of the peptide was Ac-Thr-Gly-Ser-Leu-Ser-Gly-Val-$CONH_2$ and had a molecular weight of 660.73 g/mol, simply referred to as TGSLSGV.

Figure 1.6b shows the peptide determined from biopanning with palladium nano-octahedra. Once synthesized and capped similarly as reported above, the peptide used for nanoparticle synthesis was Ac-Asn-Ala-Asn-Ala-Ile-Ser-Thr-$CONH_2$ with a molecular weight of 730.78 g/mol, referred to as NANAIST.

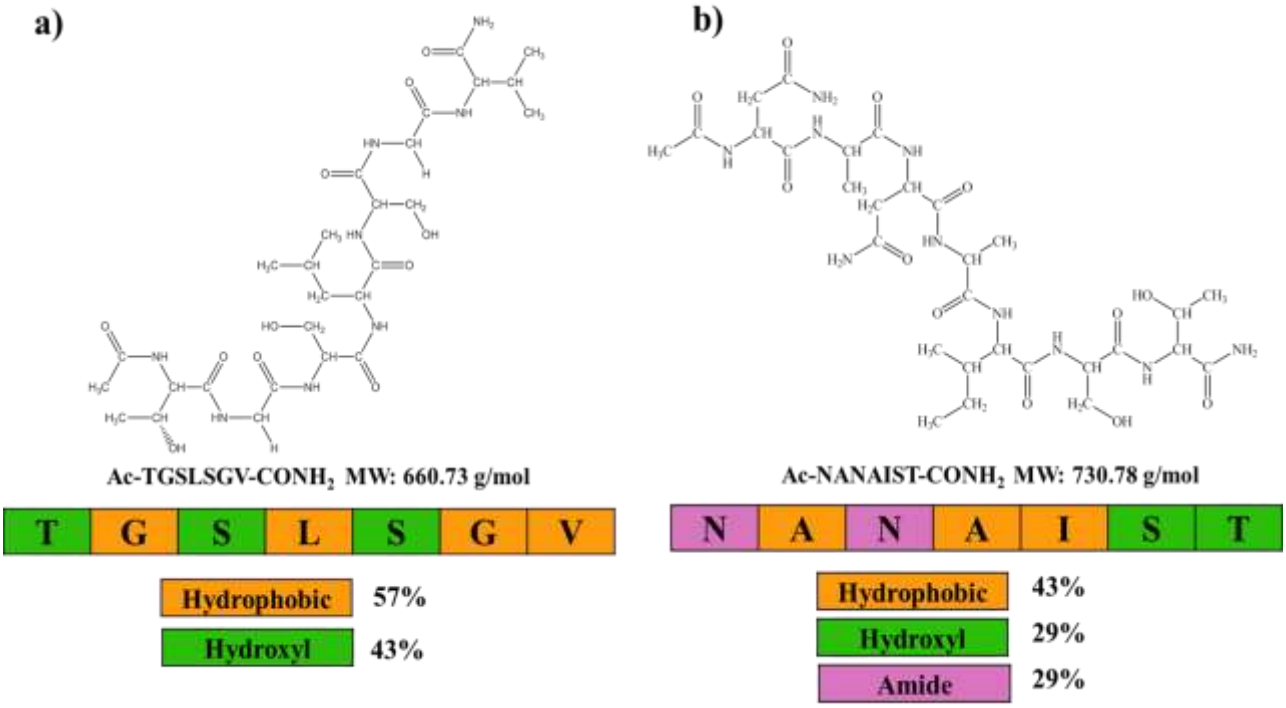

Figure 1.6 (a) Peptide Ac-TGSGLSV-$CONH_2$ selected as a capping agent through biopanning to make palladium nano-cubes. (b) Peptide Ac-NANAIST-$CONH_2$ selected as a capping agent through biopanning to make palladium nano-octahedra.

1.2.1 Palladium Nanoparticle Synthesis with Peptides from Biopanning

Peptides were used separately as capping agents in a typical nanoparticle synthesis as follows: 1.25 mM of L-ascorbic acid ($C_6H_8O_6$, Sigma) was placed in an aqueous solution with a total reaction volume of 5 mL at room temperature. A stock solution of peptide at 4 mg/mL was placed in the reaction solution with a final concentration of 0.01 mM - 0.5 mM peptide. Sodium borohydride ($NaBH_4$, Sigma) was injected into the solution at a final concentration of 0.02 mM $NaBH_4$ immediately followed by a final concentration of 2.5 mM chloropalladic (II) acid (H_2PdCl_4, Sigma). The injection of the palladium precursor was considered the initial reaction time. The control reaction was performed identically except for the injection of peptide, producing cuboctahedra nanoparticles around 20 nm in diameter, the most thermodynamically favored shape for fcc metals.[17-19] The sodium borohydride was injected to provide a burst of nucleation of palladium,[20] however it decomposes quickly in water.[21] Ascorbic acid was added to the reaction solutions to provide a slow reducing agent for the monomer-attachment growth of palladium atoms onto higher-energy facets of which the peptides show little to no binding.[6] Additionally, the ascorbic acid helped to stabilize the initial nucleation of palladium. Without ascorbic acid in solution, palladium was uncontrollably reduced by sodium borohydride and did produce well dispersed palladium nuclei. Although this mechanism is not well understood in literature, the addition of ascorbic acid was added to the control reaction and cuboctahedra were still produced indicating it did not interfere with the recognition properties of surfactants.[6,22]

Cuboctahedra seeds were produced at the initial reaction stage (at about t= 10 sec), suggesting that nucleation did not produce the resultant shape difference. Differentiation of the nanocrystals occurred after the burst of nucleation during monomer attachment with the aid of the peptide between 1 min and 1 hour. Solution samples were taken at various times after the

start of the reaction (2, 5, 10, 30 minutes and 1, 2, 5, and 10 hours) and after one hour, the nanoparticles did not change morphology or size and was then set as the final reaction time. Sizes of palladium nanocrystals were on the order of about 20 nm and only insignificant differences in size were seen within the optimal range of peptide added. Concentrations of surfactants were slightly tuned to achieve the optimal concentration for the most pristine nanocrystal shape. However, it is important to note that the difference in concentration of any one peptide did not lead to the formation of any other shape of nanocrystal other than that which it initially made. Concentrations of peptides were relatively similar indicating growth kinetics were equivalent. Because the size of nanoparticles remained at about 20 nm regardless of the presence or relative concentration of capping agent, this project focused only nanocrystal shape. Additionally, nanoparticles with twinned structures or branched/pod-like structures typically grow through different growth models,[22-27] so only single crystal nanoparticles were compared here to control cuboctahedra nanoparticles. Cuboctahedra are the most thermodynamically favored shape for fcc metals, including palladium, therefore any other shape formed was attributed to the added peptides in solution.

Nanoparticle samples were prepared with carbon substrates on copper mesh grids with 20 μL aliquots of reaction solution at various times. Transmission electron microscopy (TEM) images were imaged on a Phillips CM120 with a 120 keV operation voltage and high-resolution transmission electron microscopy (HRTEM) images were imaged on a FEI TITAN with a 300 keV operation voltage. Average frequencies of faceted particles were performed on ~100 single crystal particles per sample. Lattice spacing and facet confirmation were performed on HRTEM. Scanning electron microscopy (SEM), atomic force microscopy (AFM), and X-ray photoelectron spectroscopy (XPS) were performed on various biopanning substrates before and after

experimentation to confirm pristine conditions. Spartan ’10 was used to simulate electrostatic potential 3D mapping of peptides and HOMO/LUMO levels.

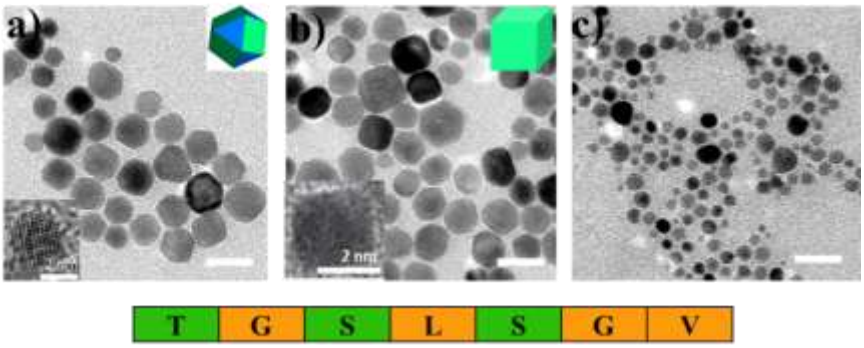

Figure 1.7 (a) TEM image of palladium nanoparticles in a control reaction. (b) TEM image of palladium nano-cubes with 0.12 mM TGSLSGV. (c) TEM image of palladium nanoparticles with 0.23 mM TGSLSGV. Scale bars 20 nm unless otherwise stated.

Cubic nanoparticles were produced with the peptide TGSLSGV demonstrating that biopanning worked successfully for finding (100) selective peptides. If biopanning had not worked to select peptides for Pd (100) surfaces, other shapes may have been formed. Additionally, if biopanning had not worked to find strongly binding peptides to palladium in general, the nanoparticles would have maintained the thermodynamically stable cuboctahedra shape as in the control reaction. Too much peptide induced small, non-faceted nanoparticles. This proved that the peptide did form strong bonds with palladium. In general, when too much capping agent is involved in a nanoparticle reaction, many nuclei form in the burst of nucleation phase and then capped heavily preventing growth. If the peptide was not considered a capping agent for the metal, it would have not disrupted the nanoparticles’ growth to such an extent.

Peptide TGSLSGV contained 57 % hydroxyl groups in its chain which was a large increase of hydroxyl groups compared to the phage display library of 24 % hydroxyl groups. This is consistent with other reports of hydroxyl groups binding well to noble metal surfaces.[10,11]

Also interestingly, the peptide TGSLSGV has a similar motif to an amino acid chain previously found to successfully cap the (100) surfaces of platinum nanocubes in our group, TLTTLTN (Ac-Thr-Leu-Thr-Thr-Leu-Thr-Asn-$CONH_2$, molecular weight: 803.92 g/mol).[6] Platinum and palladium share many similarities such as lattice constant, electronegativity, etc. and this provides further evidence that this peptide was correctly chosen for binding to the (100) surface of palladium.

Peptide NANAIST produced (111) palladium nano-octahedra and nano-tetrahedra when used as a capping agent for palladium nanoparticle synthesis. This peptide also had a higher hydroxyl/amide group ratio compared to that of the phage display library and similarly expressed an amino acid motif to that of a previous study in our group, SSFPQPN (Ac-Ser-Ser-Phe-Pro-Gln-Pro-Asn-$CONH_2$, molecular weight: 816.88 g/mol), which was found to induce Pt (111) surfaces.[6] The results with NANAIST also demonstrate the power of biopanning. Additionally, this peptide's composition and strong effect on palladium supports the claim that amide groups may preferentially bind to noble metal (111) surfaces whereas hydroxyl groups bind less selectively to both the (100) and (111) noble metal surfaces.

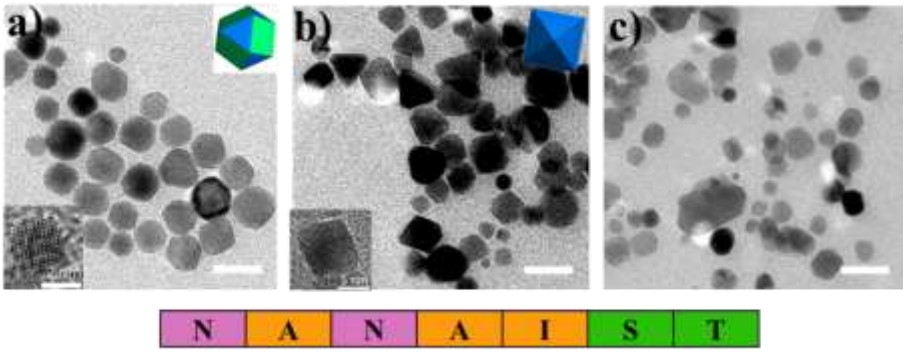

Figure 1.8 (a) TEM image of control palladium nanoparticles. (b) TEM image of palladium nano-octahedra/tetrahedra with 0.05 mM NANAIST. (c) TEM image of palladium nanoparticles with 0.09 mM NANAIST. Scale bars 20 nm unless otherwise stated.

Peptides TGSLSGV and NANAIST contained functional groups that were shown to bind strongly to noble metal surfaces in other reports. However, NANAIST had a higher binding strength to palladium than TGSLSGV because it took less peptide to fully cover all surfaces of Pd and create non-faceted spherical nanoparticles. This shows the addition of the amide group may play a crucial role in binding strongly to noble metal surfaces. All of the data involving palladium nanoparticle synthesis with peptides shows the efficacy of biopanning and provided us with new selective capping agents that work well in ambient condition nanoparticle synthesis.

1.3 Biopanning with Titania

Titania is a large band gap semiconductor required in its nano-crystalline form for many applications including pollutant degradation, photocatalysis, photovoltaics, and more.[28-30] The most common way of synthesizing crystalline titania in solution-phase synthesis is through an acid/base catalyzed sol-gel synthesis followed by calcination. Typically titanium alkoxide or titanium butoxide is used as starting material and 3D amorphous networks of titania are produced followed by calcination converting it to single crystal material. There is a driving force in the field to produce single crystal TiO_2 at ambient conditions in one step.

At the start of this project, there were limited reports on peptides used for semiconductor nanoparticle synthesis.[1,8,31] Most reports used genetically engineered M13 phages themselves in synthesis, however the reaction mechanisms and kinetics are vastly different from using pure peptides in reaction and tended to be used for 3D solution-phase ordering of nanoparticles rather than shape control.[5,32-34] Once selected, peptides are easier capping agents to use than phages themselves and can be better models for understanding the role between capping agent and substrate.

Biopanning for titania was performed similarly to that of palladium nanoparticle biopanning except for the type of substrate used. Single crystals of rutile (110) and (100) were bought cut and polished into 1 cm X 1 cm X 0.5 mm pieces (MTI Corporation) and used as substrates for biopanning. They were cleaned by washing five times with acetone, ethanol and water before use. Figure 1.9 is an Atomic Force Microscope (AFM) image of a clean rutile (100) single crystal ready for biopanning.

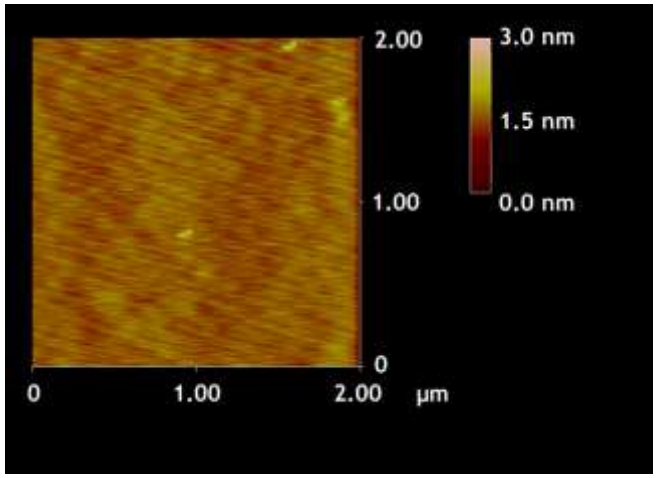

Figure 1.9 An Atomic Force Microscope (AFM) image of a rutile (100) single crystal used for biopanning.

Biopanning was performed on rutile (110) and (100) separately with a pH. D.-12 library (phage display library engineered to display 12 amino acid peptides on the pIII protein of the M13 bacteriophage (New England BioLabs, 2E9 phages/µL)). Peptide FHKSTSWHLAEL (Ac-Phe-His-Lys-Ser-Thr-Ser-Trp-His-Leu-Ala-Glu-Leu-$CONH_2$, molecular weight: 1496.69 g/mol) was found through biopanning with rutile (110) and peptide SSSTGPKKVSLP (Ac-Ser-Ser-Ser-Thr-Gly-Pro-Lys-Lys-Val-Ser-Leu-Pro-$CONH_2$, molecular weight: 1228.41 g/mol) was found through biopanning with rutile (100). The basic properties for these peptides are detailed in Figure 1.10 and 1.11 respectively. Figure 1.11 also includes LCMS (b) and HPLC (c) data to show how peptides are purified and tested for purity after synthesis.

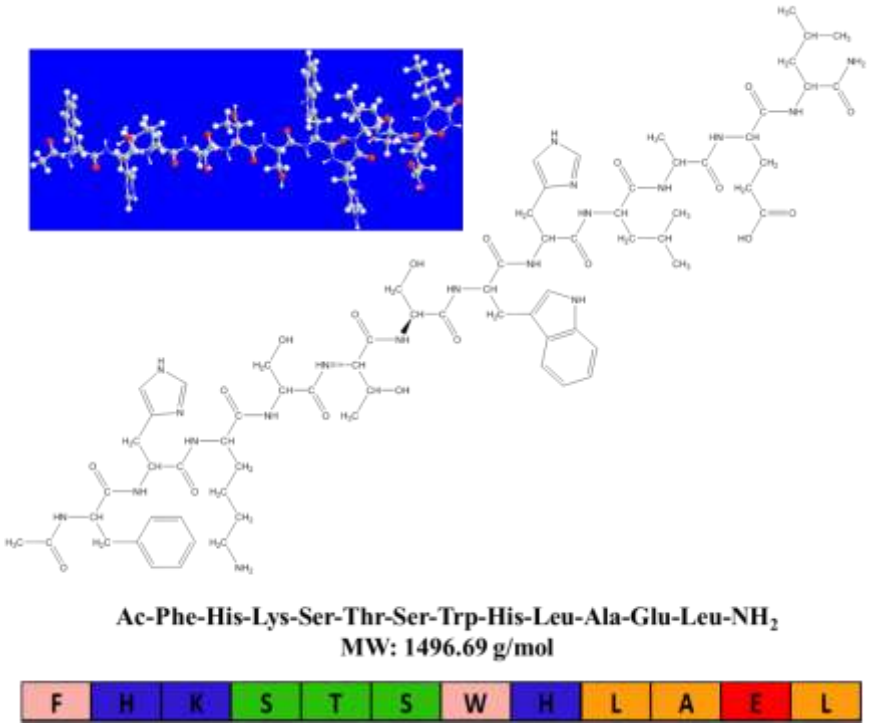

Figure 1.10 Peptide FHKSTSWHLAEL.

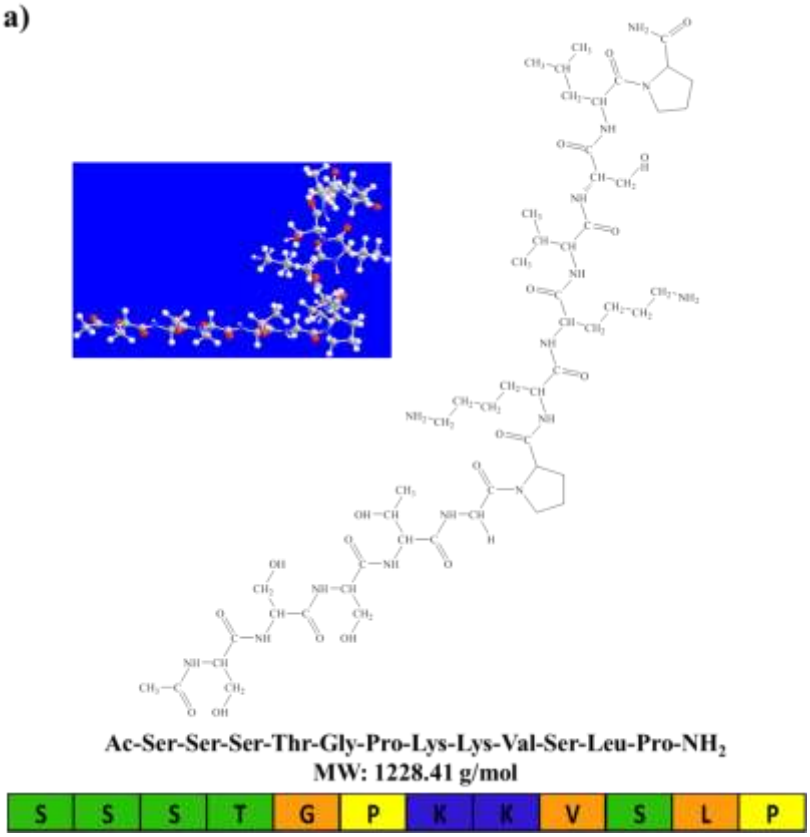

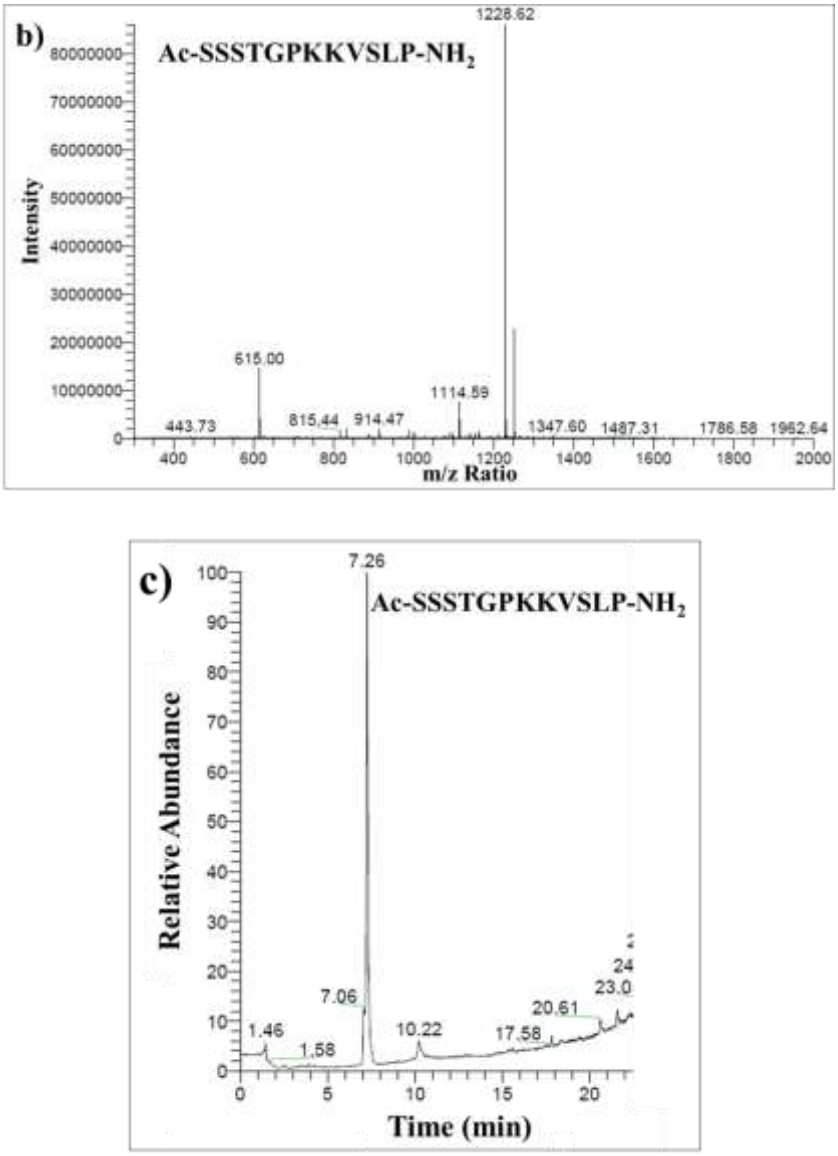

Figure 1.11 (a) Peptide SSSTGPKKVSLP (b) LCMS data for peptide SSSTGPKKVSLP indicating peptide was synthesized. (c) HPLC data for peptide SSSTGPKKVSLP indicating peptide was purified.

The biopanning results for titania were very interesting. Literature reports repeating units of the amino acids lysine,[35,36] histidine,[37] arginine,[36,38] proline,[39] and serine[40] are involved in biomineralization producing silica in organisms such as sponges, grasses and other biological systems, and that these amino acids have also been used in vitro to make silica at room

temperature and neutral pH. These results have been confirmed with arginine, lysine, and histidine for titania as well.[31] Titania and silica are both usually made through a sol-gel approach and share many other compositional similarities, therefore the ways that have proven to make silica in solution can be rationally applied to titania.

Our results also showed that serine, proline, histidine, and lysine all preferentially bound to titania in biopanning. Serine had 33 % presence in the SSSTGPKKVSLP peptide compared to the 24 % presence in the phage display library. More interestingly, most of the serine in this peptide appeared together in series in the peptide; a conformation that has shown to produce silica in nature.[40] Serine only occurred twice in the peptide FHKSTSWHLAEL, yet both serines appeared very close to each other. Histidine and lysine occurred in both peptides selected for titania in higher ratios than what was present in the phage display library, and in higher amounts than have been seen in any other phage display selection in our group for noble metal substrates. Histidine and lysine are both positively charged amino acids, whereas titania has a slightly negative surface.[41] Histidine and lysine binding favorably to a slightly negative titania surface supports the concept that electronegativity of functional groups plays a large role in favorable binding to the substrate. Additionally, two amino acids with ring groups, phenylalanine and tryptophan, appeared in this selection, which are not common in the phage display library and have not been shown previously in literature to bind favorably to titania. Ring groups (including proline) in peptides alter the peptide conformation dramatically from its linear structure and may play an additional factor in binding to substrates.

1.3.1 Titania Nanoparticle Synthesis with Peptides from Biopanning

In a typical reaction synthesis using purified peptides, a final concentration of 100 mM dihydroxybis(ammonium lactate)titanium (IV) ("TiBALDH," 50 % w/v, Alfa Aesar) was mixed into equal volume of peptides with final concentrations of 1 - 10 mM peptide. TiBALDH was used as a starting material because hydroxyl-based titanium precursors tend to hydrolyze easily and quickly in water uncontrollably. Here, nanoparticle synthesis was better controlled with a starting material system that did not form titania in the presence of water. No additional chemicals were required to form TiO_2; the peptides themselves formed TiO_2. The TiBALDH stock solution was tested by ultra violet-visible spectroscopy (UV-Vis) to confirm that no TiO_2 existed in aqueous solution before the reaction with peptides. Additionally, non-binding peptides were also tested in similar reactions and did not form any titania in solution.

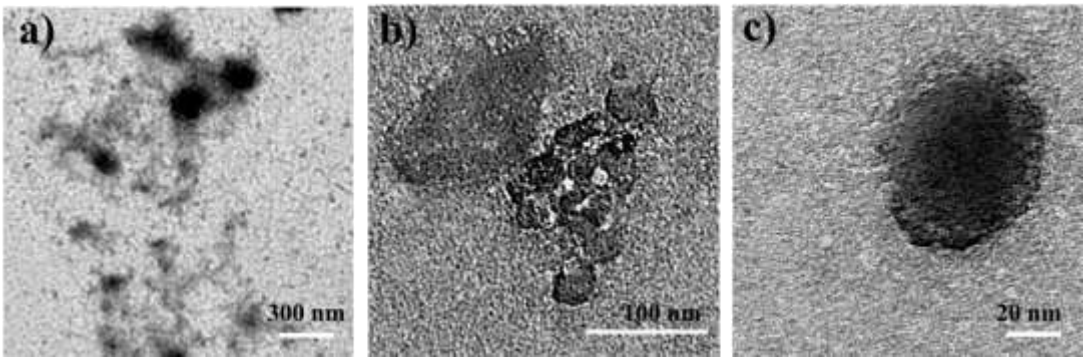

Figure 1.11 (a) Low resolution TEM image of TiO_2 made with 4.1 mM SSSTGPKKVSLP. (b and c) Higher magnification TEM image of TiO_2 made with 4.1 mM SSSTGPKKVSLP.

Peptide SSSTGPKKVSLP produced amorphous nanoparticles with random shapes. Some of the titania formed was spherical and less than 50 nm (Figure 1.11c), whereas some titania was made up of larger networks of connected spherical like titania (Figure 1.11a and b). There were not any apparent crystalline forms of titania formed from this peptide; however it induced the formation of titania which shows its strength to binding to titanium-based compounds. If the

peptides were not strong binding, no titania formation would have occurred as in the case with other non-selected peptides. Smaller spherical titania nanoparticles with diameters less than 100 nm were produced (Figure 1.11c) indicating the peptide acted as a good capping agent; in the presence of a catalyst without a capping agent, titania forms large (micron scale) amorphous networks of titania. Although no apparent crystalline titania formed in solution, the peptide produced titania in solution as well as prevented large titania networks from forming in solution, showing the value of biopanning and the unique binding capabilities of this peptide to titania.

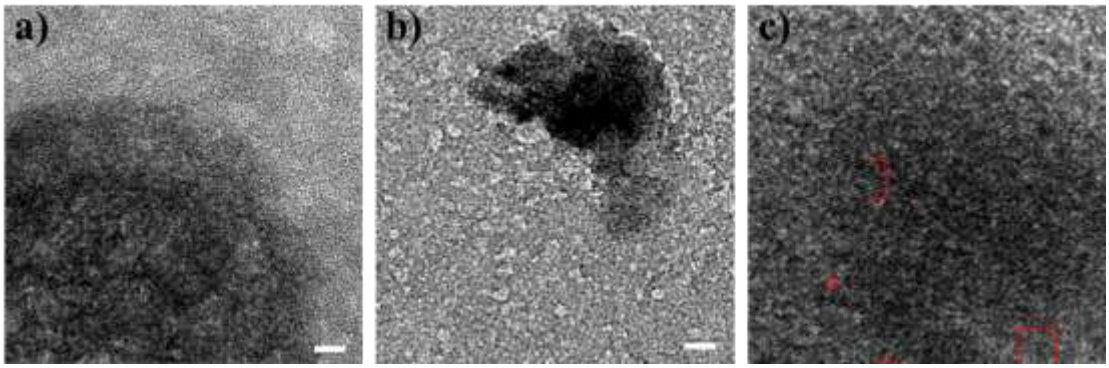

Figure 1.12 (a and b) TEM image of TiO_2 made with 1.3 mM FHKSTSWHLAEL. (c) Magnified TEM image of TiO_2 made with 1.3 mM FHKSTSWHLAEL showing anatase and monoclinic TiO_2 phases. Scale bars 10 nm.

Peptide FHKSTSWHLAEL also initiated titania formation and prevented large 3D networks of titania from forming in solution. As with peptide SSSTGPKKVSLP, there was a range of sizes and shapes of titania formed, however the solutions mainly consisted of spheres/networks of connected spheres with each sphere less than ~100 nm. Additionally, portions of the titania produced from this peptide were composed of crystalline lattice spacings of 3.54 Å, corresponding to anatase and monoclinic β–TiO_2[41] (Figure 1.12c). Both of these peptides represented promising data regarding the formation of single crystal titania nanoparticles at ambient conditions as they were able to induce titania in solution, prevented

large (micron) scale titania from forming, and created portions of crystalline titania in the case of peptide FHKSTSWHLAEL.

The differences of these peptides compared to noble metal selections helps to prove the effectiveness of the selection process for each unique substrate used in biopanning. The amino acids serine, proline, lysine, and histidine were found to bind strongly to titania, which is consistent with literature reports on the types of amino acids which bind strongly to semi-conductor surfaces, namely silica and titania. Histidine and lysine support claims that electronegativity of functional groups plays a large role in favorable binding to substrates as capping agents, whereas proline, tryptophan, and phenylalanine provide evidence that the unique formation of capping agents is an important factor for favorable binding. Lastly, tryptophan and phenylalanine are especially unique to this work and may help to provide insight into new amino acids that bind to titania favorably and induce crystalline titania at ambient conditions.

The power of nanoparticle synthesis with peptide capping agents is shown in Figure 1.13. Platinum (Pt) nano-spheres were produced with sodium borohydride and peptide TSHVSLY (molecular weight: 846.95 g/mol) from an evolved peptide, TLHVSSY, selected through biopanning with platinum reported previously in our group.[42] The nanoparticles were then washed and re-dispersed into an aqueous solution. Titania nanoparticles were synthesized in parallel with both peptides SSSTGPKKVSLP and FHKSTSWHLAEL separately based on the protocol listed above, followed by washing and re-dispersing in water. The two solutions were mixed together, washed and re-dispersed in water.

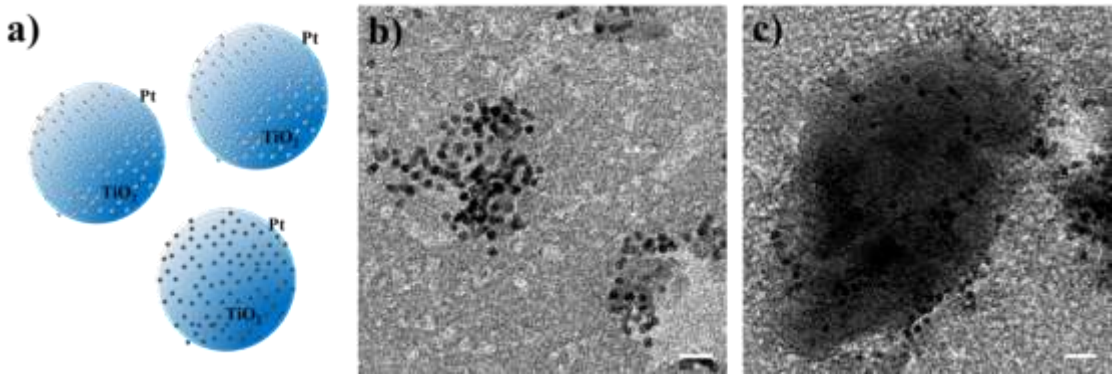

Figure 1.13 (a) Model of the TiO_2/Pt heterocatalyst system. (b) TEM image of a TiO_2/Pt heterocatalyst system with TiO_2 made from SSSTGPKKVSLP. (c) TEM image of a TiO_2/Pt heterocatalyst system with TiO_2 made from FHKSTSWHLAEL. Scale bars are 10 nm.

Figure 1.13 shows TEM images of platinum successfully adsorbed onto titania creating nano-heterostructures of platinum and titania. This system provides evidence that peptide capping agents do not prevent binding to other materials, as is the case with larger, organic capping agents. Standard handling/preparing of nanoparticles including washing with ethanol/acetone, sonicating, and centrifuging, did not disrupt the heterostructures. This system is a promising candidate in the heterocatalyst field, especially for water-splitting reactions as platinum nanoparticles on titania creates a Schottky barrier at their interface, trapping electrons produced by UV/visible light in titania, preventing recombination, and improving quantum efficiency.[43,44]

1.4 Discussion on Biopanning for Nanoparticle Synthesis

Our group has shown that peptides can be used as capping agents to regulate noble metal and semiconductor growth kinetics and control the resulting nanoparticle morphology. These results provide insight to the motifs that preferentially bind to palladium and titania and offer the opportunity to study the organic-inorganic interface further. For example, the binding strength of hydroxyl and amine groups to palladium are not simple strongly binding functional groups, they

bind depending on their relative position in the peptide and the way the peptide conforms in solution relative to the surface atomic spacing of palladium.[45] Additionally, peptides may change conformation upon substrate interactions and play a role in morphology control.[46] Peptides are versatile, dynamic capping agents that can be chemically modified to further exploit their binding to materials. Ultimately, peptide selection guides us towards judiciously determining capping agents instead of empirically choosing them through trial and error. Furthermore, peptides selected through biopanning provide capping agents capable of morphology control and forming single crystal materials at ambient conditions in aqueous solutions providing a green approach to single crystal nanoparticle synthesis.

1.5 References

1 Whaley, S. R., English, D. S., Hu, E. L., Barbara, P. F. & Belcher, A. M. Selection of peptides with semiconductor binding specificity for directed nanocrystal assembly. *Nature* **405**, 665-668 (2000).

2 Seker, U. O. S. *et al.* Adsorption Behavior of Linear and Cyclic Genetically Engineered Platinum Binding Peptides. *Langmuir* **23**, 7895-7900, doi:10.1021/la700446g (2007).

3 Sarikaya, M., Tamerler, C., Jen, A. K. Y., Schulten, K. & Baneyx, F. Molecular biomimetics: nanotechnology through biology. *Nat Mater* **2**, 577-585 (2003).

4 Sidhu, S. S. Engineering M13 for phage display. *Biomolecular Engineering* **18**, 57-63, doi:http://dx.doi.org/10.1016/S1389-0344(01)00087-9 (2001).

5 Mao, C. *et al.* Virus-Based Toolkit for the Directed Synthesis of Magnetic and Semiconducting Nanowires. *Science* **303**, 213-217, doi:10.1126/science.1092740 (2004).

6 Chiu, C.-Y. Platinum nanocrystals selectively shaped using facet-specific peptide sequences. *Nature Chemistry* **3**, 393-399, doi:10.1038/nchem.1025 (2011).

7 Fukunaga, K. & Taki, M. Practical Tips for Construction of Custom Peptide Libraries and Affinity Selection by Using Commercially Available Phage Display Cloning Systems. *Journal of Nucleic Acids* **2012**, 9, doi:10.1155/2012/295719 (2012).

8 Dickerson, M. B., Sandhage, K. H. & Naik, R. R. Protein- and Peptide-Directed Syntheses of Inorganic Materials. *Chemical Reviews* **108**, 4935-4978, doi:10.1021/cr8002328 (2008).

9 Merzlyak, A. & Lee, S.-W. Engineering Phage Materials with Desired Peptide Display: Rational Design Sustained through Natural Selection. *Bioconjugate Chemistry* **20**, 2300-2310, doi:10.1021/bc900303f (2009).

10 Naik, R. R., Stringer, S. J., Agarwal, G., Jones, S. E. & Stone, M. O. Biomimetic synthesis and patterning of silver nanoparticles. *Nat Mater* **1**, 169-172, doi:http://www.nature.com/nmat/journal/v1/n3/suppinfo/nmat758_S1.html (2002).

11 Slocik, J. M. & Naik, R. R. Probing peptide-nanomaterial interactions. *Chem. Soc. Rev.* **39**, 3454-3463, doi:10.1039/B918035B (2010).

12 Jin, M. *et al.* Synthesis of Pd nanocrystals enclosed by {100} facets and with sizes <10 nm for application in CO oxidation. *Nano Res.* **4**, 83-91, doi:10.1007/s12274-010-0051-3 (2011).

13 Aliaga, C. *et al.* Sum Frequency Generation and Catalytic Reaction Studies of the Removal of Organic Capping Agents from Pt Nanoparticles by UV−Ozone Treatment. *J Phys Chem C* **113**, 6150-6155, doi:10.1021/jp8108946 (2009).

14 Choi, S.-H. *et al.* Preparation of Polymer-stabilized Palladium–silver Bimetallic Nanoparticles by γ-irradiation and their Catalytic Properties for Hydrogenation of cis,cis-1,3-Cyclooctadiene. *Catal Lett* **105**, 59-65, doi:10.1007/s10562-005-8006-0 (2005).

15 Ding, H. *et al.* Synthesis of monodisperse palladium nanocubes and their catalytic activity for methanol electrooxidation. *Chinese Physics B* **19**, 106104 (2010).

16 Gabasch, H. *et al.* In situ XPS study of Pd(1 1 1) oxidation at elevated pressure, Part 2: Palladium oxidation in the 10−1 mbar range. *Surface Science* **600**, 2980-2989, doi:http://dx.doi.org/10.1016/j.susc.2006.05.029 (2006).

17 Yin, Y. A., P. Colloidal Nanocrystal Synthesis and the Organic–Inorganic Interface. *Nature* **437**, 664-670, doi:10.1038/nature04165 (2005).

18 Xia, Y., Xiong, Y., Lim, B. & Skrabalak, S. E. Shape-Controlled Synthesis of Metal Nanocrystals: Simple Chemistry Meets Complex Physics? *Ang. Chem. Int. Ed.* **48**, 60-103, doi:10.1002/anie.200802248 (2009).

19 Tao, A. R., Habas, S. & Yang, P. Shape Control of Colloidal Metal Nanocrystals. *Small* **4**, 310-325, doi:10.1002/smll.200701295 (2008).

20 Sun, S. & Murray, C. B. Synthesis of monodisperse cobalt nanocrystals and their assembly into magnetic superlattices (invited). *Journal of Applied Physics* **85**, 4325-4330, doi:doi:http://dx.doi.org/10.1063/1.370357 (1999).

21 Lee, H. *et al.* Morphological Control of Catalytically Active Platinum Nanocrystals. *Angewandte Chemie* **118**, 7988-7992, doi:10.1002/ange.200603068 (2006).

22 Li, D. *et al.* Direction-Specific Interactions Control Crystal Growth by Oriented Attachment. *Science* **336**, 1014-1018, doi:10.1126/science.1219643 (2012).

23 Liao, H.-G., Cui, L., Whitelam, S. & Zheng, H. Real-Time Imaging of Pt3Fe Nanorod Growth in Solution. *Science* **336**, 1011-1014, doi:10.1126/science.1219185 (2012).

24 Yuk, J. M. *et al.* High-Resolution EM of Colloidal Nanocrystal Growth Using Graphene Liquid Cells. *Science* **336**, 61-64, doi:10.1126/science.1217654 (2012).

25 Langille, M. R., Zhang, J., Personick, M. L., Li, S. & Mirkin, C. A. Stepwise Evolution of Spherical Seeds into 20-Fold Twinned Icosahedra. *Science* **337**, 954-957, doi:10.1126/science.1225653 (2012).

26 Meng, F. & Jin, S. The Solution Growth of Copper Nanowires and Nanotubes is Driven by Screw Dislocations. *Nano. Lett.* **12**, 234-239, doi:10.1021/nl203385u (2011).

27 Zhu, Y. T. *et al.* Formation of single and multiple deformation twins in nanocrystalline fcc metals. *Acta Materialia* **57**, 3763-3770, doi:http://dx.doi.org/10.1016/j.actamat.2009.04.020 (2009).

28 Linsebigler, A. L., Lu, G. & Yates, J. T. Photocatalysis on TiO2 Surfaces: Principles, Mechanisms, and Selected Results. *Chemical Reviews* **95**, 735-758, doi:10.1021/cr00035a013 (1995).

29 Ni, M., Leung, M. K. H., Leung, D. Y. C. & Sumathy, K. A review and recent developments in photocatalytic water-splitting using for hydrogen production. *Renewable and Sustainable Energy Reviews* **11**, 401-425, doi:http://dx.doi.org/10.1016/j.rser.2005.01.009 (2007).

30 Ashokkumar, M. An overview on semiconductor particulate systems for photoproduction of hydrogen. *International Journal of Hydrogen Energy* **23**, 427-438, doi:http://dx.doi.org/10.1016/S0360-3199(97)00103-1 (1998).

31 Dickerson, M. B. *et al.* Identification and Design of Peptides for the Rapid, High-Yield Formation of Nanoparticulate TiO2 from Aqueous Solutions at Room Temperature. *Chem. Mat.* **20**, 1578-1584, doi:10.1021/cm071515t (2008).

32 Huang, Y. *et al.* Programmable Assembly of Nanoarchitectures Using Genetically Engineered Viruses. *Nano. Lett.* **5**, 1429-1434, doi:10.1021/nl050795d (2005).

33 Lee, S.-W., Mao, C., Flynn, C. E. & Belcher, A. M. Ordering of Quantum Dots Using Genetically Engineered Viruses. *Science* **296**, 892-895, doi:10.1126/science.1068054 (2002).

34 Reiss, B. D. *et al.* Biological Routes to Metal Alloy Ferromagnetic Nanostructures. *Nano. Lett.* **4**, 1127-1132, doi:10.1021/nl049825n (2004).

35 Patwardhan, S., Mukherjee, N. & Clarson, S. The Use of Poly-L-Lysine to Form Novel Silica Morphologies and the Role of Polypeptides in Biosilicification. *Journal of Inorganic and Organometallic Polymers* **11**, 193-198, doi:10.1023/A:1015293712319 (2001).

36 Coradin, T., Durupthy, O. & Livage, J. Interactions of Amino-Containing Peptides with Sodium Silicate and Colloidal Silica: A Biomimetic Approach of Silicification. *Langmuir* **18**, 2331-2336, doi:10.1021/la011106q (2002).

37 Patwardhan, S. & Clarson, S. Silicification and Biosilicification. Part 6. Poly-L-Histidine Mediated Synthesis of Silica at Neutral pH. *Journal of Inorganic and Organometallic Polymers* **13**, 49-53, doi:10.1023/A:1022952931063 (2003).

38 Coradin, T., Roux, C. & Livage, J. Biomimetic self-activated formation of multi-scale porous silica in the presence of arginine-based surfactants. *J. Mat. Chem.* **12**, 1242-1244, doi:10.1039/B201616H (2002).

39 Coradin, T. & Livage, J. Effect of some amino acids and peptides on silicic acid polymerization. *Colloids and Surfaces B: Biointerfaces* **21**, 329-336, doi:http://dx.doi.org/10.1016/S0927-7765(01)00143-6 (2001).

40 Sudheendra, L. & Raju, A. R. Peptide-induced formation of silica from tetraethylorthosilicate at near-neutral pH. *Materials Research Bulletin* **37**, 151-159, doi:http://dx.doi.org/10.1016/S0025-5408(01)00807-8 (2002).

41 Zhu, J., Zhang, J., Chen, F. & Anpo, M. Preparation of high photocatalytic activity TiO2 with a bicrystalline phase containing anatase and TiO2 (B). *Mat. Lett.* **59**, 3378-3381, doi:http://dx.doi.org/10.1016/j.matlet.2005.05.072 (2005).

42 Li, Y., Whyburn, G. P. & Huang, Y. Specific Peptide Regulated Synthesis of Ultrasmall Platinum Nanocrystals. *J Am Chem Soc* **131**, 15998-15999, doi:10.1021/ja907235v (2009).

43 Wen, D., Guo, S., Wang, Y. & Dong, S. Bifunctional Nanocatalyst of Bimetallic Nanoparticle/TiO2 with Enhanced Performance in Electrochemical and Photoelectrochemical Applications. *Langmuir* **26**, 11401-11406, doi:10.1021/la100869r (2010).

44 Kowalska, E., Remita, H., Colbeau-Justin, C., Hupka, J. & Belloni, J. Modification of Titanium Dioxide with Platinum Ions and Clusters: Application in Photocatalysis. *J Phys Chem C* **112**, 1124-1131, doi:10.1021/jp077466p (2008).

45 Oren, E. E., Tamerler, C. & Sarikaya, M. Metal Recognition of Septapeptides via Polypod Molecular Architecture. *Nano. Lett.* **5**, 415-419, doi:10.1021/nl048425x (2005).

46 Heinz, H. *et al.* Nature of Molecular Interactions of Peptides with Gold, Palladium, and Pd−Au Bimetal Surfaces in Aqueous Solution. *J Am Chem Soc* **131**, 9704-9714, doi:10.1021/ja900531f (2009).

CHAPTER 2: PALLADIUM NANOPARTICLE SYNTHESIS WITH SMALL MOLECULES AS CAPPING AGENTS

2.1 Choosing Small Molecules as Capping Agents for Facet Specific Palladium Nanoparticle Synthesis

Palladium (Pd) and platinum (Pt) are the most catalytically-active metals for the oxygen reduction reaction in fuel cells.[1-4] Fuel cells are promising candidates for replacing combustion engines to help alleviate fossil fuel dependency and environmental issues from greenhouse gas emissions. Additionally, palladium and platinum are useful for other applications including heterogeneous organic catalysis and in electronics.[5] All of the applications for palladium and platinum benefit by having shape and size controlled nanoparticles.

The aim of this work included making morphology-controlled nanoparticles as well as studying the relationship of capping agent and inorganic surface. Capping agents such as PVP, CTAB, or even peptides, can induce various shapes of nanoparticles, however most capping agents are large macromolecules with complex confirmations in solution and can bind to surfaces in many ways, making it difficult to study the key interactions between capping agents and metal surfaces. On the other hand, small molecules cannot form complex shapes in solution and have limiting binding sites to the surface. Therefore their relationship with metal surface facets can be more directly studied. Understanding the inorganic-organic interactions between nanoparticles and capping agents is extremely important for being able to rationally select capping agents for nanoparticle synthesis.

Empirically choosing capping agents for nanoparticle synthesis is similar to finding a needle in a haystack due to virtually limitless combinations. Selecting peptides through a combinatorial approach, on the other hand, established particular binding motifs that induce faceted nanoparticles and gave insight to the types of interactions important for selective binding to metal surfaces.[6-9] The peptide selection work in our group and detailed in Chapter 1 lead our group to begin studying individual amino acids effects' on crystallographic surfaces, and eventually led us to judiciously choosing small molecules as capping agents in the work presented in this chapter.

In our group, Ruan[10] and colleagues mechanistically studied the effects of individual amino acids on inducing particular platinum crystallographic surfaces through density functional theory studies, Raman studies, and theories involving as energy interactions. The studies found that phenylalanine (Phe) was the major contributor to producing the (111) facet in platinum nano-octahedra and that the alternating sp^2 hybridized carbon atoms of the phenyl ring of phenylalanine lay flat on the Pt (111) surface. Density functional theory (DFT) studies also revealed that it is both the unfavorable binding energy in addition to favorable binding which directed preferred binding of amino acids to noble metal surfaces. After this was established, peptides could be turned into platinum (111) binding or non-binding capping agents simply by the addition or removal of phenylalanine anywhere in the peptide. Based on these results, it was hypothesized that benzene ring-based small molecules alone could alone induce (111) faceted nanocrystal growth of platinum. The following work by Chiu[11] found that small molecules with electronegative benzene rings and direct hydroxyl substituents such as hydroquinone, catechol, pyrogallol, and hydroxyquinol induced platinum (111) nano-tetrahedra.

I began working with small molecules with electropositive benzene rings in parallel of these studies to observe their effects on palladium nanoparticle synthesis. Platinum and palladium have similar electronic and physical properties such as Highest Occupied Molecular Orbital/Lowest Unoccupied Molecular Orbital (HOMO/LUMO) levels, lattice spacing, etc., so initial trends involving the organic-inorganic interface were applied to both systems. The results for rationally selected small molecules which induced the palladium (100) surface are shown below.

2.2 Electropositive Small Molecules for Palladium (100) Nanoparticle Synthesis

Small molecules were used separately as capping agents in a typical nanoparticle synthesis as follows: 1.25 mM of L-ascorbic acid ($C_6H_8O_6$, Sigma) was placed in an aqueous solution with a total reaction volume of 5 mL at room temperature. Stock small molecule solutions of 2 mg/mL were placed in the reaction solution with a final concentration of 0.2 mM – 1 mM small molecule to optimize nanoparticle shape. Sodium borohydride ($NaBH_4$, Sigma) was injected into the solution at a final concentration of 0.02 mM $NaBH_4$ immediately followed by a final concentration of 2.5 mM chloropalladic (II) acid (H_2PdCl_4, Sigma). The injection of the palladium precursor was considered the initial reaction time. The control reaction was performed identically except for the injection of small molecule, producing cuboctahedra nanoparticles around 20 nm in diameter, the most thermodynamically favored shape for fcc metals.[12-14] The sodium borohydride was injected to provide a burst of nucleation of palladium,[15] however it decomposes quickly in water.[16] Ascorbic acid was added to the reaction solutions to provide a slow reducing agent for the monomer-attachment growth of palladium atoms onto higher-energy facets of which the small molecules show little to no binding.[6] Additionally, the ascorbic acid helped to stabilize the initial nucleation of palladium. Without ascorbic acid in solution,

palladium was uncontrollably reduced by sodium borohydride and did produce well dispersed palladium nuclei. Although this mechanism is not well understood in literature, the addition of ascorbic acid was added to the control reaction and cuboctahedra were still produced indicating it did not interfere with the recognition properties of surfactants.[6,17]

Cuboctahedra seeds were produced at the initial reaction stage (at about t= 10 sec), suggesting that nucleation did not produce the resultant shape difference. Differentiation of the nanocrystals occurred after the burst of nucleation during monomer attachment with the aid of the ligand between 1 min and 1 hour. Solution samples were taken at various times after the start of the reaction (2, 5, 10, 30 minutes and 1, 2, 5, and 10 hours) and after one hour, the nanoparticles did not change morphology or size and was then set as the final reaction time. Sizes of palladium nanocrystals were on the order of about 20 nm and only insignificant differences in size were seen within the optimal range of small molecule added. Concentrations of surfactants were slightly tuned to achieve the optimal concentration for the most pristine nanocrystal shape. However, it is important to note that the difference in concentration of any one small molecule did not lead to the formation of any other shape of nanocrystal other than that which it initially made. Concentrations of small molecules were relatively similar indicating growth kinetics were equivalent. Because the size of nanoparticles remained at about 20 nm regardless of the presence or relative concentration of capping agent, this project focused only nanocrystal shape. Additionally, nanoparticles with twinned structures or branched/pod-like structures typically grow through different growth models,[17-22] so only single crystal nanoparticles were compared here to control cuboctahedra nanoparticles. Cuboctahedra are the most thermodynamically favored shape for fcc metals, including palladium, therefore any other shape formed was attributed to the added small molecules in solution.

Nanoparticle samples were prepared with carbon substrates on copper mesh grids with 20 μL aliquots of reaction solution at various times. Transmission electron microscopy (TEM) images were imaged on a Phillips CM120 with a 120 keV operation voltage and high-resolution transmission electron microscopy (HRTEM) images were imaged on a FEI TITAN with a 300 keV operation voltage. Average frequencies of faceted particles were performed on ~100 single crystal particles per sample. Lattice spacing and facet confirmation were performed on HRTEM. Spartan '10 was used to simulate electrostatic potential 3D mapping and HOMO/LUMO levels of small molecules. Material Studio was used to provide epitaxial matching of small molecules to palladium (100) and (111) surfaces.

3-hydroxy-2-phenylpropanoic acid (tropic acid), 2-hydroxy-2-phenylacetic acid (mandelic acid), phenylmethanol (benzyl alcohol), and 2-bromobenzoic acid were small molecules rationally selected with electro-neutral to electropositive benzene rings that successfully induced palladium (100) nano-cubes. The results are shown in Figure 2.1.

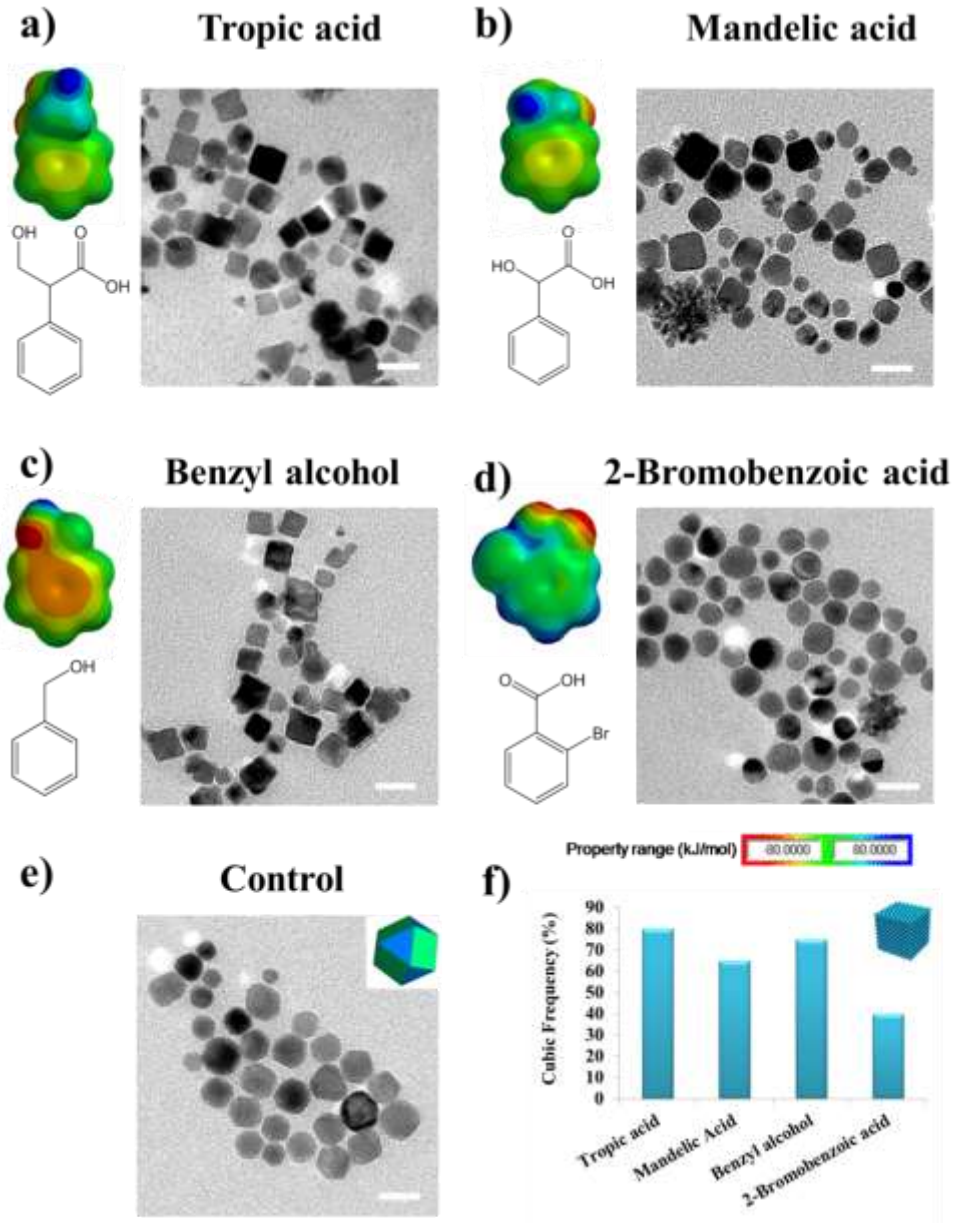

Figure 2.1 (a-d) Electrostatic potential maps and chemical structures of capping agents as well as TEM images of palladium nano-cubes with capping agents: a) 0.29 mM tropic acid b) 0.32 mM mandelic acid c) 1.0 mM benzyl alcohol and d) 0.24 mM 2-bromobenzoic acid. Scale bars of TEM images are 20 nm. (e) TEM image of control reaction palladium nano-cuboctahedra. (f) Cubic frequency plot of small molecules (a-d).

Overall, the relative concentrations of small molecules in solution to induce palladium nano-cubes were very similar indicating identical growth kinetics. Additionally, similar

concentrations of small molecules yielded palladium nano-cubes that were close to 20 nm in edge length. All four small molecules produced nano-cubes, however the completeness of the (100) surfaces creating sharp cubes relative to the type of small molecule varied. For example, tropic acid and mandelic acid only differ by one extra carbon in the substituent side group and induced similar percentages of cubes relative to the control, yet tropic acid made much more complete cubes than mandelic acid.

Also interestingly, 2-bromobenzoic acid induced very poorly formed palladium (100) nano-cubes. The percent frequency of cubes produced was low because it was often hard to detect nano-cubes from sphere-like nanoparticles; however the nanoparticles looked different from the control cuboctahedra nanocrystals indicating the small molecule did successfully interact with palladium. Literature reports that bromide ions bind very strongly to noble metal (100) surfaces.[23,24] However, as will be described below, epitaxial binding of the aryl substituents are assumed to play a major role in the outcome of the binding to the metal surface. There may have been competition between the bromine substituent of the small molecule with the carboxylic acid substituent, lessening the overall effect of the small molecule on the (100) surface.

The fundamental reasoning of why these small molecules induced palladium nano-cubes must be explained in terms of several factors. First it is important to understand the binding of capping agents and inorganic surfaces in terms of the HOMO levels of small molecules relative to palladium's d orbital levels. It is understood that a benzene ring laying flat on the surface of a noble metal can form metal-carbon bonds with electron donation from the pi orbitals of benzene to the d_z^2 and d_{yz} orbitals of the metal surface as well as back-donation from the metal to the pi^*

orbitals of the benzene.[10,25-27] The ability of a favorable interaction of the small molecule to the metal surface depends on how much the benzene ring can donate to the metal through its HOMOs and how well the metal can be an electron acceptor.[28] In order for this type of binding to occur, the HOMO level of the small molecule must be less negative than the metal's d orbital level. Our group showed that if the benzene ring is especially electronegative, for example from the addition of direct hydroxyl group substituents, the ring will have a higher HOMO level and thus increased pi electron donation to the metal atoms on the surface.[11] Additionally, a metal surface with a higher work function would be a more effective electron acceptor.

The HOMO levels of tropic acid, mandelic acid, benzyl alcohol, and 2-bromobenzoic acid are -6.73 eV, -6.90 eV, -6.39 eV, and -7.34 eV, respectively. Small molecules with electronegative benzene rings which induced platinum (111) nanocrystals reported in Chiu's work such as hydroquinone, catechol, pyrogallol, and hydroxyquinol had HOMO levels of -5.4 eV, -5.6 eV, -5.6 eV, and -5.2 eV, respectively. The HOMO levels of the electropositive small molecules were much more negative than the HOMO levels of electronegative small molecules, reinforcing the fact that the electropositive small molecules would be poor electron donators to the noble metal's d orbitals. This information leads to one reason the electropositive small molecules mentioned here did not induce palladium (111) nanocrystals. Additionally, the work function of palladium (111) is 5.59 eV and (100) is 5.25 eV; the higher work function of palladium (111) favors electron donation from the HOMO level of small molecules as mentioned above. Figure 2.2 offers schematics illustrating the favorable electron donation from electronegative small molecules to palladium's (111) surface (Figure 2.2a) and unfavorable electron donation from electropositive small molecules to palladium's (111) surface (Figure 2.2b).

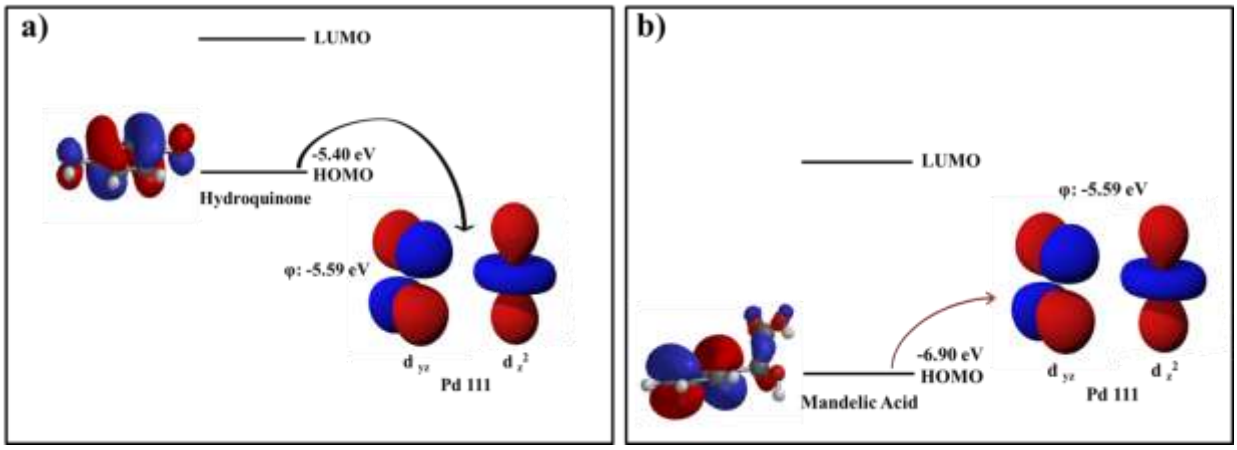

Figure 2.2 (a) Schematic showing the favorable interaction between hydroquinone's HOMOs to the d_{yz} and d_z^2 palladium orbitals upon binding of the capping agent to palladium's (111) nanoparticle surface. (b) Schematic showing the unfavorable interaction of mandelic acid's HOMOs to palladium's d orbitals upon binding to the surface of palladium (111).

Figure 2.2 and the explanation provided above helps to explain why electronegative small molecules with less negative HOMO levels help to induce noble metal (111) surfaces and why electropositive small molecules with more negative HOMO level will not induce (111) metal surfaces. However this rationale does not explain why the four small molecules mentioned above induced palladium's (100) surface in nanoparticle synthesis. Instead of favorable electron orbital interactions, there was an alternate driving force for these capping agents to induce palladium (100) nanocrystals.

2.2.1 Epitaxial Binding of Small Molecules to Palladium (100) Nanoparticles

Epitaxial binding of capping agents to metal surfaces is another important mechanism in understanding the relationship between inorganic-organic surfaces. Literature often reports functional groups that are important in binding to particular surfaces as mentioned above, yet newer reports suggest that it is not just the presence or absence of functional groups that induce favorable binding but also how the functional groups overlap with surface atoms.[7,9,29-32]

The electropositive small molecules mentioned above do not have favorable electronics to induce palladium (111) surfaces, however the location of their functional groups overlap beautifully with the top two layers of palladium (100) surface atoms. Figure 2.3 illustrates the concept of favorable epitaxial binding of tropic acid with the palladium (100) surface.

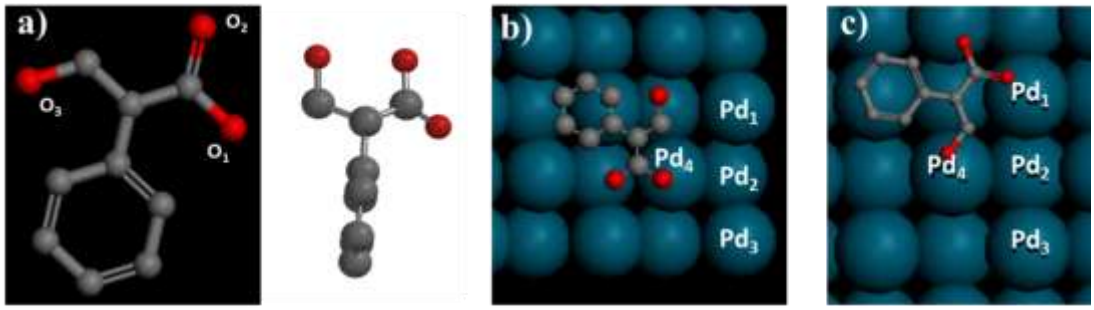

Tropic Acid	Atomic Distances
O_1-O_2	1.430 A
O_2-O_3	2.474 A
O_1-O_3	2.858 A
C-C (Benzene)	1.650 A

Palladium 100	Atomic Distances
Pd_1-Pd_3	3.890 A
Pd_1-Pd_2	1.945 A
Pd_1-Pd_4	2.751 A

Figure 2.3 (a) An illustration of tropic acid with its oxygen substituents numbered and atomic distances determined from Spartan '10 as well as a table with substituent oxygen distances. (b and c) Illustrations of tropic acid laying flat on palladium's (100) surface and atomic distances of palladium's atoms determined from Spartan '10.

These results suggest that favorable epitaxial matching of the functional groups of small molecules plays the dominant role in inducing Pd (100) nano-cubes. All of the small molecules mentioned above had substituents that overlapped with palladium's (100) surface atoms to a varied extent. Epitaxial binding may help to explain why tropic acid produced sharper cubes than mandelic acid. Although they had similar electronegativity and vary only by one carbon, tropic acid's substituents more favorably overlap with palladium's (100) surface atoms. To summarize, it is both the unfavorable electron donation from the electro-neutral/positive ring in addition to

the favorable geometric matching which are the central factors in controlling the shape evolution of palladium nanocrystals.

2.3 Chemically Reactive Small Molecules with Palladium Nanoparticle Synthesis

A different set of small molecules with electropositive benzene rings did not induce palladium (100) nanocrystals. Phenol, 2-(hydroxymethyl)phenol (2-hydroxybenzyl alcohol), benzene-1, 3, 5-triol (phloroglucinol), and 2-(4-nitrophenyl)acetonitrile (4-ntirophenylacetonitrile) did not induce well-defined palladium nanoparticles but were significantly different from the control particles indicating that these small molecules played a vital role in altering morphology. As seen in Figure 2.4, these small molecules induced polycrystalline palladium nanoparticles with defects and irregular shapes.

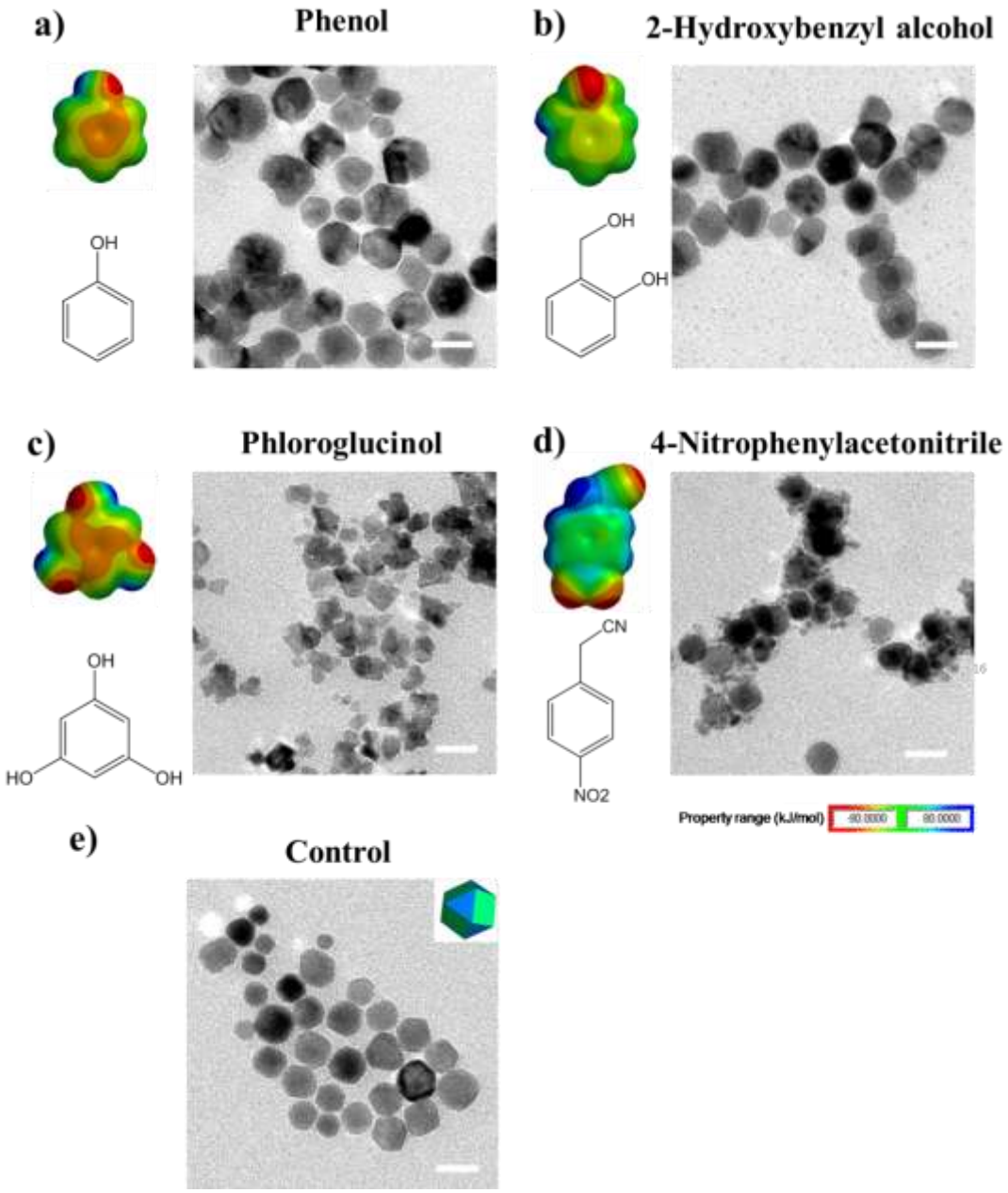

Figure 2.4 (a-d) Electrostatic potential maps and chemical structures of small molecules as well as TEM images of palladium nanoparticles with capping agents: 0.26 mM phenol (a), 0.39 mM 2-hydroxybenzyl alcohol (b), 0.16 mM phloroglucinol (c) and 0.30 mM 4-nitrophenylacetonitrile (d). Scale bars 20 nm. (e) TEM image of control reaction palladium nano-cuboctahedra.

The results of nanoparticle synthesis with these small molecules indicate it is not simply the lack of an electronegative benzene ring and favorable epitaxial matching that induce a

particular crystal facet. Instead, the reactivity of these small molecules may be playing a dominant role in nanocrystal formation. If the capping agents were simply non-binding molecules, no change of Pd growth would be seen and cuboctahedra would be formed. Additionally, if the small molecules were not somehow otherwise reactive, they would have followed the electronic/epitaxial trends of forming palladium (100) as detailed above. However, twinning planes and coalescence of the nanocrystals occurred, suggesting there may be local environment changes around the nanocrystal.

These small molecules have high reduction/oxidation potentials and may be locally reducing or oxidizing the metal surfaces, inducing twinning planes, defects, or coalescence. High strain rate, low deformation temperature, and low stacking fault energy can cause deformed twins in nanocrystalline fcc metals[22] and these conditions may provide the environment to create high energy facets through various mechanisms. Other literature reports some ligands are able to form complexes with metal precursor which cause twinning in growth.[33]

Figure 2.4a and b show nanoparticles made with phenol and hydroxybenzyl alcohol that have large defects in their surfaces. Phenol auto-decomposes into hydroquinone in solution and 2-hydroxybenzyl alcohol can also be oxidized in solution. Interestingly, the nanocrystals produced by these two small molecules look similar to palladium hexoctahedral nanoparticles with (431) surface facets exposed reported in other literature.[34] It is possible the chemical reactivity of these two small molecules are disturbing regular growth conditions and inducing kinks and steps of palladium on the surface which make up high energy facets. Benzyl alcohol, on the other hand, which has a very similar chemical structure to these two molecules but is much less reactive, induced regular low energy (100) faceted palladium nano-cubes.

Nanoparticles made by phloroglucinol and nitrophenol were branched and/or had pod-like structures connected to the bulk of each nanoparticle. The NO_2 substituent is a strong oxidizer and may be locally oxidizing the nanocrystal already formed by sodium borohydride reduction.[35] The Pd^{2+} formed by local nanoparticle oxidation would disrupt typical nucleation and growth mechanisms required for monomer attachment growth. On the other hand, phloroglucinol is also reactive and may reduce palladium monomers onto the surface of nanoparticles out of turn of typical monomer growth attachment.[36] Instead of forming single crystal nanoparticles through the traditional growth method, highly irregular nanoparticle shapes may form due to the local oxidation/reduction of palladium around the surface of the nanoparticles. Interestingly, the morphology of these nanoparticles look similar to palladium nanoparticles that have undergone leaching processes, where atoms of palladium leach and re-attach to the bulk of nanoparticles.[37]

To understand the behavior of these reactive small molecules, phenol was chosen as a model candidate to study in more detail. Phenol is known to auto-oxidize into hydroquinone, and upon introduction of a strong oxidation agent such as hydrogen peroxide, will oxidize much more quickly. Without injection of an oxidizing agent such as hydrogen peroxide, phenol induces nanoparticles with surface defects as seen in Figure 2.4a and 2.5a, indicating there is no preferential binding to a particular crystal facet, normal nanoparticle growth does not occur, and defects are created in the nanoparticles. However, upon the addition of hydrogen peroxide minutes after the irregular nanoparticles have formed (100 μL of 30 % hydrogen peroxide, H_2O_2, Fisher) palladium (111) octahedra are formed (Figure 2.5b). In this system, phenol, an unstable, electropositive small molecule, is converted to a more electronegative molecule in-situ on the nanoparticle surface, and in turn converts the nanoparticle to its predicted nanoparticle shape in

the presence of electronegative hydroquinone. This shows that phenol is a highly reactive small molecule and is not stable for single nanocrystal formation, however if it is transformed to a stable, non-reactive small molecule, even on the surface of the nanoparticle, its new stable form can induce single crystal faceted nanoparticles. This model shows the capability of altering nanoparticle surfaces in-situ after it has already been formed or potentially damaged by previous processes.

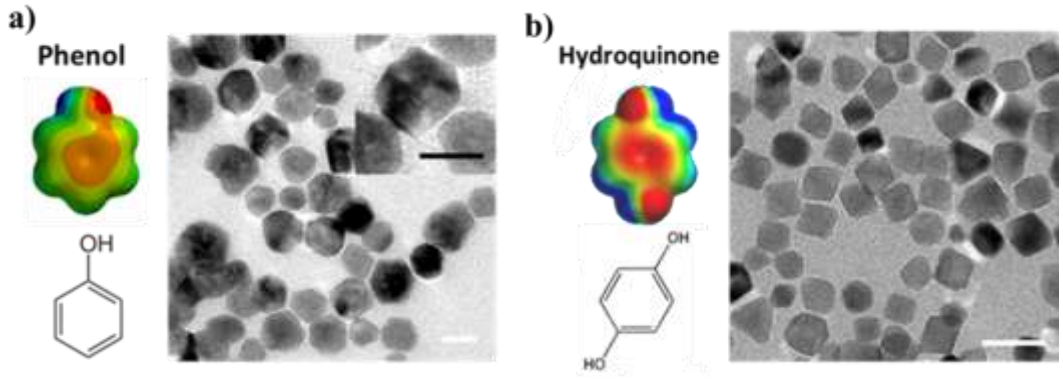

Figure 2.5 Electrostatic potential maps and chemical structures of small molecules as well as TEM images of palladium nanoparticles with: 0.26 mM phenol (a) and hydroquinone from oxidation of phenol after 1 hour (b) Scale bars 20 nm.

These results show that the electronegativity of small molecules, the geometric epitaxial matching of the substituents on small molecules, as well as the local chemical reactivity of the small molecules in solution, all must be carefully considered for nanoparticle synthesis. Reacting capping agents on the surfaces of nanoparticles is an important, yet relatively underestimated, new factor that can be manipulated to alter nanoparticle shape and size. This type of nanoparticle growth/alteration using chemical reactivity of capping agents could offer a new way of post-modifying noble metal nanoparticles.

This report shows that it is both the unfavorable electron donation from an electro-positive ring of a small molecule to palladium, in addition to the favorable geometric matching

of small molecule substituents on palladium (100) surfaces which dominate the shape evolution of palladium (100) nanocrystals for some rationally selected organic capping agents. However, when using relatively chemically unstable electropositive small molecules as capping agents, such as phenol, palladium nanoparticles can be post-modified in-situ by chemically changing the small molecule on the surface of the nanoparticles. Controlling nanoparticle synthesis creating twinning planes can provide nanocrystals with high index facets and therefore high catalytic activity.[38]

The organic-inorganic interfacial interactions of small molecules and noble metals are of high interest as they provide an understanding to the rational engineering of nanocrystal synthesis system. Steering away from choosing capping agents based on empirical results and having a logical system for choosing them based on electronics and physical interactions is key for the future in using noble metal nanocrystals in a variety of applications, such as catalysis, charge transport, functionalization and assembly. Additionally, post-modifying nanoparticles may be a promising technique for reusing nanoparticle catalysts or "self-fixing" nanoparticles in various reaction conditions.

2.4 References

1 Marković, N. M., Schmidt, T. J., Stamenković, V. & Ross, P. N. Oxygen Reduction Reaction on Pt and Pt Bimetallic Surfaces: A Selective Review. *Fuel Cells* **1**, 105-116, doi:10.1002/1615-6854(200107)1:2<105::AID-FUCE105>3.0.CO;2-9 (2001).

2 Debe, M. K. Electrocatalyst approaches and challenges for automotive fuel cells. *Nature* **486**, 43-51, doi:10.1038/nature11115 (2012).

3 Gasteiger, H. A., Kocha, S. S., Sompalli, B. & Wagner, F. T. Activity benchmarks and requirements for Pt, Pt-alloy, and non-Pt oxygen reduction catalysts for PEMFCs. *App. CatB. Env.* **56**, 9-35, doi:http://dx.doi.org/10.1016/j.apcatb.2004.06.021 (2005).

4 Koenigsmann, C. *et al.* Enhanced Electrocatalytic Performance of Processed, Ultrathin, Supported Pd–Pt Core–Shell Nanowire Catalysts for the Oxygen Reduction Reaction. *J Am Chem Soc* **133**, 9783-9795, doi:10.1021/ja111130t (2011).

5 Miyaura, N. & Suzuki, A. Palladium-Catalyzed Cross-Coupling Reactions of Organoboron Compounds. *Chemical Reviews* **95**, 2457-2483, doi:10.1021/cr00039a007 (1995).

6 Chiu, C.-Y. Platinum nanocrystals selectively shaped using facet-specific peptide sequences. *Nature Chemistry* **3**, 393-399, doi:10.1038/nchem.1025 (2011).

7 Heinz, H. *et al.* Nature of Molecular Interactions of Peptides with Gold, Palladium, and Pd−Au Bimetal Surfaces in Aqueous Solution. *J Am Chem Soc* **131**, 9704-9714, doi:10.1021/ja900531f (2009).

8 Naik, R. R., Stringer, S. J., Agarwal, G., Jones, S. E. & Stone, M. O. Biomimetic synthesis and patterning of silver nanoparticles. *Nat Mater* **1**, 169-172, doi:http://www.nature.com/nmat/journal/v1/n3/suppinfo/nmat758_S1.html (2002).

9 Slocik, J. M. & Naik, R. R. Probing peptide-nanomaterial interactions. *Chem. Soc. Rev.* **39**, 3454-3463, doi:10.1039/B918035B (2010).

10 Ruan, L. *et al.* Tailoring Molecular Specificity Toward a Crystal Facet: a Lesson From Biorecognition Toward Pt{111}. *Nano. Lett.* **13**, 840-846, doi:10.1021/nl400022g (2013).

11 Chiu, C.-Y. *et al.* Facet-Selective Adsorption on Noble Metal Crystals Guided by Electrostatic Potential Surfaces of Aromatic Molecules. *J Am Chem Soc* **135**, 15489-15500, doi:10.1021/ja406018u (2013).

12 Yin, Y. A., P. Colloidal Nanocrystal Synthesis and the Organic–Inorganic Interface. *Nature* **437**, 664-670, doi:10.1038/nature04165 (2005).

13 Xia, Y., Xiong, Y., Lim, B. & Skrabalak, S. E. Shape-Controlled Synthesis of Metal Nanocrystals: Simple Chemistry Meets Complex Physics? *Ang. Chem. Int. Ed.* **48**, 60-103, doi:10.1002/anie.200802248 (2009).

14 Tao, A. R., Habas, S. & Yang, P. Shape Control of Colloidal Metal Nanocrystals. *Small* **4**, 310-325, doi:10.1002/smll.200701295 (2008).

15 Sun, S. & Murray, C. B. Synthesis of monodisperse cobalt nanocrystals and their assembly into magnetic superlattices (invited). *Journal of Applied Physics* **85**, 4325-4330, doi:doi:http://dx.doi.org/10.1063/1.370357 (1999).

16 Lee, H. *et al.* Morphological Control of Catalytically Active Platinum Nanocrystals. *Angewandte Chemie* **118**, 7988-7992, doi:10.1002/ange.200603068 (2006).

17 Li, D. *et al.* Direction-Specific Interactions Control Crystal Growth by Oriented Attachment. *Science* **336**, 1014-1018, doi:10.1126/science.1219643 (2012).

18 Liao, H.-G., Cui, L., Whitelam, S. & Zheng, H. Real-Time Imaging of Pt3Fe Nanorod Growth in Solution. *Science* **336**, 1011-1014, doi:10.1126/science.1219185 (2012).

19 Yuk, J. M. *et al.* High-Resolution EM of Colloidal Nanocrystal Growth Using Graphene Liquid Cells. *Science* **336**, 61-64, doi:10.1126/science.1217654 (2012).

20 Langille, M. R., Zhang, J., Personick, M. L., Li, S. & Mirkin, C. A. Stepwise Evolution of Spherical Seeds into 20-Fold Twinned Icosahedra. *Science* **337**, 954-957, doi:10.1126/science.1225653 (2012).

21 Meng, F. & Jin, S. The Solution Growth of Copper Nanowires and Nanotubes is Driven by Screw Dislocations. *Nano. Lett.* **12**, 234-239, doi:10.1021/nl203385u (2011).

22 Zhu, Y. T. *et al.* Formation of single and multiple deformation twins in nanocrystalline fcc metals. *Acta Materialia* **57**, 3763-3770, doi:http://dx.doi.org/10.1016/j.actamat.2009.04.020 (2009).

23 Peng, H.-C., Xie, S., Park, J., Xia, X. & Xia, Y. Quantitative Analysis of the Coverage Density of Br– Ions on Pd{100} Facets and Its Role in Controlling the Shape of Pd Nanocrystals. *J Am Chem Soc* **135**, 3780-3783, doi:10.1021/ja400301k (2013).

24 Xiong, Y. *et al.* Synthesis and Mechanistic Study of Palladium Nanobars and Nanorods. *J Am Chem Soc* **129**, 3665-3675, doi:10.1021/ja0688023 (2007).

25 Morin, C., Simon, D. & Sautet, P. Chemisorption of Benzene on Pt(111), Pd(111), and Rh(111) Metal Surfaces: A Structural and Vibrational Comparison from First Principles. *J. Phys. Chem. B.* **108**, 5653-5665, doi:10.1021/jp0373503 (2004).

26 Morin, C., Simon, D. & Sautet, P. Density-Functional Study of the Adsorption and Vibration Spectra of Benzene Molecules on Pt(111). *J. Phys. Chem. B.* **107**, 2995-3002, doi:10.1021/jp026950j (2003).

27 Anderson, A. B., McDevitt, M. R. & Urbach, F. L. Structure and electronic factors in benzene coordination to Cr(CO)3 and to cluster models of Ni, Pt, and Ag (111) surfaces. *Surface Science* **146**, 80-92, doi:http://dx.doi.org/10.1016/0039-6028(84)90230-9 (1984).

28 Koel, B. E., Crowell, J. E., Mate, C. M. & Somorjai, G. A. A high-resolution electron energy loss spectroscopy study of the surface structure of benzene adsorbed on the rhodium(111) crystal face. *The Journal of Physical Chemistry* **88**, 1988-1996, doi:10.1021/j150654a014 (1984).

29 Atanasoska, L. L., Buchholz, J. C. & Somorjai, G. A. Low-energy electron diffraction study of the surface structures of adsorbed amino acid monolayers and ordered films deposited on copper crystal surfaces. *Surface Science* **72**, 189-207, doi:http://dx.doi.org/10.1016/0039-6028(78)90388-6 (1978).

30 Feng, J. *et al.* Adsorption mechanism of single amino acid and surfactant molecules to Au {111} surfaces in aqueous solution: design rules for metal-binding molecules. *Soft Matter* **7**, 2113-2120, doi:10.1039/C0SM01118E (2011).

31 Kilin, D. S., Prezhdo, O. V. & Xia, Y. Shape-controlled synthesis of silver nanoparticles: Ab initio study of preferential surface coordination with citric acid. *Chemical Physics Letters* **458**, 113-116, doi:http://dx.doi.org/10.1016/j.cplett.2008.04.046 (2008).

32 Wegner, D. *et al.* Single-Molecule Charge Transfer and Bonding at an Organic/Inorganic Interface: Tetracyanoethylene on Noble Metals. *Nano. Lett.* **8**, 131-135, doi:10.1021/nl072217y (2007).

33 Carbone, L. *et al.* Multiple Wurtzite Twinning in CdTe Nanocrystals Induced by Methylphosphonic Acid. *J Am Chem Soc* **128**, 748-755, doi:10.1021/ja054893c (2005).

34 Zhang, L. *et al.* Synthesis of Convex Hexoctahedral Palladium@Gold Core–Shell Nanocrystals with {431} High-Index Facets with Remarkable Electrochemiluminescence Activities. *ACS Nano* **8**, 5953-5958, doi:10.1021/nn501086k (2014).

35 Habas, S. E., Lee, H., Radmilovic, V., Somorjai, G. A. & Yang, P. Shaping binary metal nanocrystals through epitaxial seeded growth. *Nat Mater* **6**, 692-697, doi:http://www.nature.com/nmat/journal/v6/n9/suppinfo/nmat1957_S1.html (2007).

36 Stein, H. N. & Tendeloo, H. J. C. The oxidation of phloroglucinol as a model for humification processes. *Plant Soil* **11**, 131-138, doi:10.1007/BF01435102 (1959).

37 Collins, G., Schmidt, M., O'Dwyer, C., McGlacken, G. & Holmes, J. D. Enhanced Catalytic Activity of High-Index Faceted Palladium Nanoparticles in Suzuki–Miyaura Coupling Due to Efficient Leaching Mechanism. *ACS Catalysis* **4**, 3105-3111, doi:10.1021/cs5008014 (2014).

38 Tian, N., Zhou, Z.-Y., Sun, S.-G., Ding, Y. & Wang, Z. L. Synthesis of Tetrahexahedral Platinum Nanocrystals with High-Index Facets and High Electro-Oxidation Activity. *Science* **316**, 732-735, doi:10.1126/science.1140484 (2007).

CHAPTER 3: THE SYNTHESIS OF GOLD-PALLADIUM NANOPARTICLES FOR THE BENZYL ALCOHOL OXIDATION REACTION

3.1 Gold-Palladium Synergistic Effects in Catalysis

Gold (Au) and palladium (Pd) as solitary catalysts are effective heterogeneous catalysts for a wide range of organic reactions.[1-3] However in the last several decades, the combination of the elements has been proven to be much more active in catalytic reactions,[4] including hydrogen fuel cells,[5] pollution control,[6] hydrogen peroxide formation,[7,8] carbon monoxide oxidation,[9] the hydrodesulfurization (HDS) reaction,[10] alcohol oxidation,[11-14] and acetoxylation. For example, in the United States alone, 4.8 million tons of vinyl acetate are produced over AuPd catalysts annually.[4]

There are two proposed mechanisms by which gold and palladium synergistically affect each other's catalytic properties: the ensemble effect and the ligand effect. The ensemble effect occurs in a catalyst when a certain number of atoms in a particular geometric orientation either facilitate a particular catalytic process or prevent a specific catalytic process. The ligand effect occurs from electronic modifications due to hetero-nuclear metal bonding. Both effects are generated when making alloy or bimetallic nanoparticle systems, however one effect usually plays a larger role depending on the specific system. In this report, as in most accepted literature, the term "alloy" will refer to two metals that are mixed irrespective of their intimacy or amounts of mixing, and "bimetallic" will refer to two metals segregated within a (nano) structure. "Intermetallic" is a more general term, which may refer to either alloy or bimetallic.

In AuPd systems, the ligand effect, or sometimes known as the electronic effect, occurs when charge is transferred from palladium to gold. This occurs inherently because of gold's very strong electron affinity, higher electronegativity, and lower work function (Φ_{Au} = 5.3 eV, Work function of Pd: Φ_{Pd} = 5.6 eV). Specifically, Au gains s and p electrons from Pd, but loses some of its 5d electrons,[15] whereas Pd loses some of its s and p electronic character, but gains some d electrons.[10,15-17] Adding d electrons to palladium shifts the d band center away from the Fermi level and causes the d band to narrow. For late transition metals like Au and Pd, the enhancement of d electrons is much more important than s or p character in terms of chemisorption and catalytic properties because of the Fermi level shifts. A result of this effect prevents palladium from binding to substrates as strongly, which in turn prevents poisoning of the catalyst and hence, more catalytically active overall.[18]

There is a ~5% lattice mismatch between Au and Pd (the lattice constant of Au = 4.080 Å and the lattice constant of Pd = 3.890 Å). Upon alloying, some literature reports Pd may adopt the lattice spacing of Au in certain cases.[17,19] By stretching the Pd-Pd bond lengths, the Fermi level within palladium's d band rises, which narrows its d band even further.[4] This also prevents poisoning based on the same principles described above.

The small mismatch of Au and Pd's lattice spacing and the charge transfer from Pd to Au because of the Coulomb attraction presented above helps to describe the reason for the ensemble effect between Au and Pd. The ensemble effect, sometimes referred to as the promotional effect, occurs in AuPd systems because of the easy diffusion of Au and Pd. The ensemble effect is considered a "diluting" effect, because gold, which is sometimes considered the less active metal, covers palladium until there is a critical number of palladium atoms exposed on the surface in the right orientation/spacing for desired catalytic reactions.[16,20-22] This effect is unique

to gold and palladium because of their electronic attractions described above and small lattice mismatch. The ensemble effect is considered more dominant than the ligand effect for direct catalytic enhancement and selectivity,[18,23] whereas the ligand effect is essential for catalytic recyclability.

The promotional role of gold onto palladium was recently suggested by Mingshu Chen and coworkers for the different facets of AuPd.[24] They found that the rate of formation of vinyl acetate was significantly enhanced on the AuPd (100) surface compared with the AuPd (111) surface. In both cases, gold functioned to isolate palladium atom pairs on its surface. However in the AuPd (100) case, two noncontiguous, suitably spaced palladium atoms were formed from the addition of the gold, which facilitated ethylene surface species suitably spaced apart to make desirable products (vinyl acetate) and prevent undesirable by-products. To our knowledge however, this was the first paper that described a "structure-activity" relationship between gold and palladium and their (100) and (111) surfaces.

Both the ligand and ensemble effect of Au on Pd ultimately help to promote weaker binding of substrates which prevents self-poisoning of the catalyst and turns-off side reactions. Additionally, gold with palladium has been proven to enhance both metals' overall catalytic activity, selectivity, and stability. These advantages, along with primitive data about the difference between the (100) and (111) AuPd surfaces for catalysis inspired our knowledge of controlled nanoparticle synthesis to be applied to a catalytic experiment involving the comparison and efficiency of (100) and (111) AuPd nanostructures.

In this study, AuPd nanoparticles were synthesized in a solution starting with Pd nano-cubes as seeds. Both AuPd nano-cubes exposing (100) facets and nano-octahedra exposing (111)

facets were produced, and both nano-cubes and nano-octahedra each had two morphologies, a coreshell type structure and a pod-like structure. These nanoparticles were used in a model benzyl alcohol oxidation study to determine which nanoparticle facet was more catalytically active. To our knowledge, this was the first experimental study of the (100) and (111) AuPd nanoparticle surfaces in catalysis.

3.1.1 The Importance, State-of-the-Art, and Mechanisms of the Benzyl Alcohol Oxidation Reaction

There are several model heterogeneous catalysis reactions to consider when testing a catalytic material such as alcohol oxidation,[11-14] decomposition reactions,[10] hydrogen peroxide formation,[7] and hydrogenation reactions.[25] The benzyl alcohol oxidation reaction is an especially useful probe-reaction for illustrating basic and foundational properties of a catalyst for multiple reasons. Alcohol substituents of phenols are much easier to oxidize than those on primary or secondary carbons; therefore they offer a reaction that is viable to catalytic systems in their early stages. Also, it is beneficial to use a catalytic substrate that is at least partially water soluble (solubility of benzyl alcohol in water, 4.29 g/100 mL) and also produces water soluble products when using nanoparticle systems made from solution phase nanoparticle synthesis. In most noble metal nanoparticle reactions, catalysts are coated with water soluble capping agents during their synthesis such as polyethylene glycol (PEG), polyvinylpyrrolidone (PVP), ethylene glycol (EG), cetyltrimethylammonium bromide (CTAB), trioctylphosphine oxide (TOPO), or others.[26] And despite washing techniques, capping agents remain on the surface of heterogeneous catalysts, so it is advantageous to use a substrate that is soluble with all other species in the reaction, including capping agents, solvents, co-solvents, etc. Additionally, benzyl alcohol is readily available, relatively non-toxic, and is stable within a wide range of temperatures and pressures.

After the reaction is complete, the solution can be handled and analyzed in air with very few precautions.

Benzaldehyde is the most desirable product from the benzyl alcohol oxidation reaction because it is extremely valuable in both commercial and laboratory processes.[27,28] For example, benzaldehyde is an important intermediate in in the perfume industry,[29] as well as in laboratory settings.[30] The other products of benzyl alcohol oxidation are benzoic acid, benzyl benzoate, toluene, dibenzylether, the hemiacetal, dibenzylacetal, anthracene, stilbene, and water through various pathways. Great care is taken in creating the right catalyst under the right conditions to selectively make benzaldehyde.

The exact mechanisms of benzyl alcohol oxidation in the presence of AuPd structures is still somewhat controversial and seems to depend on the specific catalysts as well as the reaction parameters used. Literature reports that the adsorption of the hydroxyl hydrogen is the first step of the catalytic cycle and that removing the beta-hydrogen from benzyl alcohol is the rate limiting step in catalysis.[31,32] Other research has shown that once formed, benzaldehyde and benzoic acid may be compete for active sites with benzyl alcohol, inhibiting continued catalysis, and that the addition of a base may prevent the competition.[33] Additionally, a base may function as a "promoter" or "co-catalyst" to deprotonate benzyl alcohol, ensuring the oxidation step the rate-limiting step. Yet still others claim the addition of a base is not necessary.[14]

Despite the kinetic details and ambiguities, it is accepted that there are four pathways for the conversion of benzyl alcohol catalysis: oxidation, disproportionation, dehydration, and condensation reactions.[13,14,32,34] The oxidation reaction forms benzaldehyde directly and benzoic acid when over-oxidized (Equations 1a and 1b). The disproportionation reaction forms

benzaldehyde, toluene and water (Equation 2). The dehydration reaction forms dibenzylether (Equation 3). The self-condensation reactions may form benzyl benzoate, dibenzyl acetal, anthracene and stilbene (Equations 4a, b, c, and d).[35] The two main pathways for benzyl alcohol oxidation in solution phase synthesis are the oxidation and disproportionation reactions.

Oxidation Reactions:

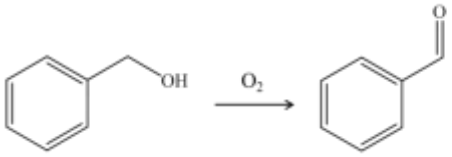

Equation 1a

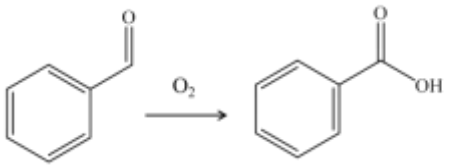

Equation 1b

Disproportionation Reaction:

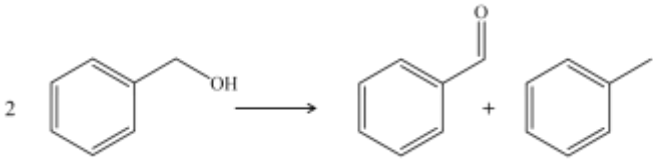

Equation 2

Dehydration Reaction:

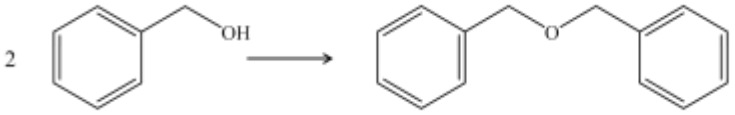

Equation 3

Condensation Reactions:

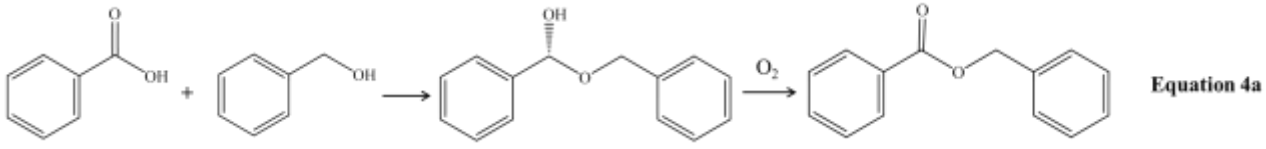

Equation 4a

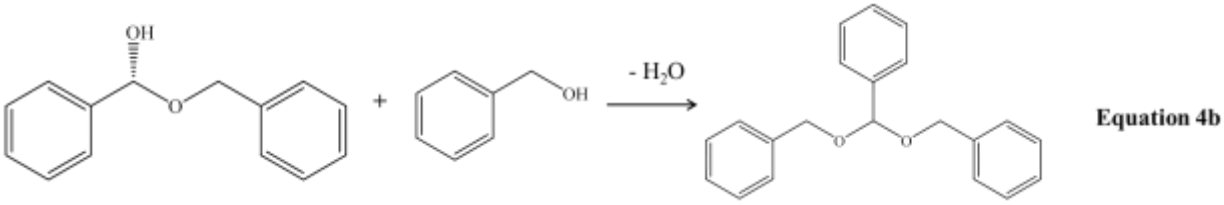

Equation 4b

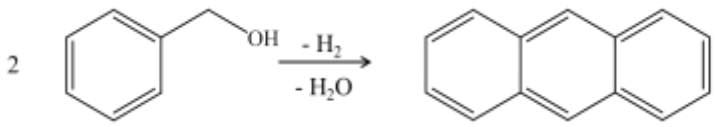

Equation 4c

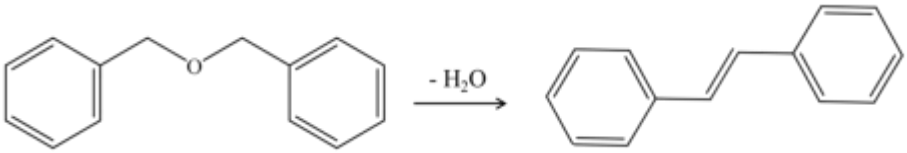

Equation 4d

Catalytic activity is typically measured in terms of percent conversion, the relative ratio of the product of interest over the remaining starting material in solution, turn over number (TON), which is defined as the moles of the product of interest over the moles of the catalyst being used, and/or turn over frequency (TOF), which is the moles of product produced over the moles of catalyst used per unit of time. Activity, selectivity, and recyclability of catalysts for the benzyl alcohol oxidation reaction differ dramatically based on experimental conditions. Solution-phase benzyl alcohol oxidation is categorized by "mild condition" catalysis and regular catalysis. Mild condition benzyl alcohol oxidation occurs at temperature below 120 °C and pressures below 0.3 MPa of gas above solution. A table of different parameters and their ranges for the mild condition benzyl alcohol oxidation reaction is summarized below:

Parameter	Range
Temperature	Mild Conditions: ≤ 120 °C
Pressure	Mild Conditions: ≤ 0.3 MPa
Phase	Solution-Phase
Gas Above Reaction Solution	Air, O_2, N_2

Oxidant	Air, O_2, H_2O_2, Chromate, Permanganate
Solvent	None, Toluene, Ethanol, Water
Base	Diols (1,2-propanediol), Triols, NaOH, K_2CO_3, KF
Support	Titania (TiO_2), Activated Carbon (AC), Alumina (Al_2O_3), Silica (SiO_2), Ceria (CeO_2), Fe_2O_3, hydroxyapatite (HAP) ($Ca_{10}(PO_4)_6(OH)_2$), Nb_2O_5, MgO, ZnO, Zeolites
Wt % of Catalyst on Support	1%-5% by Mass of Catalyst on Support
Mass Ratio Benzyl Alcohol: Catalyst	50-40,000:1

Table 3.1 Common parameters of mild condition benzyl alcohol oxidation reactions.

All parameters vary widely from group to group, and there are many variables to choose from for each parameter. None of the parameters listed are more accepted than any others, and scientists still constantly look for newer choices of supports, bases, etc. as well as methods of preparation of their catalysts to increase performance. For example, oxidants such as chromate and permanganate were used more in the past but are more often replaced now by oxygen gas, air, or hydrogen peroxide, which are less expensive, more environmentally friendly, and less toxic.[29] Choosing the detailed parameters of the benzyl alcohol oxidation reaction depends on the particular AuPd nanoparticle catalyst system made, and many parameters are adjusted over time to find the most suited for the catalyst to thrive.

3.2 The Synthesis of Palladium Nano-Cubes and Etched Nano-Cubes as Seeds for Subsequent AuPd Nanoparticles

Palladium nano-cubes were synthesized according to a previously reported method by Xia and coworkers.[36] In short, 87 mM PVP (polyvinylpyrrolidone, average molecular weight 40,000 g/mol, Sigma), 31 mM L-ascorbic acid ($C_6H_8O_6$, Sigma), and 230 mM potassium bromide (KBr, Fisher) were added together in equal ratios of water while stirring. After the mixture was heated to 80 °C, 17.4 mM Na_2PdCl_4 (sodium tetrachloropalladate (II), Sigma) was injected in one shot to the mixture and the solution was left stirring at 80 °C for three hours.

Nanoparticle samples were prepared with carbon substrates on copper mesh grids with 20 μL aliquots of reaction solution at various times. Transmission electron microscopy (TEM) images were imaged on a Phillips CM120 with a 120 keV operation voltage and high-resolution transmission electron microscopy (HRTEM) images were imaged on a FEI TITAN with a 300 keV operation voltage. Average frequencies of faceted particles were performed on ~100 single crystal particles per sample. Lattice spacing and facet confirmation were performed on HRTEM. Scanning transmission electron microscopy (STEM) was also performed on the FEI TITAN for elemental mapping, lines scans, and high-angle dark field imaging (HAADF) of nanoparticles.

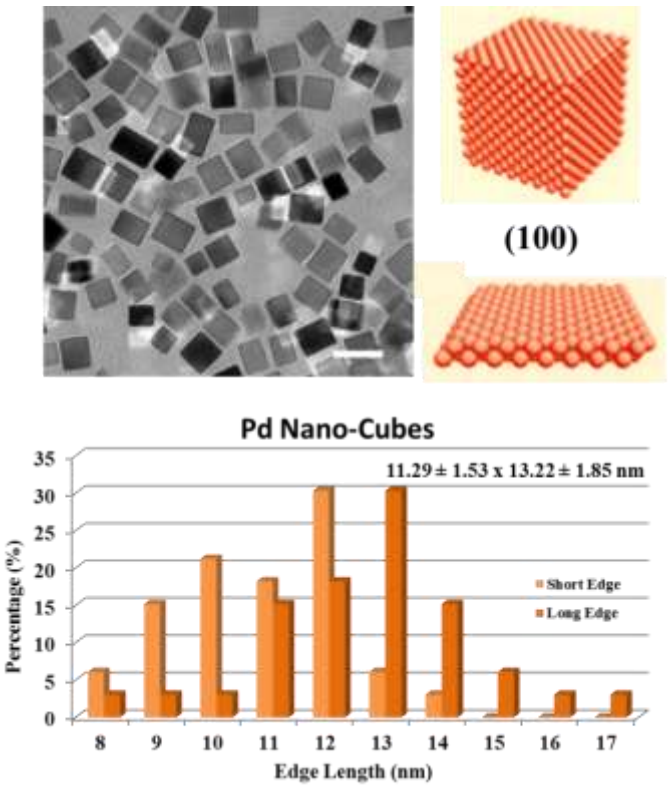

Figure 3.1 Transmission Electron Microscope (TEM) image of palladium nano-cubes and nano-rectangular prisms known collectively as palladium nano-cubes. Scale bar is 20 nm.

When the reaction was complete, the nanoparticles were collected and washed through three cycles of a standard ethanol (Pharmco-AAPER) and acetone (Sigma) washing technique to remove excess chemicals in the reaction and to remove some of the PVP from the surface of the nanoparticles. Briefly, the nanoparticles were collected by centrifuge at 12,000 rpm for 20 minutes. The supernatant was decanted and then ethanol and acetone were added in a volumetric ratio of 1:3. The solution was sonicated for 10 minutes and then centrifuged at 12,000 rpm for 20 minutes. This washing cycle was performed three times. The nano-cubes were re-dispersed into 10 mL of water and used as "seeds" for some of the subsequent nanoparticle synthesis in this work. The average edge-length of the nanoparticles was ~11 x 13 nm. As previously reported, the nanoparticles are a range of nano-cubes and nano-rectangular prisms, all with (100) surface facets, herein simply described as nano-cubes.

Using bromide ions as a capping agent in solution phase synthesis for making palladium (100) nano-cubes is an established chemical route because of bromide's preferential binding to (100) surfaces over (111) surfaces.[37] However, removing the bromide ions from the (100) surfaces is difficult. Xia and co-workers showed through XPS (X-ray photoelectron spectroscopy) and ICP-MS (Inductively Coupled Plasma-Mass Spectrometry) that there are is crucial ~0.8 bromide ions per surface Pd atom for the nano-cubes reported here to make sharply faceted palladium nano-cubes. With no bromide in solution (and only PVP as a stabilizing agent) palladium cuboctahedra were formed, with insufficient bromide on the surface of palladium truncated cubes were formed, and with too much bromide in solution, palladium nuclei were decreased and nanoparticle size was increased due to a bromide-palladium complex formed. They found a strong chemisorption interaction between bromide and palladium (II) on the surface of the cubes and that the only way to remove the majority of the bromide ions was through either a reduction process or further growth of the nano-cubes. [38] Washing the nanoparticles was not enough to remove the bromide to grow gold on the palladium; the nanoparticles needed to be stringently chemically processed or used as seeds to remove the bromide ions and used as potential effective catalysts.

Other papers have shown that oxidation of palladium nano-cubes could remove bromide ions from the surface, creating new shapes and allowing subsequent growth more easily. To remove the bromide ions from palladium nano-cubes through an oxidation process, several methods were considered.[39] A combination of air/Cl^- in solution has been shown to etch Pd nanoparticles and even prevent twinning in early stages of growth.[40] Oxygen gas could be bubbled into solution. Iron (III) chloride can etch palladium seeds in early stages of growth, altering its growth pattern without including iron into the palladium nanoparticles.[41]

Hydrochloric acid can perform oxidative etching of palladium in aqueous solution, and its mechanisms have been studied and controlled in several works.[42,43] Using hydrogen peroxide was also considered as an oxidizing agent from work in earlier studies in our lab with palladium. Oxygen gas (O_2), hydrochloric acid (HCl) and hydrogen peroxide (H_2O_2) oxidations offer the "cleanest" methods of chemical oxidation, not leaving behind additional ions that could potentially alter the growth of Pd.

In an attempt to remove bromide from the (100) surfaces of palladium, HCl was used as an oxidative etchant through the following process: in an 8 mL reaction solution, 200 µL of washed Pd nano-cubes and 6 mM PVP was mixed and heated to 80 °C. Various amounts of 1.2 M HCl was added to reaction solutions to see the effect of increasing amounts of HCl on palladium nano-cubes. Reaction samples were taken from solution after 20 minutes of reaction time and observed by TEM to see the effect of HCl on the system.

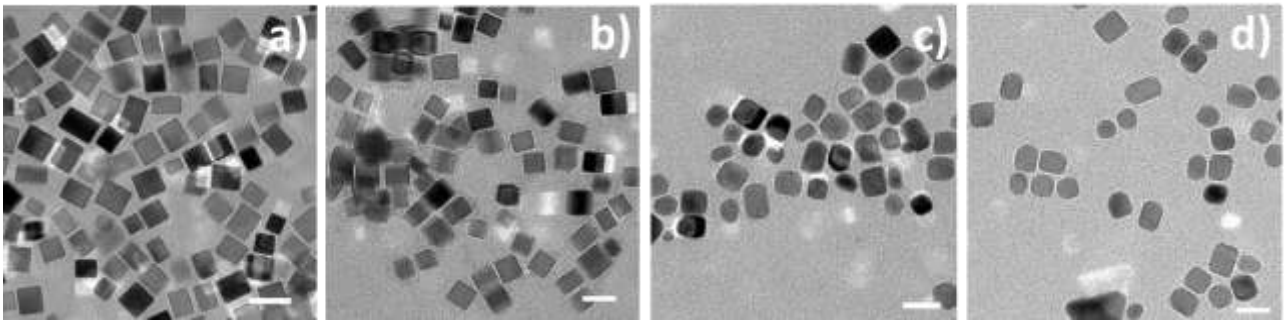

Figure 3.2 (a) Pd nano-cubes before reaction with HCl. (b) Pd nano-cubes after 20 minutes with 3.7 mM HCl. (c) Pd "nano-cubes" after 20 minutes with 31 mM HCl. (d) Pd "nano-cubes" after 20 minutes with 73 mM HCl. All scale bars are 20 nm.

After 20 minutes of reacting with HCl, there was no (100) facets remaining although bromide was still in solution, indicating the hydrochloric acid successfully removed enough bromide from the surface of palladium to lose the (100) shape. However the PVP-Pd interactions were not disrupted by HCl as nanoparticles remained mono-disperse in solution. Increasing the

amount of HCl in solution eventually to over-etching as seen by the disappearance of mono-disperse nanoparticles and the appearance of fused, enlarged palladium masses in solution.

In a parallel attempt to etch the palladium nano-cubes, palladium nano-cubes were etched with oxygen gas and hydrochloric acid through a synthesis as follows: in an 8 mL reaction solution, 200 µL of washed Pd nano-cubes and 6 mM PVP was mixed and heated to 80 °C. Oxygen gas was purged into the system through a needle at a rate of about one oxygen bubble every two seconds. Once mixed and heated to 80 °C, 200 µL of 1.2 M HCl was added to the reaction solution (final concentration of HCl = 30 mM). Reaction samples were taken from solution at different time intervals and observed by TEM to see the effect of HCl/O_2 on the system.

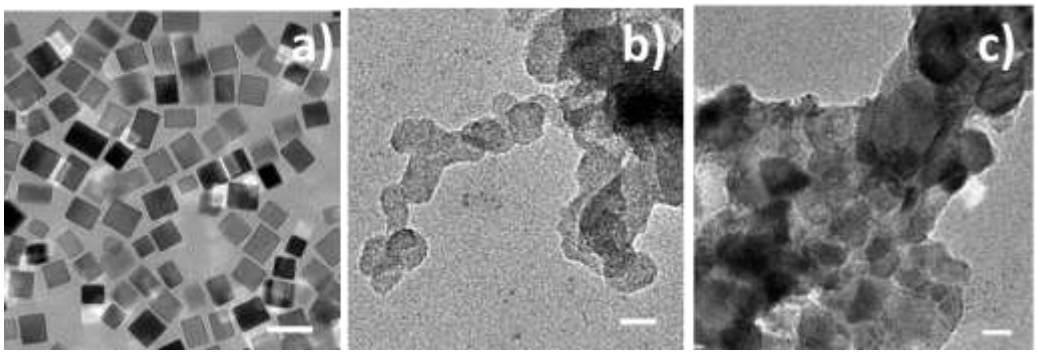

Figure 3.3 (a) Pd nano-cubes before reaction with HCl/O_2 gas. (b) Pd "nano-cubes" after 20 minutes of reacting with 30 mM HCl/O_2 gas. (c) Pd "nano-cubes" after 45 minutes of reacting with 30 mM HCl/O_2 gas. All scale bars are 20 nm.

As shown above, the addition of oxygen gas with hydrochloric acid reacted aggressively with the nano-cubes. (The addition of oxygen gas alone in a similar reaction had no effect on the nanoparticles.) The loss of (100) facets by HCl/O_2 showed that bromide ions must have been removed from the palladium surface in this oxidation process. Based on the results, loss of mono-disperse nanoparticles indicate that either too much bromide and/or PVP must have been removed from the surface of the nanoparticles to cause the fusion of the nanoparticles. Even

when limiting the oxygen gas bubbling time and amount, these systems could not be used for subsequent gold addition to make well dispersed AuPd nanoparticles. Overall, this process proved too intense for the removal of some bromide ions on the palladium (100) surfaces.

3.2.1 The Synthesis of Gold-Palladium Core-Shell and Pod-Like Nano-Cubes

Though oxidative etching was found to be an effective method of removing some bromide ions and creating new shapes, gold had the ability to etch palladium directly through a type of galvanic replacement reaction. Because the standard reduction potential of an $AuCl_4^-/Au$ pair, 0.99 V vs SHE (standard hydrogen electrode) is higher than that of $Pd^{2+/}Pd$ pair, 0.92 V vs SHE, palladium nanostructures suspended in solution can be oxidized by $HAuCl_4$ according to the following replacement reaction:

$$3\ Pd\ (s) + 2\ AuCl_4^-\ (aq) \rightarrow 2\ Au\ (s) + 3\ Pd^{2+}\ (aq) + 8\ Cl^-\ (aq) \quad \textbf{Equation 5}$$

In our novel synthesis, 37 mM PVP, 2 mL of washed Pd nano-cubes, and 1.96 mM citric acid (Sigma) was added together and heated to 80 °C in a total of 152 mL of water. After five minutes at 80 °C (to ensure the solution was thoroughly heated), 8 mL of 0.25 mM $HAuCl_4$ (chloroauric acid, Sigma) was added to the mixture in one shot. The nanoparticles were collected and washed by a stringent washing technique to obtain clean surfaces for the following benzyl alcohol oxidation reaction. First, the nanoparticles were collected by centrifuge at 12,000 rpm for 20 minutes and then washed three times with ethanol and acetone in a volumetric ratio of 1:3 as described above. Following this, the nanoparticles were dispersed in 20 mL of glacial acetic acid (J. T. Baker) and stirred for 5 hours. Then, the nanoparticles were collected from the glacial acetic acid through centrifuge and washed with ethanol: acetone for five cycles. At the end of

this procedure, the nanoparticles were re-dispersed into 2 mL of ethanol for the subsequent synthesis and catalysis.

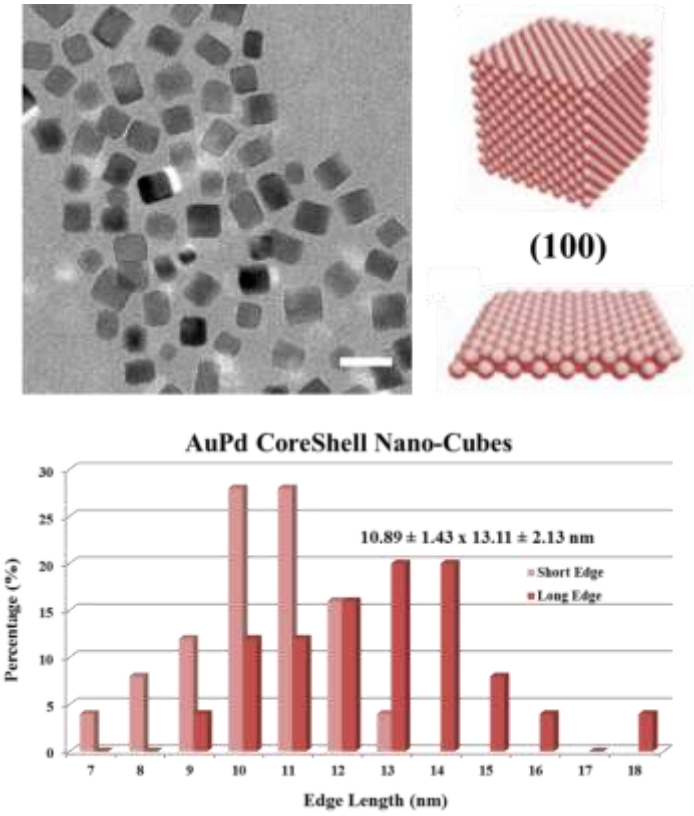

Figure 3.4 TEM image of AuPd coreshell nano-cubes. Scale bar is 20 nm.

Heat and time were extremely important in this reaction as Au^{3+} is readily reduced to Au^{0} in solution, especially when heated or in the presence of a reducing agent such as citric acid. Additionally, only a very small amount of gold precursor was necessary to perform this reaction without over growing the gold on palladium; based on the equation above, two gold atoms replace three palladium atoms per oxidation. Other scientists have made large, overgrown, bulbous structures by using more gold than reported here.[44] The reducing agent, citric acid, was responsible for the coreshell structure produced. Without citric acid, the gold in solution took longer to reduce and formed pod-like structures as mentioned in the next section. With citric

acid, the gold reduced quickly and all directly onto the nano-cubes without time to produce directionally grown structures on itself.

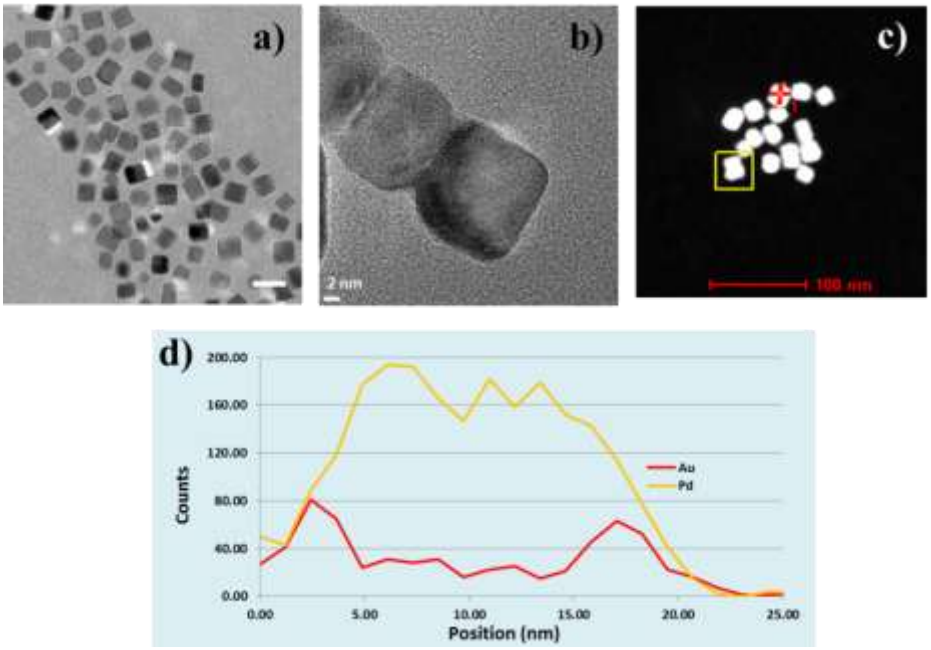

Figure 3.5 (a) TEM image of AuPd coreshell nano-cubes. Scale bar is 20 nm. (b) HR-TEM image of AuPd coreshell nano-cubes. Scale bar is 2 nm. (c) A High Angle Annular Dark Field (HAADF) STEM image of AuPd coreshell nano-cubes. Scale bar is 20 nm. (d) An STEM line profile of AuPd coreshell nano-cubes.

The morphology of the AuPd coreshell nanoparticles were nano-cubes with (100) facets exposed. These nanoparticles were slightly smaller compared with the seed palladium nanoparticles, indicating that gold etched the palladium successfully. Furthermore, gold replaced much of the palladium based on STEM data. The STEM line scan profile (Figure 5d) shows that both Au and Pd reside in the entirety of the nanoparticle, indicating an alloy-type structure. However, there is more gold on the outside of the nanoparticles as indicated by higher gold counts near the edges of the nanoparticles, so these nanoparticles are referred to as “coreshell” structures. Based on the size of nanoparticles and the easy diffusion of Au into Pd as detailed above, it makes sense that the nanoparticles retain an alloy structure throughout the nanoparticle.

For pod-like morphologies of AuPd nano-cubes, the synthetic conditions were very similar to AuPd coreshell nano-cubes except there was no citric acid added to solution and slightly more gold precursor was added. 37 mM PVP and 2 mL of washed Pd nano-cubes was added together and heated to 80 °C in a total of 136 mL of water. After five minutes at 80 °C, 24 mL of 0.25 mM $HAuCl_4$ was added to the mixture in one shot. The nanoparticles were then collected and washed in the same way described for the AuPd coreshell nano-cubes.

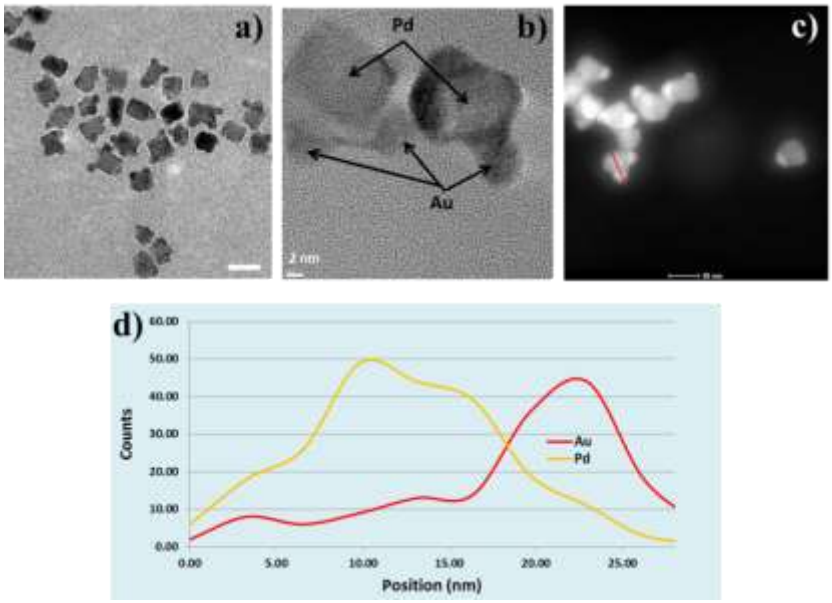

Figure 3.6 (a) TEM image of AuPd pod-like nano-cubes. Scale bar is 20 nm. (b) HR-TEM image of AuPd pod-like nano-cubes. Scale bar is 2 nm. (c) A High Angle Annular Dark Field (HAADF) STEM image of AuPd pod-like nano-cubes. Scale bar is 20 nm. (d) An STEM line profile of AuPd pod-like nano-cubes.

The bulk of the AuPd pod-like nano-cubes had similar atomic morphology as the AuPd coreshell nano-cubes described above; an alloy-type structure of Au and Pd throughout the nanoparticle with slightly more Au on the outside of the nanoparticle. However, these AuPd nano-cubes additionally have gold growths in the corners of the nanoparticles. The nanoparticles were the same size as the AuPd coreshell cubes with the addition of the pods that were ~1-2 nm. There are about three gold pods per nanoparticle, meaning that about 3/8 of the corners of

palladium nano-cubes were replaced with gold. The galvanic replacement that occurred of the corners gave rise to directional growth of gold. Because no citric acid was used in this reaction, gold reduced more slowly in solution and was able to preferentially reduce and bind to itself instead of palladium. This has been reported elsewhere for different types of AuPd structures, such as AuPd "bulb" structures[44] and AuPd "tad-pole" structures.[45] These nanoparticles represent a novel structure of Au and Pd together, and may prove to be useful for catalysis. However in studying the difference between AuPd (100) and (111) surfaces, it was not appropriate to use these nanoparticles (or the AuPd pod-like nano-octahedra) since the pods were entirely gold and spherical (non-faceted).

3.2.2 The Synthesis of Gold-Palladium Core-Shell and Pod-Like Nano-Octahedra

To synthesize palladium nano-octahedra, the palladium nano-cubes described above were used as seeds.105 mM PVP and 1 mL of un-washed palladium nano-cubes were added together in a total of 8 mL water while stirring and heated to 90 °C. Then, 2 mL of 21 mM Na_2PdCl_4 was injected in several shots into the reaction mixture. The solution was left stirring for 24 hours. The nano-octahedra were collected and washed for two cycles in a standard ethanol/acetone washing technique and then re-dispersed into 5 mL of water for subsequent gold replacement reactions. The palladium nano-octahedra collected here had an average edge length of ~19 nm. They are significantly larger than the palladium cubes due to the seeded growth synthesis. However, all catalytic activities are surface site normalized and did not disrupt the catalytic study between the (100) and (111) AuPd surfaces.

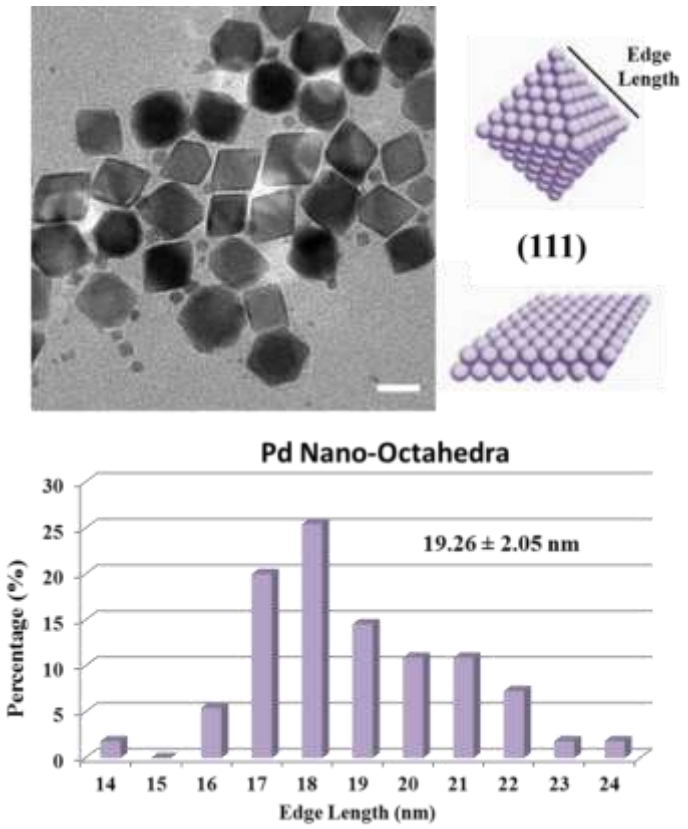

Figure 3.7 TEM image of palladium nano-octahedra. Scale bar is 20 nm.

The synthesis of AuPd coreshell nano-octahedra was exactly the same as the one reported for the synthesis of AuPd coreshell nano-cubes, except that cubes were replaced for octahedra.

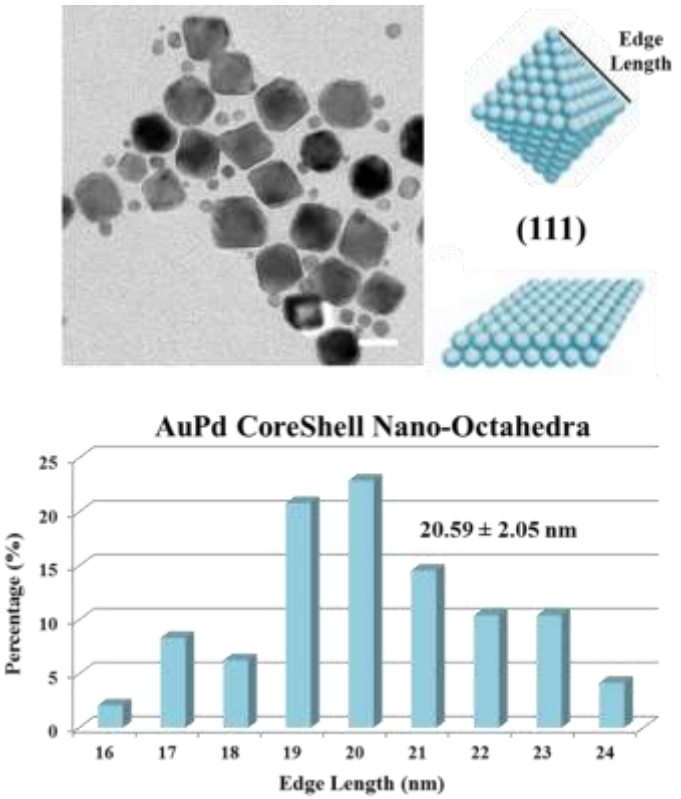

Figure 3.8 TEM image of AuPd coreshell nano-octahedra. Scale bar is 20 nm.

Small palladium nuclei were present in the final washed solution of palladium nano-octahedra and remained present for the AuPd nano-octahedra reactions. However, AuPd coreshell and pod-like morphologies looked similar to the AuPd cube structures overall, indicating the palladium nuclei did not play a negative role in the synthesis of the AuPd nano-octahedra. Additionally, because our study focused on the catalytic activity of (100) and (111) surfaces of AuPd, the small nuclei were not considered as an important factor for the benzyl alcohol oxidation reaction because spherical nanoparticles have equal ratios of (100) and (111) surfaces exposed.

As in the bulk palladium octahedra, the AuPd coreshell octahedra had an overall morphology of octahedra with (111) surface facets exposed. These nanoparticles were slightly larger than their Au-lacking counterpart. This is different from the AuPd coreshell cube reaction,

where the AuPd nanoparticles were smaller than their Pd cube counterpart. There may have been less galvanic replacement in this reaction and just more growth and diffusion. One reason for this may have been due to the fact that making the palladium octahedra required more PVP than making palladium cubes, which could have protected the outer layer of palladium from galvanic replacement. The STEM line profile scan for these nanoparticles show an alloy-type structure of Au and Pd, with slightly more Au on the outside of the nanoparticles.

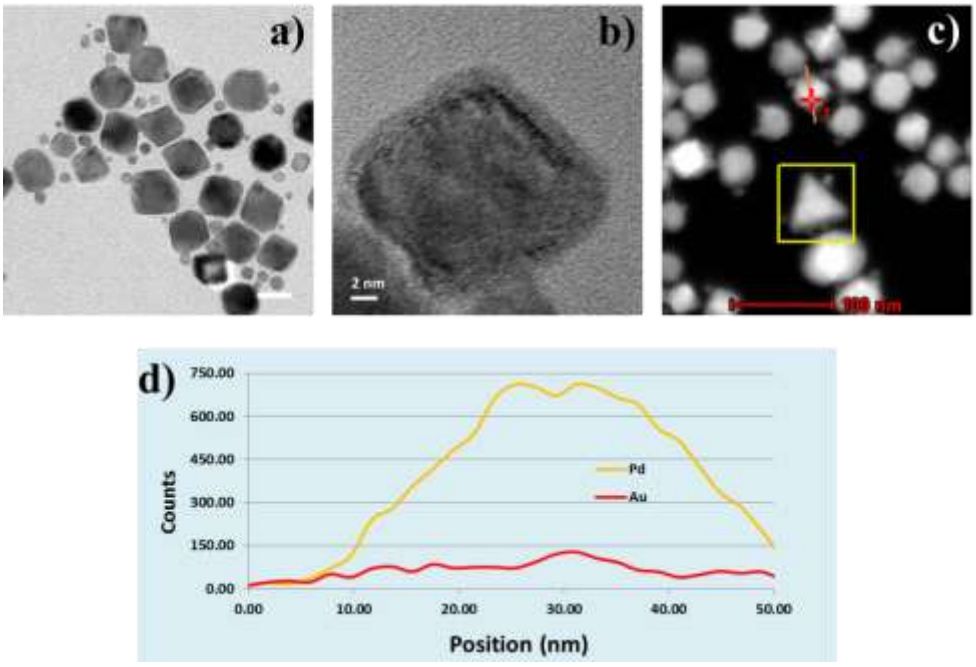

Figure 3.9 (a) TEM image of AuPd coreshell nano-octahedra. Scale bar is 20 nm. (b) HR-TEM image of AuPd coreshell nano-octahedra. Scale bar is 2 nm. (c) A High Angle Annular Dark Field (HAADF) STEM image of AuPd coreshell nano-octahedra. Scale bar is 20 nm. (d) An STEM line profile of AuPd coreshell nano-octahedra.

The synthesis of AuPd pod-like nano-octahedra was exactly the same as the one reported for the synthesis of AuPd pod-like nano-cubes, except that cubes were replaced for octahedra.

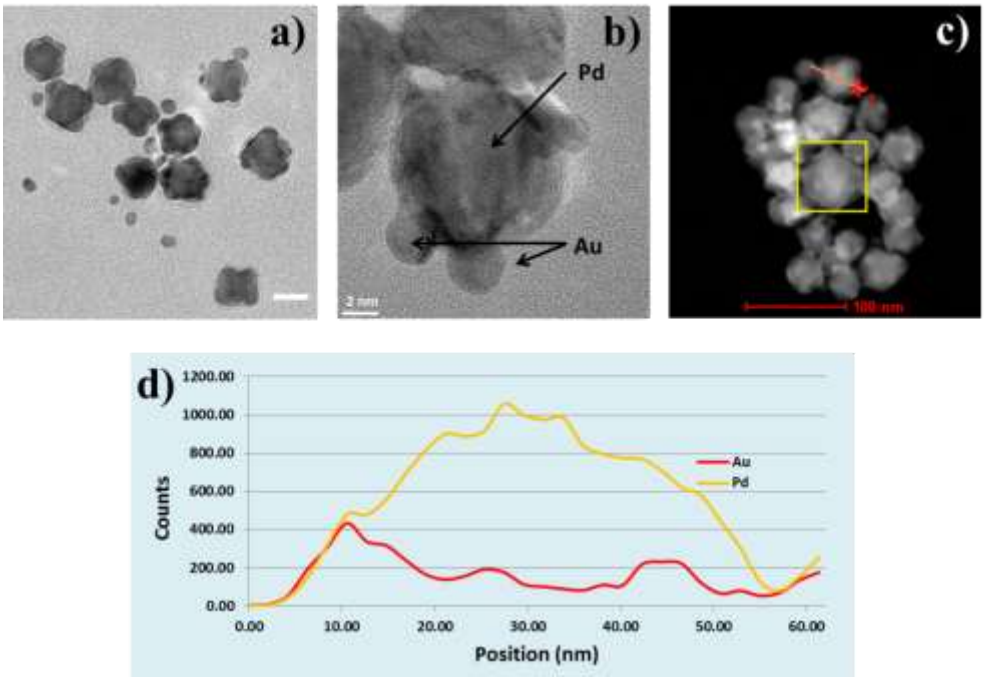

Figure 3.10 (a) TEM image of AuPd pod-like nano-octahedra. Scale bar is 20 nm. (b) HR-TEM image of AuPd pod-like nano-octahedra. Scale bar is 2 nm. (c) A High Angle Annular Dark Field (HAADF) STEM image of AuPd pod-like nano-octahedra. Scale bar is 20 nm. (d) An STEM line profile of AuPd pod-like nano-octahedra.

The morphology of the AuPd pod-like nano-octahedra shows similar morphology and structure as the AuPd coreshell nano-octahedra. The overall structure is an alloy structure of Au and Pd with more Au on the outside of the nanoparticle. The nanoparticles were the same size as the AuPd coreshell octahedra with the addition of the pods that were ~1-2 nm. Interestingly, the gold pods on these structures were much less defined than on the AuPd pod cubes. This is consistent with the fact that the gold did not etch the palladium as much as with the cubes, but instead grew onto the nanoparticles. In this way, there were not etched and re-grown portions of gold but rather more uniformed growth on the nanoparticles. However, gold pods were still produced and these nanoparticles still present a novel AuPd (111) structure that should be considered for future catalytic purposes.

The atomic spacing of all of the AuPd nanoparticles was found to be ~2.78 Å, which is in range of the accepted value for Pd-Pd (bulk Pd = 2.75 Å) and near the range of Pd-Au atomic spacing (~2.83 Å).[19] The lattice spacing found from HRTEM helped to confirm the presence and morphology of AuPd structures and insinuates there is a presence of Pd-Au bonding. Conclusive evidence regarding the bonding modes of Au and Pd would require more advanced studies using EXAFS and XRD to determine if palladium's lattice spacing expanded to take on gold's lattice spacing or if there was a mutual change in lattice constants, etc. To summarize, the four types of AuPd nanoparticles made are shown below:

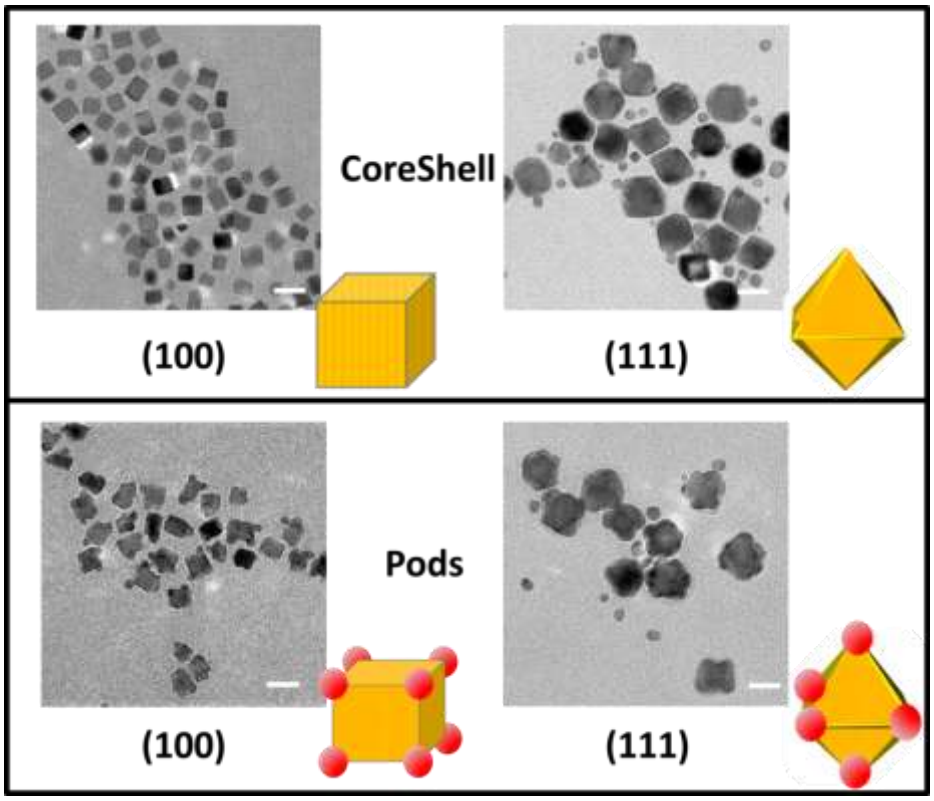

Figure 3.11 TEM images and model nanoparticles of AuPd coreshell and pod-like nano-cubes and nano-octahedra. Scale bars are 20 nm.

3.3 The Synthesis of Gold-Palladium Nanoparticles on Titania as a Support for the Benzyl Alcohol Oxidation Reaction

Only the coreshell AuPd structures were used for the benzyl alcohol oxidation reaction. In order to test the behavior and difference of the (100) and (111) surfaces, the pod-like morphologies of gold on palladium were not considered as they add non-(100) surfaces of only gold into the reaction mixture. In this report, Degussa P25 TiO_2 (Aeroxide) was used as a support for the AuPd nanoparticles for several reasons that were believed to create the best three-phase heterogeneous catalytic system possible.

In general, a nanoparticle catalyst support must have high surface area, be highly miscible in the reaction solution, and is desirable to be electronically conducting in order to assist in the catalytic process. Supports are used in heterogeneous nanoparticle catalysis to ensure nanoparticles remain well-dispersed during catalysis. However, they can also play a vital role in the chemical and physical activity of the catalysts, and may even be involved in the catalysis itself. For model oxidation reactions, activated carbon, titania, or other metal oxides such as SiO_2, CeO_2, Al_2O_3, Fe_2O_3, MgO, or ZnO are usually considered. However, activated carbon must be prepared through several washing cycles before it can be used in reactions. And some metal oxides such as Al_2O_3 and Fe_2O_3, as well as some zeolites, have been known to be too acidic for the benzyl alcohol reaction and led to enhanced by-product formation such as benzyl benzoate, dibenzyl acetal, and dibenzylether.[11,34] On the other hand, titania is readily available in most labs, is not overly acidic, has a high surface area, and has been shown to turn off the disproportionation and self-condensation reactions in literature.[13]

To adsorb AuPd nanoparticles onto titania (TiO_2) for catalysis, both the titania and nanoparticles were stirred in an ethanol solution for one hour. Our best results yielded 2.5 % by

mass of Au and Pd on titania. In a typical reaction, 0.002 mmol of Au and 0.042 mmol of Pd was attached to 2.44 mmol of TiO_2 in 10 mL of ethanol. The reaction mixture was then drop-casted onto glass slides and dried by air. Oxygen plasma was applied to the thin films for 5 minutes to try to remove remaining PVP and bromide on the surfaces of the AuPd nanoparticles. Lastly, the thin films of supported catalyst were placed into the catalytic reaction solution for catalysis.

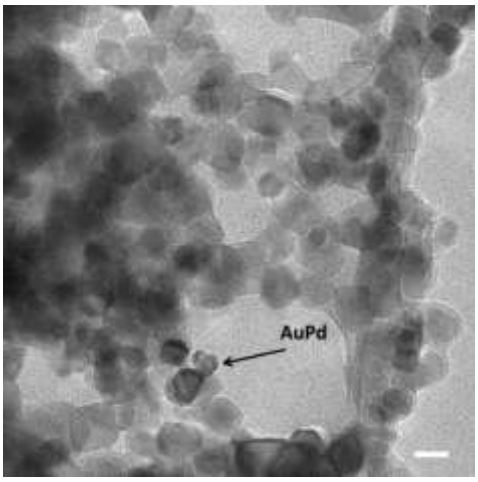

Figure 3.12 TEM image of AuPd pod-like octahedra on TiO_2. Scale bars are 20 nm.

3.4 The Catalytic Behavior of Gold-Palladium Nano-Cubes and Nano-Octahedra on Titania in the Benzyl Alcohol Oxidation Reaction

The benzyl alcohol oxidation reaction was carried out under mild conditions due to our group's interest in ambient condition, green chemistry. Our system occurred at a temperature of 85 °C and a pressure of 0.2 MPa O_2, both on the milder side of the mild oxidation conditions. In a typical reaction, a total of 0.002 mmol of Au and 0.042 mmol of Pd were used on 2.44 mmol of titania. A low-pressure reactor was used in an oil bath while stirring at 1200 rpm for a total of an eight-hour reaction. Both solvent-free conditions and using ethanol as a solvent gave similar results, so the solvent-free method was continued for simplicity of the reaction. After eight hours of reaction, a portion of the solution was centrifuged and then tested on a Gas Chromatography

Mass Spectrometer (GCMS) for relative amounts of chemicals in the reaction solution. The table below summarizes the data of the benzyl alcohol oxidation reaction for the coreshell Au/Pd nano-cubes and nano-octahedra.

Reaction	Products	% Conversion	TON
AuPd CoreShell Cubes @TiO_2	Benzaldehyde	25%	10215
AuPd CoreShell Octahedra @TiO_2	Benzaldehyde	13%	1733
AuPd Coreshell Cubes	Benzaldehyde	1%	523
Pd Cubes	Benzaldehyde	< 1%	0.005
TiO_2	Benzaldehyde	5%	N/A

Table 3.2 Benzyl alcohol oxidation results for various AuPd@TiO_2 nanostructures.

The TON in Table 2 was measured in terms of the total moles of gold present in the reaction. Based on newer reports involving AuPd catalysts, it is believed that gold is the active metal in this reaction, especially under mild conditions.[4,14,33] However, the electronic and ensemble effects that gold and palladium have with each other were essential for the reaction's performance, as detailed previously. Testing gold nanoparticles alone was not appropriate as the catalytic test was based on gold on palladium nanoparticles. However, reports of AuPd nanoparticle systems have surpassed Au systems alone in many works.[4,11,13] The palladium cubes' performance on the catalytic reaction was clear evidence that the gold in the reaction played the essential role in oxidation. Support-free catalysis did not work in this system due to nanoparticle aggregation in the reaction solution.

These results show that the AuPd (100) surface is more catalytically active for the benzyl alcohol oxidation reaction than the AuPd (111) surface. Under the same conditions, the AuPd nano-cubes were twice as effective as oxidizing benzyl alcohol. Interestingly, the only product in all of our syntheses was benzaldehyde. The selectivity of benzaldehyde may have been due to several reasons. In general, mild conditions generally yield benzaldehyde, benzoic acid, and sometimes benzyl benzoate.[13] However, the fact that only benzaldehyde was produced in the reactions indicate that some other driving force may have been the cause. Titania has been known to help inhibit the over-oxidation from benzaldehyde to benzoic acid, and this may be the cause of the high selectivity in these reactions.[34] In the reactions without titania (Pd cubes and AuPd coreshell cubes) such a small amount of benzaldehyde was produced and any amount of benzoic acid produced from that may have been undetected in the GCMS.

Conversion did not reach 100 % possibly due to inhibition of active sites from benzaldehyde under solvent-free conditions,[33] however the superior performance of AuPd (100) nano-cubes shows that AuPd (100) surfaces are more catalytically active for the benzyl alcohol oxidation reaction than AuPd (111) surfaces. The reaction used here was environmentally friendly and highly selective. The majority of current literature reports involving the benzyl alcohol oxidation reaction use AuPd nanoparticles that have been made through impregnation, sol-immobilisation, or basic co-reduction methods without any type of face-specific control. This project reveals a novel approach of applying controlled nanoparticle synthesis on heterogeneous organic catalysis to help elucidate the specific mechanisms by which catalysts perform.

3.5 References

1 Hashmi, A. S. K. & Hutchings, G. J. Gold Catalysis. *Ang. Chem. Int. Ed.* **45**, 7896-7936, doi:10.1002/anie.200602454 (2006).

2 Miyaura, N. & Suzuki, A. Palladium-Catalyzed Cross-Coupling Reactions of Organoboron Compounds. *Chemical Reviews* **95**, 2457-2483, doi:10.1021/cr00039a007 (1995).

3 Landon, P., Collier, P. J., Papworth, A. J., Kiely, C. J. & Hutchings, G. J. Direct formation of hydrogen peroxide from H2/O2 using a gold catalyst. *Chem. Comm.*, 2058-2059, doi:10.1039/B205248M (2002).

4 Gao, F. & Goodman, D. W. Pd-Au bimetallic catalysts: understanding alloy effects from planar models and (supported) nanoparticles. *Chem. Soc. Rev.* **41**, 8009-8020, doi:10.1039/C2CS35160A (2012).

5 Trimma, D. L., Önsan, Z. Ilsen. Onboard Fuel Coversion for Hydrogen-Fuel-Cell-Driven Vehicles. *Catalysis Reviews: Science and Engineering* **43**, 31-84, doi:10.1081/CR-100104386 (2001).

6 Bonarowska, M., Malinowski, A., Juszczyk, W. & Karpiński, Z. Hydrodechlorination of CCl2F2 (CFC-12) over silica-supported palladium–gold catalysts. *App. CatB. Env.* **30**, 187-193, doi:http://dx.doi.org/10.1016/S0926-3373(00)00231-9 (2001).

7 Pritchard, J. *et al.* Direct Synthesis of Hydrogen Peroxide and Benzyl Alcohol Oxidation Using Au−Pd Catalysts Prepared by Sol Immobilization†. *Langmuir* **26**, 16568-16577, doi:10.1021/la101597q (2010).

8 Edwards, J. K. *et al.* Direct synthesis of hydrogen peroxide from H2 and O2 using TiO2-supported Au–Pd catalysts. *Journal of Catalysis* **236**, 69-79, doi:http://dx.doi.org/10.1016/j.jcat.2005.09.015 (2005).

9 Xu, J. *et al.* Biphasic Pd−Au Alloy Catalyst for Low-Temperature CO Oxidation. *J Am Chem Soc* **132**, 10398-10406, doi:10.1021/ja102617r (2010).

10 Venezia, A. M., La Parola, V., Deganello, G., Pawelec, B. & Fierro, J. L. G. Synergetic effect of gold in Au/Pd catalysts during hydrodesulfurization reactions of model compounds. *Journal of Catalysis* **215**, 317-325, doi:http://dx.doi.org/10.1016/S0021-9517(03)00005-8 (2003).

11 Enache, D. I. *et al.* Solvent-Free Oxidation of Primary Alcohols to Aldehydes Using Au-Pd/TiO2 Catalysts. *Science* **311**, 362-365, doi:10.1126/science.1120560 (2006).

12 Hou, W., Dehm, N. A. & Scott, R. W. J. Alcohol oxidations in aqueous solutions using Au, Pd, and bimetallic AuPd nanoparticle catalysts. *Journal of Catalysis* **253**, 22-27, doi:http://dx.doi.org/10.1016/j.jcat.2007.10.025 (2008).

13 Hutchings, G. J. Selective oxidation using supported gold bimetallic and trimetallic nanoparticles. *Catalysis Today* **238**, 69-73, doi:http://dx.doi.org/10.1016/j.cattod.2014.01.033 (2014).

14 Meenakshisundaram, S. *et al.* Oxidation of alcohols using supported gold and gold-palladium nanoparticles. *Faraday Discussions* **145**, 341-356, doi:10.1039/B908172K (2010).

15 Rodriguez, J. Physical and chemical properties of bimetallic surfaces. *Surface Science Reports* **24**, 223-287, doi:http://dx.doi.org/10.1016/0167-5729(96)00004-0 (1996).

16 Yi, C. W., Luo, K., Wei, T. & Goodman, D. W. The Composition and Structure of Pd−Au Surfaces. *J. Phys. Chem. B.* **109**, 18535-18540, doi:10.1021/jp053515r (2005).

17 Sárkány, A., Geszti, O. & Sáfrán, G. Preparation of Pdshell–Aucore/SiO2 catalyst and catalytic activity for acetylene hydrogenation. *Applied Catalysis A: General* **350**, 157-163, doi:http://dx.doi.org/10.1016/j.apcata.2008.08.012 (2008).

18 Liu, P. & Norskov, J. K. Ligand and ensemble effects in adsorption on alloy surfaces. *Physical Chemistry Chemical Physics* **3**, 3814-3818, doi:10.1039/B103525H (2001).

19 Lee, A. F. *et al.* Structural and Catalytic Properties of Novel Au/Pd Bimetallic Colloid Particles: EXAFS, XRD, and Acetylene Coupling. *The Journal of Physical Chemistry* **99**, 6096-6102, doi:10.1021/j100016a053 (1995).

20 Gao, F., Wang, Y. & Goodman, D. W. CO Oxidation over AuPd(100) from Ultrahigh Vacuum to Near-Atmospheric Pressures: The Critical Role of Contiguous Pd Atoms. *J Am Chem Soc* **131**, 5734-5735, doi:10.1021/ja9008437 (2009).

21 Gao, F., Wang, Y. & Goodman, D. W. CO Oxidation over AuPd(100) from Ultrahigh Vacuum to Near-Atmospheric Pressures: CO Adsorption-Induced Surface Segregation and Reaction Kinetics. *J Phys Chem C* **113**, 14993-15000, doi:10.1021/jp9053132 (2009).

22 Han, P., Axnanda, S., Lyubinetsky, I. & Goodman, D. W. Atomic-Scale Assembly of a Heterogeneous Catalytic Site. *J Am Chem Soc* **129**, 14355-14361, doi:10.1021/ja074891n (2007).

23 Ponec, V. Alloy catalysts: the concepts. *Applied Catalysis A: General* **222**, 31-45, doi:http://dx.doi.org/10.1016/S0926-860X(01)00828-6 (2001).

24 Chen, M., Kumar, D., Yi, C.-W. & Goodman, D. W. The Promotional Effect of Gold in Catalysis by Palladium-Gold. *Science* **310**, 291-293, doi:10.1126/science.1115800 (2005).

25 Hugon, A., Delannoy, L., Krafft, J.-M. & Louis, C. Selective Hydrogenation of 1,3-Butadiene in the Presence of an Excess of Alkenes over Supported Bimetallic Gold−Palladium Catalysts. *J Phys Chem C* **114**, 10823-10835, doi:10.1021/jp100479b (2010).

26 Yin, Y. A., P. Colloidal Nanocrystal Synthesis and the Organic–Inorganic Interface. *Nature* **437**, 664-670, doi:10.1038/nature04165 (2005).

27 Brink, G.-J. t., Arends, I. W. C. E. & Sheldon, R. A. Green, Catalytic Oxidation of Alcohols in Water. *Science* **287**, 1636-1639, doi:10.1126/science.287.5458.1636 (2000).

28 Pagliaro, M., Campestrini, S. & Ciriminna, R. Ru-based oxidation catalysis. *Chem. Soc. Rev.* **34**, 837-845, doi:10.1039/B507094P (2005).

29 Pillai, U. R. & Sahle-Demessie, E. Oxidation of alcohols over Fe3+/montmorillonite-K10 using hydrogen peroxide. *Applied Catalysis A: General* **245**, 103-109, doi:http://dx.doi.org/10.1016/S0926-860X(02)00617-8 (2003).

30 Markó, I. E., Giles, P. R., Tsukazaki, M., Brown, S. M. & Urch, C. J. Copper-Catalyzed Oxidation of Alcohols to Aldehydes and Ketones: An Efficient, Aerobic Alternative. *Science* **274**, 2044-2046, doi:10.1126/science.274.5295.2044 (1996).

31 Nowicka, E. S., Meenakshisundaram. Taylor, Stuart H. Bethell, Donald. Knight, David W. Hutchings, Graham J. Selective Oxidation of Alcohols Using Supported Gold Palladium Nanoparticles.

32 Meier, D. M., Urakawa, A. & Baiker, A. In Situ PM-IRRAS Study of Liquid-Phase Benzyl Alcohol Oxidation on Palladium. *J Phys Chem C* **113**, 21849-21855, doi:10.1021/jp908071m (2009).

33 Skupien, E. *et al.* Inhibition of a Gold-Based Catalyst in Benzyl Alcohol Oxidation: Understanding and Remediation. *Catalysts* **4**, 89-115 (2014).

34 Li, G. *et al.* Solvent-free oxidation of benzyl alcohol with oxygen using zeolite-supported Au and Au–Pd catalysts. *Catal Lett* **110**, 7-13, doi:10.1007/s10562-006-0083-1 (2006).

35 Sreekumar, R. & Pillai, C. N. Reactions of benzyl alcohol and dibenzyl ether over zeolites. *Catal Lett* **19**, 281-291, doi:10.1007/BF00767069 (1993).

36 Jin, M. *et al.* Synthesis of Pd nanocrystals enclosed by {100} facets and with sizes <10 nm for application in CO oxidation. *Nano Res.* **4**, 83-91, doi:10.1007/s12274-010-0051-3 (2011).

37 Xiong, Y. *et al.* Synthesis and Mechanistic Study of Palladium Nanobars and Nanorods. *J Am Chem Soc* **129**, 3665-3675, doi:10.1021/ja0688023 (2007).

38 Peng, H.-C., Xie, S., Park, J., Xia, X. & Xia, Y. Quantitative Analysis of the Coverage Density of Br– Ions on Pd{100} Facets and Its Role in Controlling the Shape of Pd Nanocrystals. *J Am Chem Soc* **135**, 3780-3783, doi:10.1021/ja400301k (2013).

39 Zheng, Y., Zeng, J., Ruditskiy, A., Liu, M. & Xia, Y. Oxidative Etching and Its Role in Manipulating the Nucleation and Growth of Noble-Metal Nanocrystals. *Chem. Mat.* **26**, 22-33, doi:10.1021/cm402023g (2013).

40 Xiong, Y. *et al.* Understanding the Role of Oxidative Etching in the Polyol Synthesis of Pd Nanoparticles with Uniform Shape and Size. *J Am Chem Soc* **127**, 7332-7333, doi:10.1021/ja0513741 (2005).

41 Xiong, Y. *et al.* Size-Dependence of Surface Plasmon Resonance and Oxidation for Pd Nanocubes Synthesized via a Seed Etching Process. *Nano. Lett.* **5**, 1237-1242, doi:10.1021/nl0508826 (2005).

42 Liu, M., Zheng, Y., Zhang, L., Guo, L. & Xia, Y. Transformation of Pd Nanocubes into Octahedra with Controlled Sizes by Maneuvering the Rates of Etching and Regrowth. *J Am Chem Soc* **135**, 11752-11755, doi:10.1021/ja406344j (2013).

43 Zhang, J. *et al.* Shape-Controlled Synthesis of Palladium Single-Crystalline Nanoparticles: The Effect of HCl Oxidative Etching and Facet-Dependent Catalytic Properties. *Chem. Mat.* **26**, 1213-1218, doi:10.1021/cm403591g (2013).

44 Lim, B. *et al.* Synthesis of Pd−Au Bimetallic Nanocrystals via Controlled Overgrowth. *J Am Chem Soc* **132**, 2506-2507, doi:10.1021/ja909787h (2010).

45 Camargo, P. H. C., Xiong, Y., Ji, L., Zuo, J. M. & Xia, Y. Facile Synthesis of Tadpole-like Nanostructures Consisting of Au Heads and Pd Tails. *J Am Chem Soc* **129**, 15452-15453, doi:10.1021/ja077505a (2007).

CONCLUSION AND OUTLOOK

In my thesis work, I found interesting functional peptide motifs for palladium, platinum, and titania which induced morphological and crystalline nanoparticles. For the noble metals platinum and palladium, I found that hydroxyl and amide groups bind well to noble metal surfaces, and that hydroxyl groups bind to the (100) surface more effectively whereas amide groups bind better to the (111) surfaces. For titania, I found that histidine, lysine, and serine bind particularly well to this semiconductor and are even involved in the initial formation of titania from its water-stable precursor. Additionally, proline and other ring group amino acids were found frequently in the peptides selected for titania. These results show that it is both the conformation of peptides as well as functional groups that are important for the specific binding to inorganic surfaces in solution. Peptides as capping agents also allowed for the successful creation of heterostructures exemplified between nanoparticles of platinum and titania. These results further show that peptides are not only good capping agents in ambient condition nanoparticle synthesis for controlling morphology of metals but also that they can be versatile, dynamic ligands in solution.

In the second chapter of this work, I showed that electro-neutral to electropositive aryl small molecules are driven by their substituents' epitaxial binding to noble metal surfaces and less by their electrostatic potentials. A special set of reactive electropositive small molecules create defects and irregularly shaped nanoparticles. These results offer the potential of post-modification of nanocrystals as well as make nanoparticles with high energy facets for catalysis and electronic applications.

AuPd nano-cubes and nano-octahedra were the focus of the third chapter of this work. These nanostructures were made to detect the difference in catalysis of (100) and (111) surfaces of AuPd for the benzyl alcohol oxidation reaction. It was found that the (100) AuPd surface was more catalytically active under mild oxidative conditions and that the system used for this work had selective conversion to benzaldehyde.

Since the beginning of this work, studies have been published adding the knowledge of the capping agent-nanoparticle surface relationship in combination with the interactions of the solvent, the ligand-ligand interactions, etc. to make 3D superstructures of nanoparticles suspended in solution as well as to make more complex nanoparticle structures in solution. In 2011, Chad Mirkin and colleagues paved the way to making a variety of rational 3D colloid suspensions using DNA as ligands by outlining general guidelines.[1] Since then, various groups have taken advantage of creating unique nanocrystal suspensions with interesting properties. Earlier this year, Chan and colleagues made satellite-core structures of gold nanoparticles linked together by unique strands of DNA to create different 3D shapes in solution.[2] Figure 1 shows various gold superstructures made from the same approach but with different-sized linkers of DNA, different lengths of ligand PVP, and different sized gold nanoparticles. Not only is the synthesis of these systems interesting for future nanoparticle superstructure synthesis, but the literature also reported in-vivo studies of the efficiency of the superstructures being endocytosed by macrophages as well as their fluorescence properties in rat tumors in vitro. With improved understanding of nanoparticle synthesis, more complex systems will be made and used for every field of science.

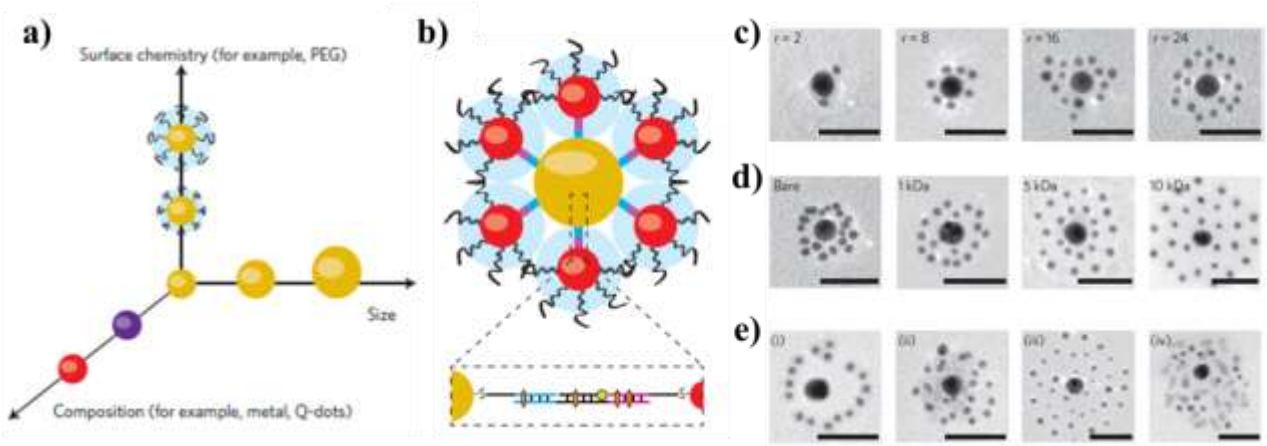

Figure 1 (a) Schematic showing core-satellite structures are made through a dynamic relationship between linker size and functionality (y-axis), nanoparticle size (x-axis) and nanoparticle composition (z-axis). (b) A schematic of a core-satellite structure, where the yellow and red spheres represent the core and satellite nanoparticles, respectively. The black lines around the satellite structures represent polyvinylpyrrolidone (PVP), and the blue/purple lines between the core and satellite structures represent the DNA linkages. (c) Transmission electron microscopy (TEM) images of gold core-satellite structures with various core to satellite ratios. (d) TEM images of gold core-satellite structures with increasing molecular weights (lengths) of PVP. (e) TEM images of core-satellite nanostructures with various DNA linkages and the introduction of other types of nanoparticles.[2]

As technology advances in terms of equipment for physical observation of materials as well computer software, so will our understanding of the fundamental concepts of nanocrystal systems. There are constantly new reports of density-functional theory (DFT) studies on nanoparticle surfaces and their relationship to ligands,[3-6] which all add to the consideration of how nanoparticles can be more successfully made under the most environmentally friendly conditions. Additionally, new novel morphologies of nanocrystals will continue to evolve their optical, physical, and chemical properties. For example, high index facets can be more catalytically active than lower energy facets for many reactions; however their synthetic conditions are usually more complex and harder to stabilize in solution for long periods of time, especially with noble metals. In a recent report, colleagues in Ireland have successfully made

(730) high index palladium nanocrystals and used them to show their superior activity to low energy (100) facets in Suzuki-Miyaura coupling reactions.[7] Figure 2a shows palladium nano-cubes made through the same approach as detailed in Chapter 3 of this work and then used as seeds to create surface concave palladium nanoparticles with (730) facets exposed (Figure 2b). During the catalytic reaction, the concave nanoparticles were not stable and faced severe leaching. The increased leaching of the high energy facets compared to the low energy facets actually allowed for better performance, and in this way, a negative effect of high energy facet stabilization was turned into a helpful part of the catalytic system.

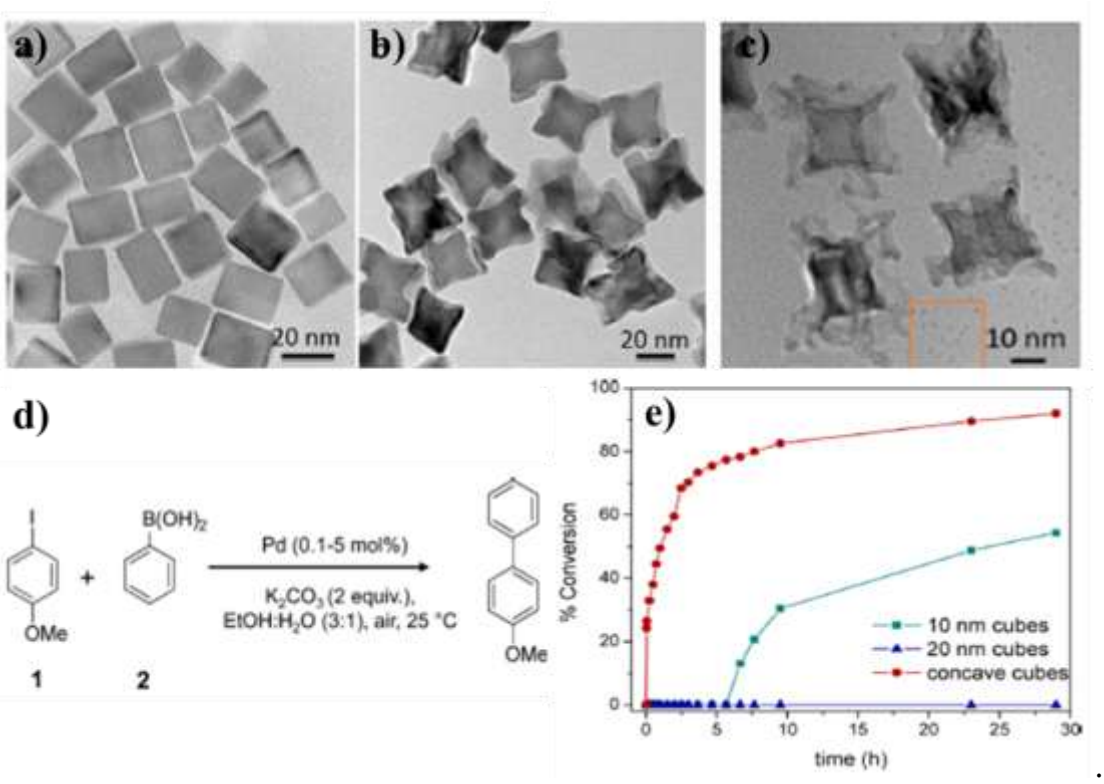

Figure 2 (a) TEM image of palladium nano-cubes made through the same approach detailed in Chapter 3. (b) TEM image of palladium concave cubic nanoparticles used for the Suzuki-Miyaura coupling reaction. (c) TEM image of leached palladium concave cubic nanoparticles after the Suzuki-Miyaura coupling reaction. (d) The Suzuki-Miyaura coupling reaction performed in this study. (e) The % conversion of substrate from the various types of palladium nano-cubes.[7]

High energy facets also enhance optical properties, as shown in work by Zhang and co-workers in China.[8] In their work, convex hexoctahedral AuPd core-shell nanoparticles with (431) index facets exposed show enhanced electrochemiluminescence (ECL) properties compared to their lower energy facet counterparts due to the abundant AuPd kinks and steps as surface sites for the ECL reaction of luminol and hydrogen peroxide. This work offers the potential for more intricate bioanalytical detection methods using high index nanoparticles.

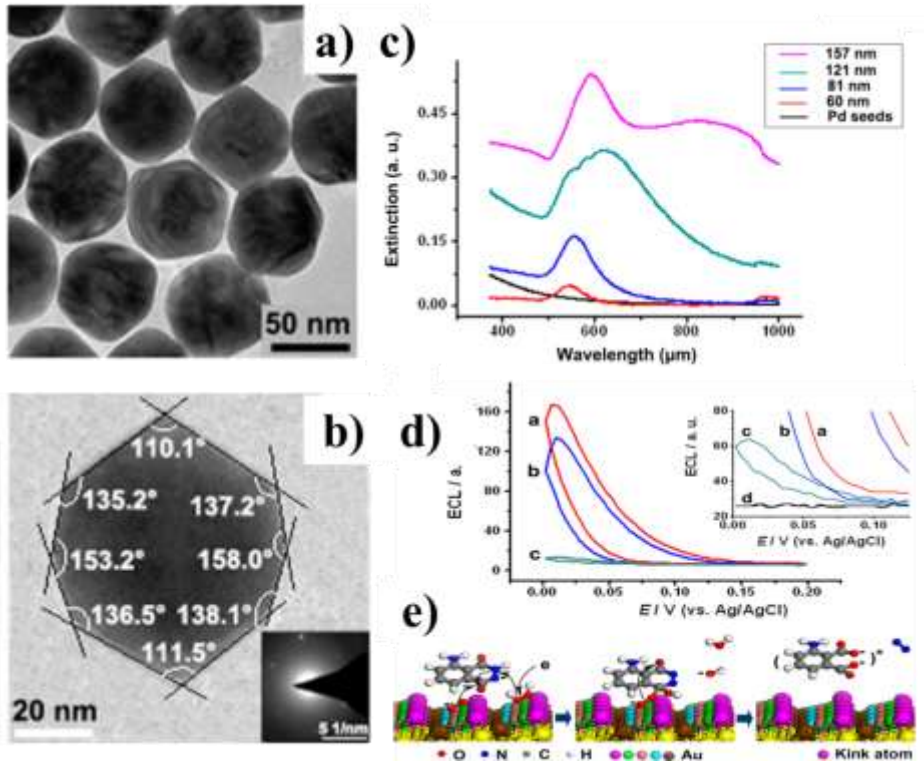

Figure 3 (a and b) TEM images of AuPd core-shell convex hexoctahedral nanoparticles. (c) A graph of extinction spectra of palladium nano-cubes and different-sized hexoctahedral nanoparticles. (d) Electrochemiluminescence (ECL) potential curves for the reaction of luminol and hydrogen peroxide with AuPd core-shell convex hexoctahedral (inset a), concave trisocahedral (inset b), truncated octahedral nanoparticles (inset c), and the bare glassy carbon electrode (inset d). (e) A schematic of the ECL reaction mechanism of luminol and hydrogen peroxide on the convex hexoctahedral nanoparticles.[8]

In years to come, I see the field of nanoparticle synthesis continuing to grow as nanoparticles become increasingly popular in catalysis, electronics, and the environmental and medical industries. My work adds knowledge to an area of Inorganic Chemistry and Materials Science and Engineering that yearns to be further studied. As we continue to better understand nanoparticle systems, we will also be able to be more creative in our syntheses, structures, and applications of these materials.

References

1 Macfarlane, R. J. *et al.* Nanoparticle Superlattice Engineering with DNA. *Science* **334**, 204-208, doi:10.1126/science.1210493 (2011).

2 Chou, L. Y. T., Zagorovsky, K. & Chan, W. C. W. DNA assembly of nanoparticle superstructures for controlled biological delivery and elimination. *Nat Nano* **9**, 148-155, doi:10.1038/nnano.2013.309.http://www.nature.com/nnano/journal/v9/n2/abs/nnano.2013.309.html#supplementary-information (2014).

3 Fischer, G., Poteau, R., Lachaize, S. & Gerber, I. C. Surfaces of a Colloidal Iron Nanoparticle in Its Chemical Environment: A DFT Description. *Langmuir* **30**, 11670-11680, doi:10.1021/la502963n (2014).

4 Morin, C., Simon, D. & Sautet, P. Chemisorption of Benzene on Pt(111), Pd(111), and Rh(111) Metal Surfaces: A Structural and Vibrational Comparison from First Principles. *J. Phys. Chem. B.* **108**, 5653-5665, doi:10.1021/jp0373503 (2004).

5 Slocik, J. M. & Naik, R. R. Probing peptide-nanomaterial interactions. *Chem. Soc. Rev.* **39**, 3454-3463, doi:10.1039/B918035B (2010).

6 Morin, C., Simon, D. & Sautet, P. Density-Functional Study of the Adsorption and Vibration Spectra of Benzene Molecules on Pt(111). *J. Phys. Chem. B.* **107**, 2995-3002, doi:10.1021/jp026950j (2003).

7 Collins, G., Schmidt, M., O'Dwyer, C., McGlacken, G. & Holmes, J. D. Enhanced Catalytic Activity of High-Index Faceted Palladium Nanoparticles in Suzuki–Miyaura Coupling Due to Efficient Leaching Mechanism. *ACS Catalysis* **4**, 3105-3111, doi:10.1021/cs5008014 (2014).

8 Zhang, L. *et al.* Synthesis of Convex Hexoctahedral Palladium@Gold Core–Shell Nanocrystals with {431} High-Index Facets with Remarkable Electrochemiluminescence Activities. *ACS Nano* **8**, 5953-5958, doi:10.1021/nn501086k (2014).